Defence Research and Development Canada
Recherche et développement pour la défense Canada

CAN UNCLASSIFIED

DRDC | RDDC
technologysciencetechnologie

Ultimate and residual strength of benchmark hull models

Malcolm J. Smith
DRDC – Atlantic Research Centre

Defence Research and Development Canada

Scientific Report

DRDC-RDDC-2019-R021

March 2019

CAN UNCLASSIFIED

Canada

IMPORTANT INFORMATIVE STATEMENTS

Endorsement statement: This publication has been peer-reviewed and published by the Editorial Office of Defence Research and Development Canada, an agency of the Department of National Defence of Canada. Inquiries can be sent to: Publications.DRDC-RDDC@drdc-rddc.gc.ca.

Abstract

The ultimate and residual strength in vertical bending of three benchmark hull girder models are evaluated using nonlinear finite element analysis (FEA) and using Smith's simplified method. The benchmark models are evaluated in three conditions: intact, with simulated grounding damage, and with simulated collision damage. Two different Smith's method calculations are performed for each model, in which load shortening curves are generated either using the International Association of Classification Societies (IACS) analytical formulas, or by interpolating from the ULTMAT database of pre-calculated curves. Smith's method predictions using the IACS formulas are found to agree well with FEA predictions for interframe collapse of longitudinal structure with high-column slenderness, whereas Smith's method does not agree well with FEA when an overall collapse mode is predicted. For structures with low-column slenderness, Smith's method is found to predict ultimate strengths that are higher than the FEA predictions. Gross damage to the main deck and shear strake, or to the hull bottom, is found to reduce ultimate strength by more than 50% in some cases. In percentage terms, strength reductions are up to three to four times the percentage reduction in the effective cross sectional area. Overall collapse is the preferred mode of failure with collision damage, whereas interframe collapse is preferred with grounding damage.

Significance to defence and security

Ultimate strength defines the overall load-carrying capacity for the hulls of large surface combatants. Ultimate strength can vary over the life of a vessel depending on design changes to the vessel and in-service degradation effects such as corrosion and deformations. Major damage incidents can severely reduce the remaining or residual strength to an extent that safety of the vessel is compromised. The present work is part of an international collaboration to validate tools for predicting ultimate and residual strength using realistic test cases. Through this effort, knowledge of the operational limits of the Royal Canadian Navy (RCN) hulls is enhanced, thus supporting the Department of National Defence (DND)'s aims in naval materiel assurance.

Résumé

On évalue la résistance à la rupture et la résistance résiduelle en flexion verticale de trois modèles de référence de poutres-coques au moyen de l'analyse non linéaire par éléments finis et de la méthode simplifiée de Smith. Les modèles de référence sont évalués selon trois conditions : intact, avec simulation d'avaries causées par un échouage, puis avec simulation d'avaries causées par une collision. En utilisant la méthode de Smith, on effectue, pour chaque modèle, deux calculs dans lesquels les courbes de raccourcissement de charge sont générées par les formules analytiques de l'IACS, l'Association internationale des sociétés de classification, ou par interpolation à partir de la base de données de courbes précalculées ULTMAT. On a constaté que la méthode de Smith combinée aux formules de l'IACS concordait bien avec les prévisions de l'analyse par éléments finis pour l'écrasement entre membrures de la charpente longitudinale avec coefficient d'élancement élevé de la colonne, mais elle ne concordait pas avec l'analyse par éléments finis lorsqu'un écrasement général était prévu. Pour les charpentes avec coefficient d'élancement bas de la colonne, on a constaté que la méthode de Smith permettait de prévoir des résistances limites plus élevées que celles de l'analyse par éléments finis. On a également constaté que les avaries importantes au pont principal et à la virure de carreau, ou au fond de la coque, réduisaient la résistance à la rupture de plus de 50 % dans certains cas. En pourcentage, les réductions de la résistance sont de trois à quatre fois plus élevées que celle de la section transversale efficace. L'écrasement général est le mode de défaillance privilégié pour les avaries causées par une collision, tandis que l'écrasement entre membrures est celui pour les avaries causées par un échouage.

Importance pour la défense et la sécurité

La résistance à la rupture détermine la capacité portante globale de la coque des grands navires de combat de surface. La résistance à la rupture peut varier tout au long de la vie d'un navire en fonction des changements à sa conception et des effets de la dégradation en service tels que la corrosion et les déformations. Les incidents qui causent de graves avaries peuvent réduire considérablement la résistance restante ou résiduelle au point où la sécurité du navire s'en trouve compromise. Les présents travaux font partie d'une collaboration internationale visant à valider les outils de prévision de la résistance à la rupture et de la résistance résiduelle par des jeux d'essai réalistes Ces efforts ont permis d'accroître la connaissance des limites opérationnelles des coques de la Marine royale canadienne (MRC), ce qui vient appuyer les objectifs du ministère de la Défense nationale (MDN) en matière d'assurance de l'équipement naval.

Table of contents

List of figures

List of tables

1 Introduction

Traditionally, global strength of ships was based on longitudinal stresses and deflections due to an applied design bending moment; the ultimate strength, i.e., the largest bending moment a hull can withstand before collapsing, was not directly considered. However, modern ship design standards, such as the Common Structural Rules for Bulk Carriers and Oil Tankers published by the International Association of Classification Societies [1], now require that large vessels be designed for hull girder ultimate strength. Similarly, naval design standards, such as Lloyd's Register's Naval Ship Rules [2], offer notations covering the assessment of ultimate hull girder strength.

Analogous to the ultimate strength, the residual strength is the maximum load carrying capacity of a hull in a damaged condition. This is important both at the design stage, when anticipating likely damage scenarios, and in-service, when in the aftermath of a damage event. Depending on the damage to the structure, the residual strength and the mode of collapse may differ considerably from the intact ultimate strength. Assessment of residual strength has been introduced in some commercial and naval ship standards [1],[2].

Predicting ultimate or residual strength requires a numerical analysis tool that can account for material elasticity, plasticity and buckling instability of the longitudinal structure while also taking into account the effect of imperfections. Specialized methods such as Smith's method [3], and nonlinear finite element methods, are most commonly used for this calculation.

A Collaborative Project under Technical Panel 4 of the Maritime Group of The Technical Cooperation Program (TTCP) is investigating the survivability and resilience of damaged or degraded naval platforms [4]. A component of this project is a round-robin comparison of ultimate and residual strength predictions for benchmark test problems. The present document summarizes the DRDC contribution to this effort.

Results are provided for three benchmark test cases: two UK box girder designs and a US Navy design for a generic or "notional" destroyer. These benchmark test cases were modelled and analysed with the Canadian DND's finite element software tools Trident Modeller and (VAST) [5], and with DRDC's in-house ultimate strength analysis software ULTMAT [6]. Section 2 of the report describes the modelling and analysis methodology used and Section 3 provides the results of all of the analyses. Some further interpretation of the results is given in Section 4, and final conclusions and recommendations are given in Section 5.

2 Methodology

2.1 Model definition

Two groups of simplified hull structures are modelled and analysed in both the intact and damaged conditions. The present section defines the geometries and other properties for each of the simplified hull structures. Section 2.2 describes the analysis approaches used for all of the models.

2.1.1 Structures Software Test Kit (SSTK) designs

The SSTK designs are numerical models representing highly simplified hull structures that were devised by the UK Ministry of Defence (MoD) for use in benchmarking structures analysis codes [7]. Two of the SSTK configurations are considered in this study: a rectangular box girder (Model A), and a semi-circular box girder (Model C). The overall dimensions of the two models are summarized in Table 1, and views of the model geometry and cross section arrangement of the midbody are given in Figure 1 and Figure 2.

Table 1: *Dimensions of the SSTK models.*

Dimension	Model A	Model C
Length, L (m)	100	115
Breadth, B (m)	15	15
Overall depth, D (m)	10	7.5
Transverse frame spacing (m)	2.5	2.5
Compartment length (m)	10	10

Nominal material properties to be used for the SSTK models are summarized in Table 2. A bilinear material model in tension and compression is assumed.

Table 2: *Material properties of the SSTK models.*

Elastic Modulus (MPa)	207,000
Poisson's ratio	0.3
Yield stress (MPa)	235
Tangent modulus (MPa)	203

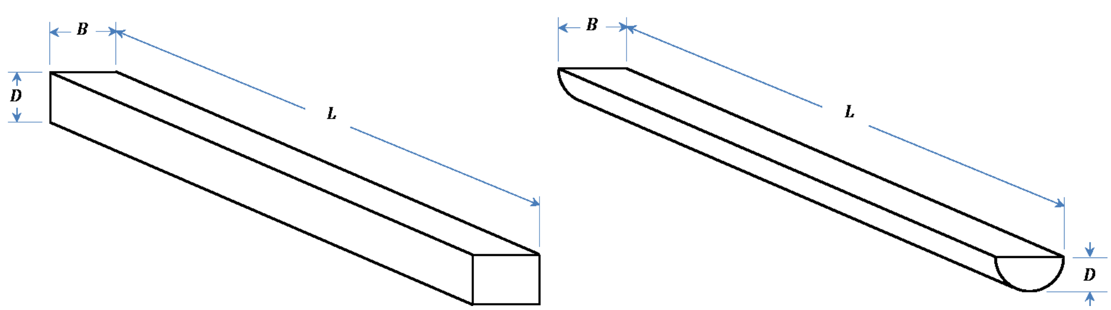

Figure 1: *SSTK Model A (top), and Model C (bottom).*

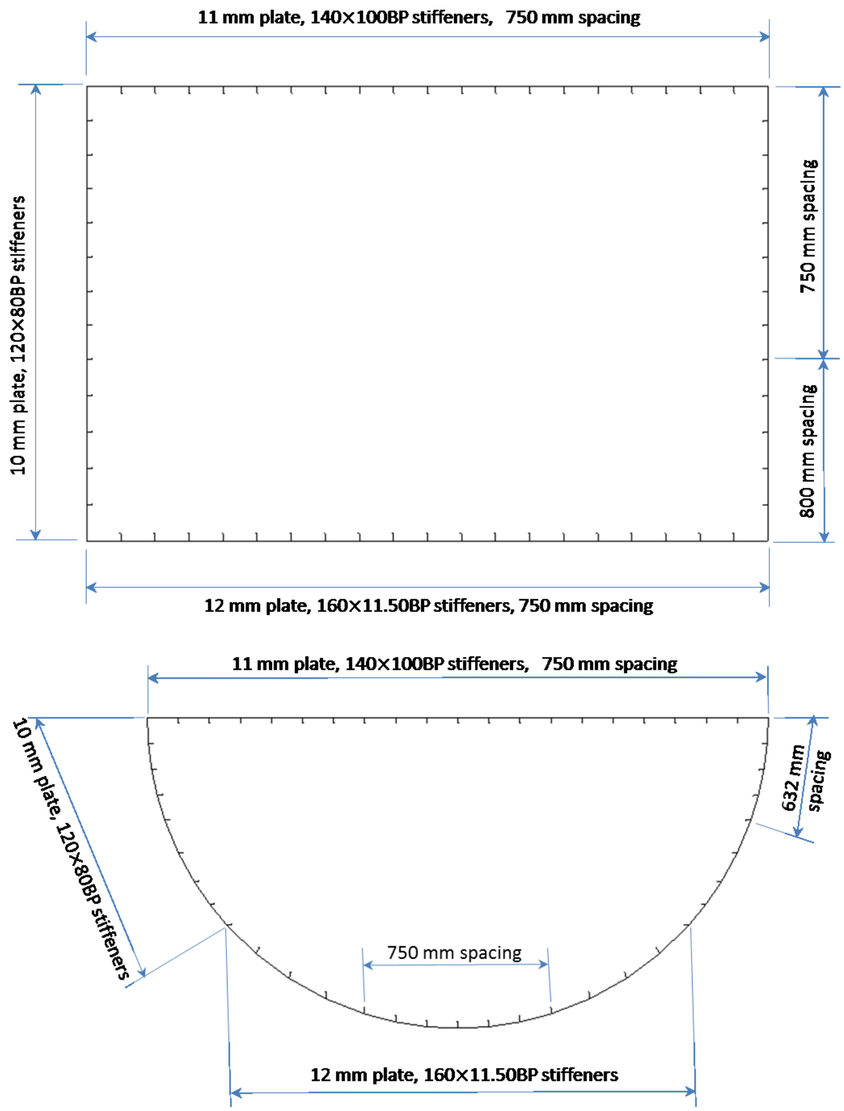

Figure 2: *SSTK midbody cross section arrangement: Model A (top), and Model C (bottom).*

Two gross damage cases are to be investigated for each of the SSTK models. Gross damage is represented as a complete disablement or removal of the damaged structure. Of particular interest to the present work is whether the loss of the damaged structure changes the mode of failure under extreme bending, and for this reason relatively large damage areas are investigated.

Collision and grounding damage cases for SSTK-A and SSTK-C are sketched in Figure 3 and Figure 4, respectively. The damage length is assumed to be a full length of the compartment in each case. All structure inside the red box, including plating, transverse frames, longitudinal stiffeners, is completely disabled, whereas all structure outside the box remains fully intact.

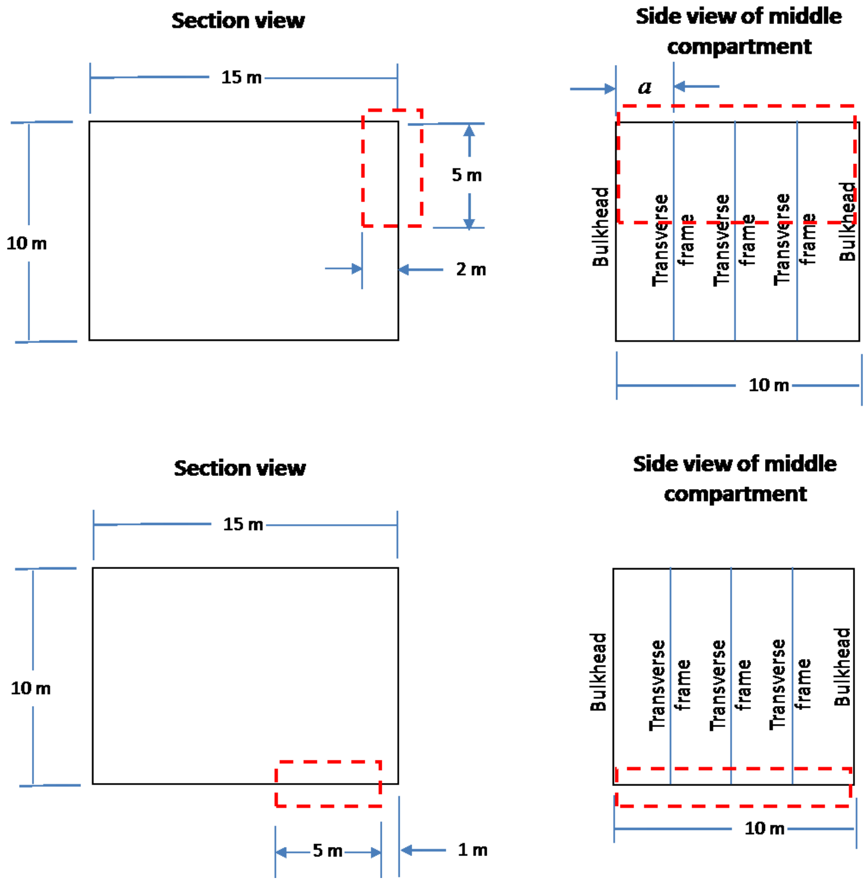

Figure 3: *Collision damage case (top) and grounding damage case (bottom) for SSTK-A.*

Table 3 summarizes the cross sectional areas of the SSTK models in the intact and damaged condition.

Table 3: *Cross sectional areas of the SSTK models.*

Model	**Intact**	**Collision damage**		**Grounding damage**	
	Area (m^2)	Area (m^2)	Area ratio	Area (m^2)	Area ratio
SSTK-A	0.646	0.564	0.873	0.554	0.858
SSTK-C	0.504	0.418	0.829	0.427	0.847

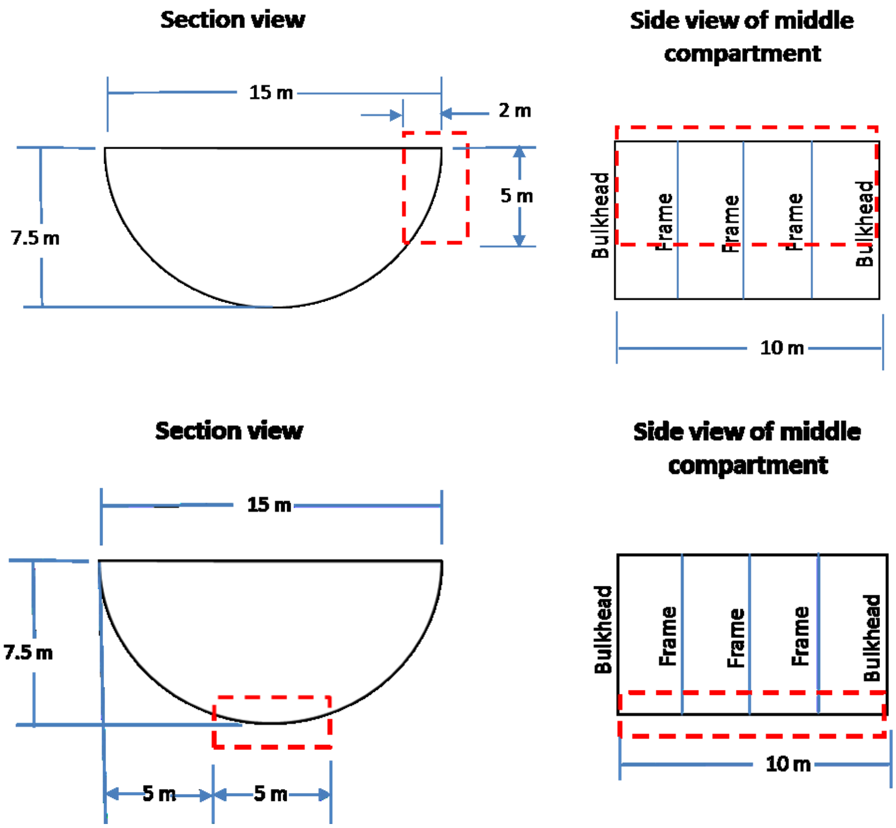

Figure 4: *Collision damage case (top) and grounding damage case (bottom) for SSTK-C.*

Both of the SSTK models use bulbplate sections for longitudinals. As none of the analysis tools used in the present work supports the use of bulbplate sections, these are modelled as equivalent angle sections. Table 4 gives the angle section equivalents for the bulbplates used in the SSTK models. The equivalents are determined such that the overall depth, flange area, web thickness, and the total area of the section are the same as in the corresponding bulbplate.

Table 4: *Angle equivalents to bulbplates.*

Bulbplate	Depth (mm)	Width (mm)	Web thickness (mm)	Flange thickness (mm)
140×100BP	140	33.64	10	11
120×80BP	120	29	8	10
160×11.50BP	160	39.83	11.5	12

2.1.2 Notional destroyer design

The notional destroyer design was described in the 2009 ISSC Committee V.5 report (Naval Ship Design) [8] and in an unpublished document by Naval Surface Warfare Center (NSWC) Carderock [9]. The design is based on the 5415 hull form. It is a single-hulled vessel with four continuous decks. The hull is built from a high strength steel with a yield strength of 355 MPa, although some portions of the deck and hull plating are fabricated from the high-tensile strength steel HY80. Lines of form and cross section arrangements for the midsection, forward and aft quarters are given in [9]. For the present study, the middle compartment of the vessel (between FR220 and FR254) is considered. This is modelled a parallel midbody geometry based on the midships section (Station 10). For this study, the spacing of transverse web frames is 1.905 m (75 in). In the original specification document, the compartment length was defined as 11.43 m, i.e., six frame bays. During the course of this work, the author considered that it would be more advantageous to use a seven frame bay, or 13.335 m, compartment length for definition of imperfections and damage.

Nominal material properties for the two steels used in this design are summarized in Table 5.

Table 5: *Material properties of the notional destroyer.*

	HSS	HY80
Elastic modulus (MPa)	207000	207000
Poisson's ratio	0.3	0.3
Yield stress (MPa)	355	550
Tangent modulus (MPa)	2000	2000

Collision and grounding damage cases defined for the notional destroyer design are shown in Figure 6. As with the SSTK models, the simplified approach of modelling damage is used. All structure within the indicated damage regions is considered to be completely disabled or removed. In the collision damage case, the damage extends longitudinally three full frame bays and this includes the two most centrally positioned transverse web frames. The transverse frames that are on the edge of the damage zone are considered to be intact. In the grounding case, the damage is considered to extend a full compartment length, affecting all web frames, but leaving the bulkheads intact.

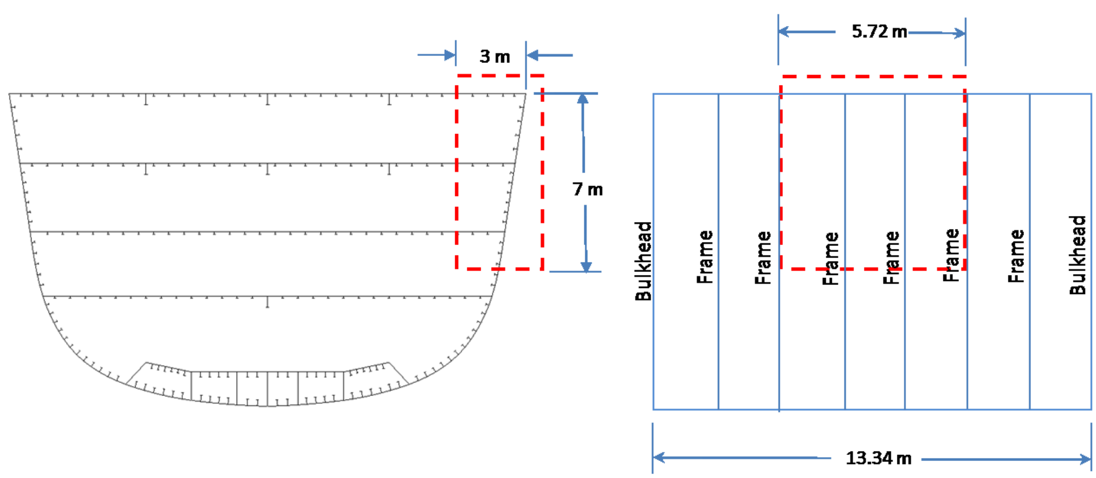

Figure 5: *Collision damage case for the destroyer model.*

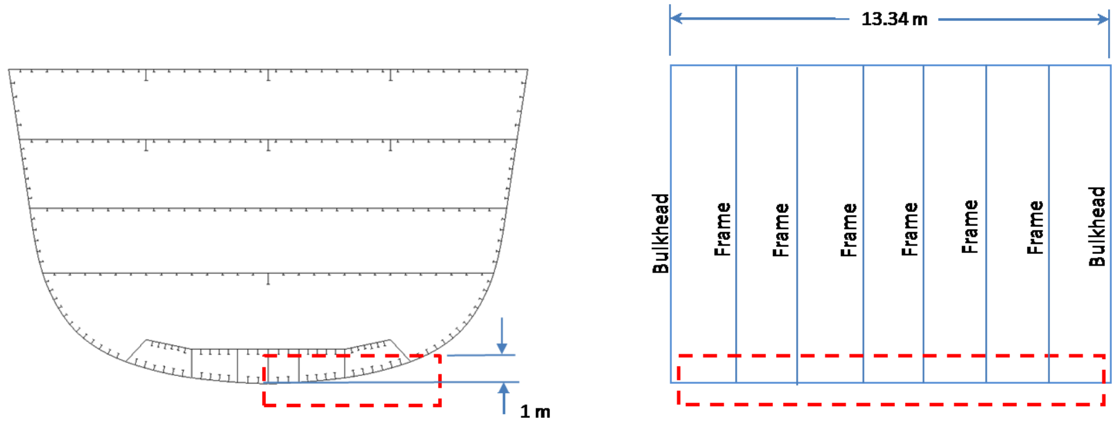

Figure 6: *Grounding damage case for the destroyer model.*

Table 6: *Cross sectional areas of the destroyer model.*

Intact	**Collision damage**		**Grounding damage**	
Area (m^2)	Area (m^2)	Ratio	Area (m^2)	Ratio
1.357	1.227	0.904	1.234	0.909

2.2 Analysis methodology

Two different methods will be used to determine the ultimate and residual strengths of the hull structures described in Section 2.1.

2.2.1 Smith's method

Smith's method [3] is one of the most commonly used methods for determining the intact ultimate strength of steel monohull vessels. It has been adopted by classification society rules [1] and has also been proposed for residual strength of damaged vessels [1],[10],[11]. It assumes beam-like behaviour of the hull girder, and determines the ultimate bending moment considering elasto-plastic collapse and yielding of the longitudinal structure between transverse web frames. The models used in Smith's method are therefore single-frame bay models of the most critical cross sections.

The ULTMAT program [6] will be used in the present work for Smith's method analysis. It uses an incremental-iterative method in which a progressively increasing curvature is applied to a cross section. At each step of the calculation, the longitudinal strain in each structural unit is determined, assuming the section remains plane under bending. Using this strain, the average stress in each independently acting unit is determined by either (a) interpolating from a database of pre-calculated load-shortening curves for stiffened panels [12]; or (b) using the analytical formulas for the load-shortening behaviour taken from the Common Structural Rules [1]. The peak value of the bending moment determined using the incremental method is the ultimate strength of the cross section.

Smith's method normally uses a curvature-controlled incremental approach, where curvature is incremented vertically to produce a sagging or hogging bending in the hull. This is sufficient when determining vertical ultimate strength of an intact symmetric hull structure. But when the structure is damaged asymmetrically, applied curvature in the vertical direction results in both vertical and horizontal bending moment components, and does not give a true measure of the vertical ultimate strength. Instead, a bi-axial ultimate strength calculation using a moment-controlled incremental method is more appropriate when assessing damaged structure, and this is the method used to assess asymmetrically damaged cross sections.

Welding of the longitudinal stiffeners to the plating is assumed to result in (1) distortion of hull and deck plating, and distortion of the longitudinal stiffeners; and (2) residual stresses in the form of tensile yield stresses in the heat affected zones (HAZ) close to the longitudinal welds, and compressive residual stresses in the plating outside of the HAZ. Both types of imperfections may influence the ultimate strength of intact vessels and the residual strength of damaged vessels.

In Smith's method, imperfections are usually implicit in the definition of the load shortening formulas or curves. ULTMAT's native library of load-shortening curves assumes for "average" plate imperfections a maximum normal plate deflection of $0.1\beta^2 t$, where

$$\beta = \left(\frac{b}{t}\right)\sqrt{\sigma_y/E} \tag{1}$$

is the plate slenderness parameter, in which b is the width of plating between adjacent longitudinal supports, t is the plate thickness, σ_y is the yield strength, and E is the elastic modulus. The "average" level of initial out-of-straightness of longitudinal stiffeners are assumed to be between $0.0008a$ and $0.0015a$, depending on the value of the column slenderness parameter,

$$\lambda = \left(\frac{a}{\pi r}\right)\sqrt{\sigma_y/E} \tag{2}$$

in which a is the effective length of the beam-column between transverse supports, r is the radius of gyration of the combined stiffener and effective width of attached plating. Average longitudinal compressive residual stress in plating is taken to be 15% of the yield stress. Average imperfections are assumed for all of the cross sections analyzed in the present work.

Table 7 summarizes the distortions and residual stress levels to be included in the modes.

Table 7: *Imperfection level for all models.*

Max plate deflection, δ_p	$0.1\beta^2 t$
Max stiffener deflection, δ_s	$0.0015a$
Longitudinal residual stress, σ_r	$-0.15\sigma_y$

ULTMAT cross sections are generated from Trident finite element (FE) models using the cross sectioning tool in DRDC's Ultmat Modeller software. This tool takes a section through the FE model in a user-defined plane and automatically identifies elements intersecting the plane. This collection of intersected elements is further reduced to create a cross section comprised of stiffeners and plate elements. Plates and stiffeners are then grouped into independently acting structural units. Longitudinally stiffened panel units are comprised of a single longitudinal stiffener and a width of attached plating. Failure is in yielding in tension and in elasto-plastic buckling or yielding in compression. Hard corners elements are junctions of plating that fail in yielding in tension and compression. The notional destroyer cross section also has a few transversely stiffened panel units, which are used for the webs of deep girders. These are assumed to fail by plate buckling or yielding in compression and by yielding in tension. The plating attached to longitudinals normally extends half the distance to the neighbouring stiffener on each side. For a hard corner, the width of each plate segment is the lesser of half the distance to the next longitudinal support or $20t$, where t is the plate thickness [1].

The three cross section models for the SSTK and notional destroyer designs in the intact condition are shown in Figure A.1 through Figure A.3 in Annex A. The same models are used for hogging and sagging analysis. The transverse frame spacing defines the effective length of the structural units making up the cross section. This is important for determining the column slenderness of the longitudinal stiffened panels. The effective length is 2.5 m for the SSTK models, and 1.905 m for the destroyer model. Tranversely stiffened panels have an additional parameter defining the spacing of transverse stiffeners, which is assumed to be 476.25 mm in the destroyer model. The stiffener spacing parameter is needed by ULTMAT to determine the aspect ratio of the individual plate panels in compression.

Two simple ways of introducing damage in the ULTMAT cross sections are to either delete damaged structure or reduce its effectiveness. The latter approach was used to create the collision and grounding damage models. Reducing effectiveness to zero has the same effect as deleting the structure, except that the original organization of the structure into structural units is preserved. To model damage, the effectiveness of all plate and stiffener elements inside the damage area is reduced to zero. Where a plate crosses the boundary of the damage area, its effectiveness is reduced according to the percentage of its cross sectional area that is inside the damaged area. The effectiveness of a longitudinally stiffened panel unit is the combined effectiveness of the longitudinal stiffener and the two plates that comprise it. The grounding and collision damage models for the three designs are shown in Figure A.4 through Figure A.6 in Annex A.

2.2.2 Nonlinear Finite Element Analysis (FEA)

Nonlinear FEA is seeing increasing use for ultimate strength assessment of ship hulls. A detailed study by Amlashi and Moan [13] demonstrated its application to a bulk carrier. Some recent applications of nonlinear FEA to residual strength assessment of damaged ships were performed by Muis Alie et al [14] and by Petricic [15]. Hull and damage geometries can be more realistically modeled with nonlinear FEA than with other methods. The main disadvantage is that the modelling effort and computationally time required with nonlinear FEA is generally much higher than with other methods. Obtaining a convergent solution with nonlinear FEA can also be difficult near collapse and in the post-collapse region.

2.2.2.1 Meshing

Surface geometry models for the SSTK and notional destroyer designs are created using DRDC's SubSAS software [16] and are shown in Figure 7 through Figure 9. A two-compartment long parallel midbody section of each of these models is meshed with first-order shell and beam elements. The two compartment section is centred around a central compartment, with half compartment sections on either end. The ½+1+½ compartment arrangement was chosen for modelling of structural damage up to one compartment in length and compartment-length collapse modes.

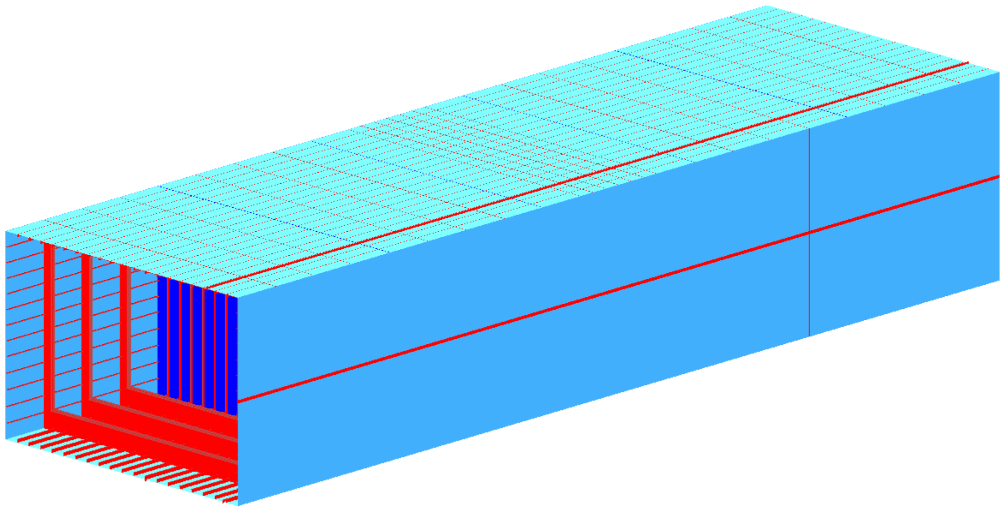

Figure 7: *SubSAS geometric model of SSTK-A.*

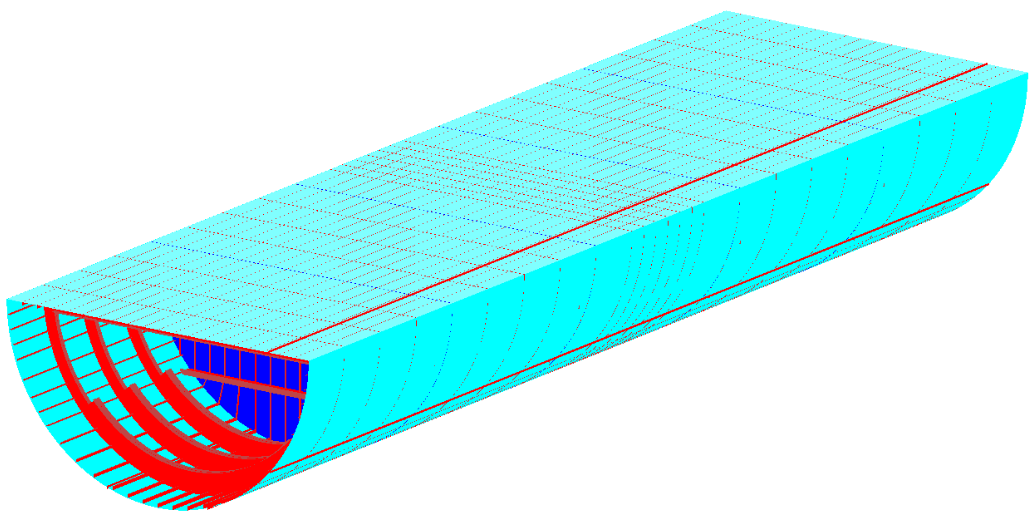

Figure 8: *SubSAS geometric model of SSTK-C.*

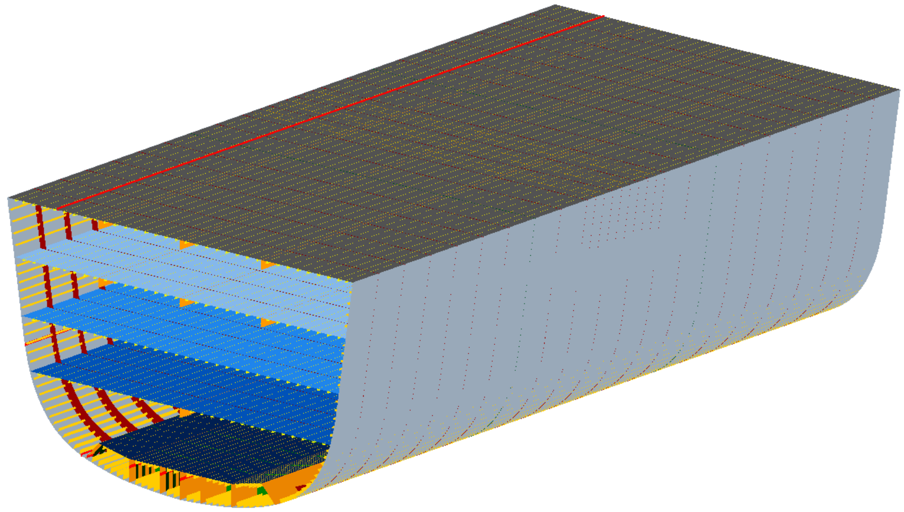

***Figure 9:** SubSAS geometric model of the notional destroyer.*

SubSAS generates the FE meshes predominantly using 4-node quadrilateral shell elements, with 3-node shell elements used occasionally to avoid badly shaped quadrilaterals. Shell elements are used for the plating, transverse frames and some longitudinals. The meshes are specialized for hogging and sagging to optimize the model size to the analysis case. Generally additional refinement is only used on the side of the hull girder in compression. All longitudinals are modelled with shell elements in the SSTK models. Longitudinals on the tension side of the notional destroyer are modelled as beam elements while compression-side longitudinals are meshed with shell elements. This helps to limit the growth of the model size. Element sizes used in the three sets of models are summarized in Table 8. These were considered to be adequate based on previous work by the author and in the published literature [13],[17]. The destroyer model has an intermediate mesh to effect a smoother transition between the base mesh and the refined zone.

***Table 8:** Element sizes used in the FE models.*

Parameter	SSTK-A	SSTK-C	Destroyer
Edge length, base (mm)	200	200	300
Edge length, transition zone (mm)	-	-	200
Edge length, refined zone (mm)	100	100	100
Refined longitudinal webs (# elem)	5	5	4
Refined longitudinal flanges (# elem)	4	4	4

The finite element meshes generated for the SSTK-A and SSTK-C models are shown in Figure B.1 through Figure B.8 in Annex B, where the different meshes for the hogging and sagging load cases are noted.

2.2.2.2 Imperfections

Distortions are applied to the FE models subsequent to meshing using imperfection objects provided in SubSAS. The total out-of-plane distortion in a single plate panel, w_{0p}, is

$$w_{0p} = \delta_p \left(0.8 \sin\frac{\pi x}{a} + 0.2 \sin\frac{3\pi x}{a}\right) \sin\frac{\pi y}{b} + \delta_s \sin\frac{\pi x}{a} \tag{3}$$

whereas the total out-of-plane column distortion in the stiffener, w_{0s}, is

$$w_{0s} = \delta_s \, sin\frac{\pi x}{a} \tag{4}$$

In the above, x is the longitudinal direction, and y is the transverse direction; δ_p is the amplitude of distortion in the plating and δ_s is the amplitude of distortion in the longitudinal stiffener; b is the local spacing of stiffener, and a is the frame spacing. The terms in the parenthesis are the contributions to the plate distortions in the first and third longitudinal modes. Values for δ_p and δ_s are defined in Table 7. Plate distortion is positive toward the stiffened side of the panel. Thus the Mode 1 component of plate distortion is always positive, whereas the Mode 3 component is alternating. The stiffener distortion is positive toward the stiffened side of the panel, but alternates from frame bay to frame bay.

Separate SubSAS objects are used to create the three components of distortion in the structure. Figure 10 shows the mode 1 and mode 3 components of distortion over the bottom plate of SSTK-A hogging model. In this case Mode 1 distortions are only applied to the central compartment of the model, and the Mode 3 component is applied only to the two central bays of the compartment. These distortions are also applied to the side shell. The sagging models have similar distortions applied to the decks and side shell.

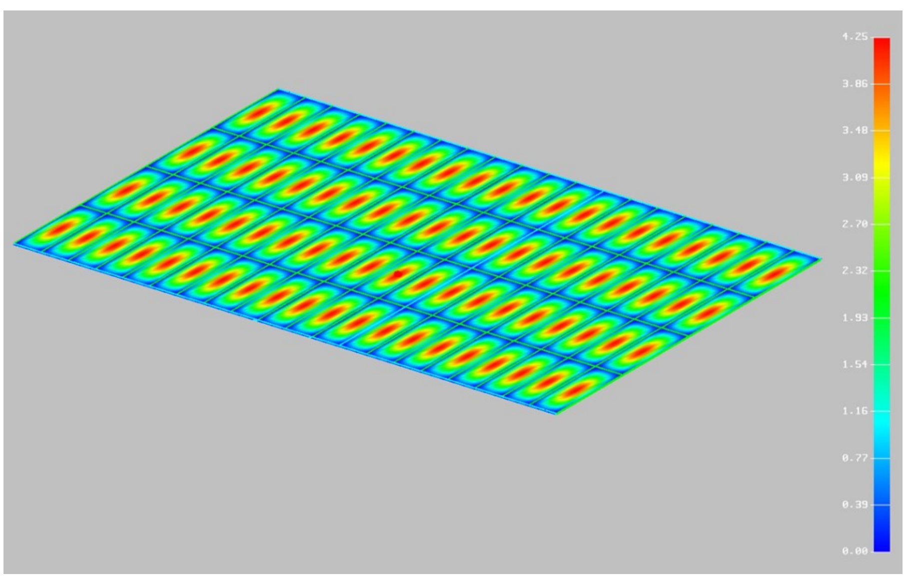

Figure 10: *Mode 1 plating distortion (mm) for bottom plate of SSTK-A.*

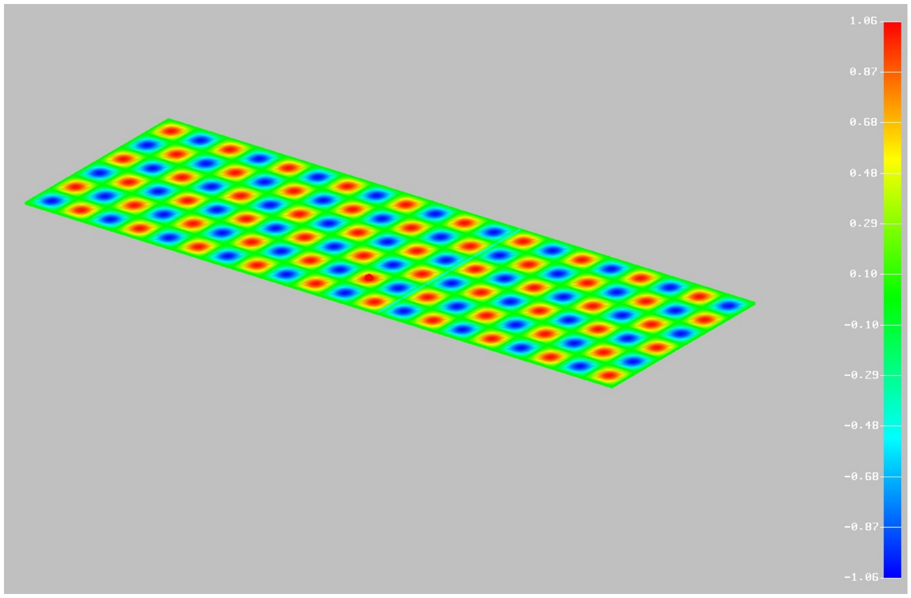

Figure 11: *Mode 3 plating distortion (mm) for bottom plate of SSTK-A.*

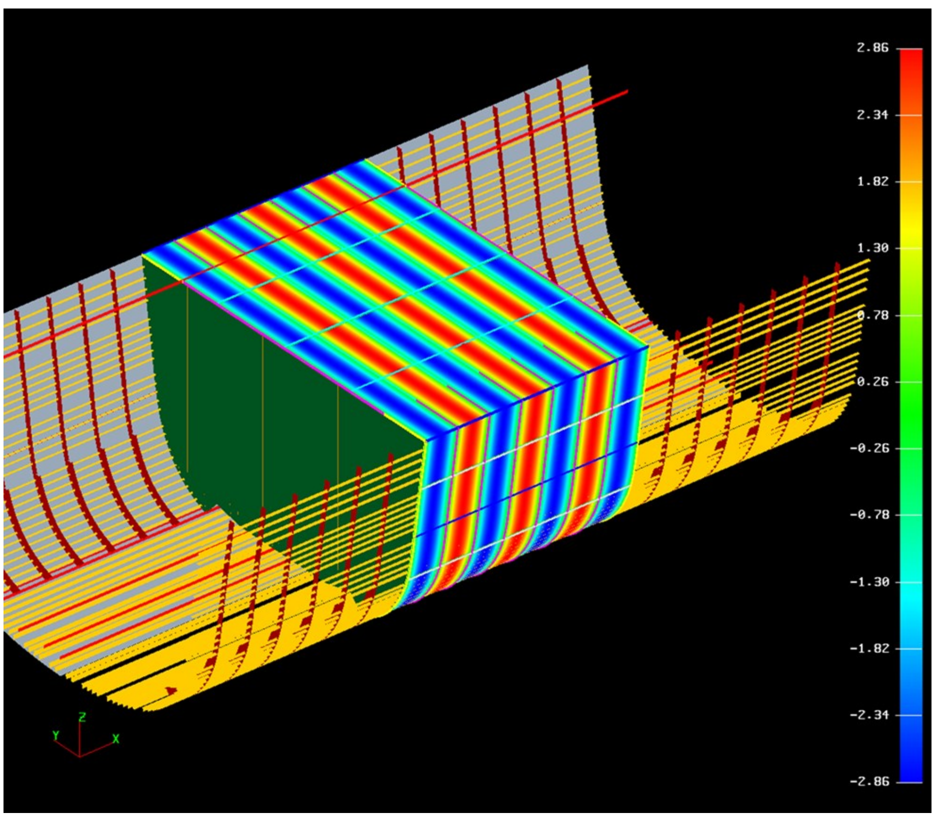

Figure 12: *Stiffener distortion (mm) in the destroyer model*

Residual stresses are accounted for by modifying the constitutive properties of the structural material to produce a response similar to what would occur if residual stresses were present. The stress-strain curve for a plate panel is approximated by considering the resistance in tension and compression averaged over the width of a plate panel. This produces curves like those in Figure 13. The slope of the elastic regimes is slightly different in tension and compression. The trilinear character of the compression curve is the result of early yielding that occurs when a compressive residual stress is present. As the FEA software requires the same properties in tension and compression in a given element, the stress-strain curve for compression is only applied to the elements on the compression side of the girder, and the tension curve is applied to the elements on the tension side.

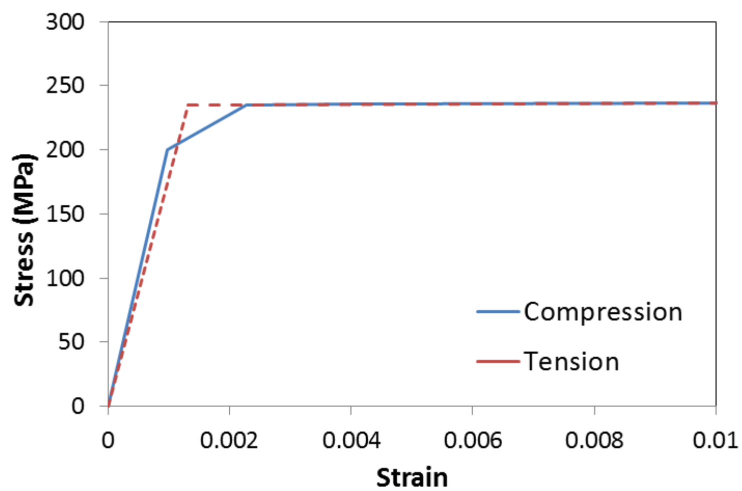

Figure 13: *Constitutive properties used in the SSTK FE models.*

2.2.2.3 Load and solution method

A pure bending moment load is applied to one end of the model, with the other end held fixed. Nodes in the end plane are tied together to a single central master node using multipoint constraints. This allows end nodes to rotate together in a rigid plane when a rotation or moment is applied to the master node. The master node is located approximately at the elastic neutral axis of the section. No other loads (e.g., hydrostatic pressure loads) are applied to the structure. The arrangement of constraint and loading is shown in Figure 14.

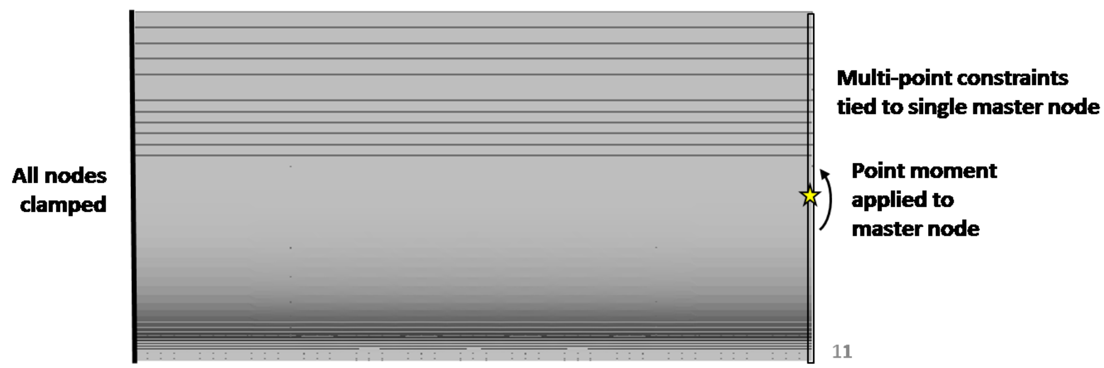

Figure 14: *Load and constraint arrangement.*

A vertical bending moment M is applied to the master node, in a direction of either hogging or sagging. The nonlinear solution algorithm increments fractions of this load in a series of load steps and solves the equations of static equilibrium at each load step. Multiple iterations are required at each load step to converge to the solution. The orthogonal trajectory solution method in the VAST finite element program is used to perform the nonlinear FEA. This method is an arc-length type of solution method that uses a Newton-Raphson formulation of the static equilibrium equations at each load step. The Newton-Raphson equation for any given load step is [5]

$$\boldsymbol{K_T}^{(k-1)} \Delta \boldsymbol{U}^{(k)} = \left(\lambda^{(k-1)} + \Delta\lambda^{(k)}\right)\boldsymbol{R} - (\boldsymbol{f}_{int})^{(k-1)} \tag{5}$$

Where $\boldsymbol{K_T}$ is the tangent stiffness matrix at the current load step, $\Delta\boldsymbol{U}$ is the incremental displacement vector being solved for, $\boldsymbol{R}$ is the reference external load vector, $\boldsymbol{f}_{int}$ is an internal force vector evaluated using the current element stresses, and λ is the load parameter. In this formula (k) indicates the k^{th} iteration within the current load increment. Eqn (5) has two unknowns to solve for: $\Delta\boldsymbol{U}$ and the increment to the load parameter $\Delta\lambda$. The size of the load parameter increment is regulated by the arc-length equation:

$$\left(\boldsymbol{U}^{(k-1)} + \Delta\boldsymbol{U}^{(k)}\right)^T \left(\boldsymbol{U}^{(k-1)} + \Delta\boldsymbol{U}^{(k)}\right) + \gamma\left(\lambda^{(k-1)} + \Delta\lambda^{(k)}\right)^2 = \Delta\ell^2 \tag{6}$$

where $\Delta\ell$ is the arc length, and γ is a scaling factor. Solution of (5) and (6) together gives $\Delta\boldsymbol{U}^{(k)}$ and $\Delta\lambda^{(k)}$. Iterations are performed until the solution converges, i.e.,

$$\frac{\Delta\boldsymbol{U}^{(k)} \cdot \left[\lambda^{(k)}\boldsymbol{R} - (\boldsymbol{f}_{int})^{(k-1)}\right]}{\Delta\boldsymbol{U}^{(1)} \cdot \left[\lambda^{(1)}\boldsymbol{R} - \tilde{\boldsymbol{f}}_{int}\right]} \leq \varepsilon \tag{7}$$

where ε is a user-defined convergence tolerance, and where $\tilde{\boldsymbol{f}}_{int}$ is the interval force vector from the previous load step. To help optimize the number of loads steps and iterations, the orthogonal trajectory method in VAST has a self-adjusting arc length in which the arc-length is updated as,

$$\Delta\ell = \widetilde{\Delta\ell}\left(\frac{N_D}{N}\right)^{\mu},\ \Delta\ell \le \alpha\Delta\ell_0 \tag{8}$$

where N is the number of iterations required to converge the previous load step, N_D is the desired or optimal number of iterations, $\widetilde{\Delta\ell}$ is the arc length from the previous load step, $\Delta\ell_0$ is the arc length in the initial load step, and μ and α are user-defined growth parameters. Table 9 summarizes the solution parameters used for the present work.

Table 9: Nonlinear solution parameters.

ε	0.0025
N_D	5
μ	0.5
α	1.0

With the use of the arc-length relation (8), the calculated incremental load step $\Delta\lambda$ can be positive or negative, allowing solutions to be determined in the pre-collapse and post-collapse region. Although solutions in the post-collapse region have little physical meaning in themselves, it is useful to carry the analysis at least part way into the post-collapse region to ensure that the global maximum load has been reached and to help identify the mode of collapse. When carried sufficiently far into the post-collapse region, the solution of (5) eventually breaks down, usually due to the loss of positive definiteness in the tangent stiffness, $\boldsymbol{K_T}$. The nonlinear FE analyses conducted for the present study were carried out until well into the post-collapse region, or until the solution would no longer converge.

2.2.2.4 Post-processing

With the approach described for applying bending moment loads to finite element models, the bending moment at each load step can be determined directly from the computed values for the applied load $\lambda\boldsymbol{R}$. Thus determining the ultimate strength from the FEA results is straightforward provided a clear peak value can be determined from the computed load parameters.

Ultimate strength results for ship hull girders are often presented in the form of bending moment versus curvature relationships. The use of curvature implicitly assumes beam-like behaviour of the structure under bending. While this fits well with the Smith's method approach, it is less suitable for application to 3D FEA models since curvature cannot be determined unambiguously from the deformations of an FEA model undergoing a combination of global bending, local compression and bending, plasticity and buckling.

Instead, by estimating the difference in the rotations of two cross section positions, it is possible to calculate a pseudo-curvature for the hull structure between the two sections. It is a pseudo-curvature, and not a real curvature, because in a 3D FEA model undergoing pure bending, a plane transverse section does not remain plane due to local deformation effects. Thus rotation of a given section is an approximation to the idealized rotations of beam theory.

The approach developed for this study is to determine pseudo-curvature between two cross sections located at the two transverse frames or bulkheads that are close to and which bracket a significant portion of the collapse region. The rotation of each of these cross sections is determined by using the deformations in the longitudinal direction at the major connection points (e.g., the keel, and deck/shear strake intersections). Figure 15 illustrates the process of determining pseudo-curvature for a case of interframe collapse.

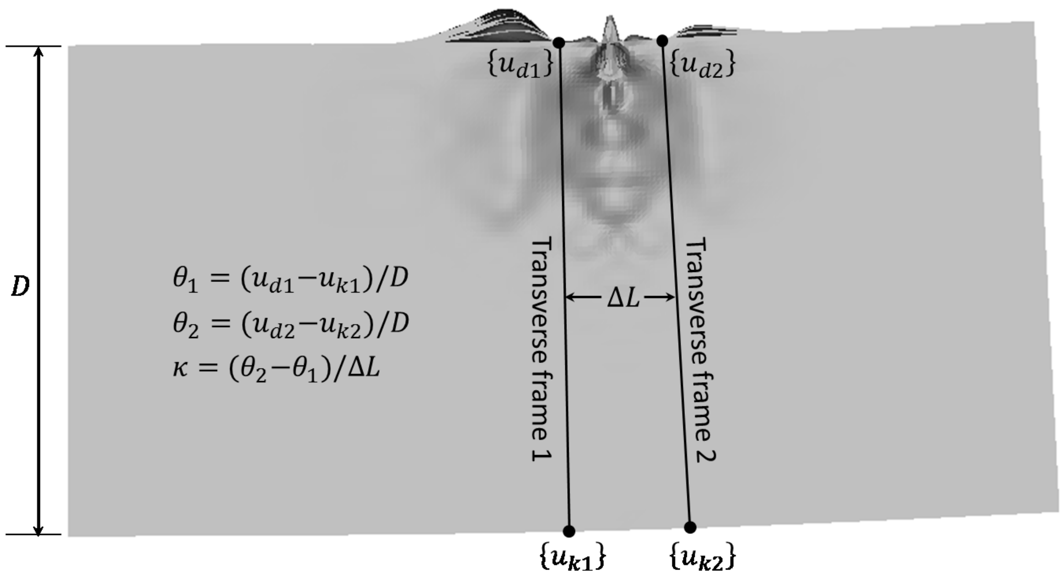

Figure 15: *Determining pseudo-curvature from finite element results.*

3 Results

3.1 SSTK-A results

The ultimate strengths in hogging and sagging for the intact SSTK-A are summarized in Table 10, and the moment versus curvature relationships are shown in Figure 16. A positive vertical bending moment is used for hogging, and a negative moment for sagging. The ULTMAT results are calculated using the two different load-shortening methods: analytical formulas in the Common Structural Rules [1] (IACS), and interpolation from ULTMAT's native database of load-shortening curves [12] (LSC). Also, the single FEA curve shown in Figure 16 was obtained through analysis of separate models for hogging and sagging.

Table 10: *Ultimate strengths in MNm for the intact SSTK-A.*

	Hogging	Sagging
ULTMAT/IACS	456.3	-397.0
ULTMAT/LSC	411.5	-331.1
FEA	465.7	-399.7

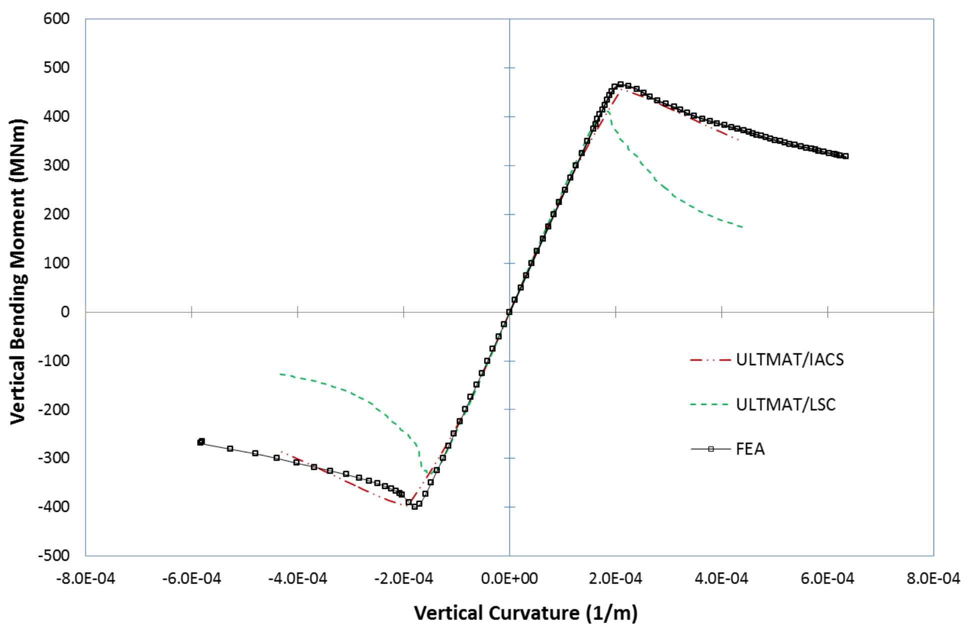

Figure 16: *Moment vs curvature for SSTK-A in the intact condition.*

The ultimate strengths predicted by the two ULTMAT methods differ widely in both hogging and sagging. ULTMAT/IACS is within 2% of the FEA ultimate strengths in both hogging and sagging, while the ULTMAT/LSC approach predicts strengths that are 12% to 17% lower than the FEA results. The ULTMAT/IACS and nonlinear FEA moment-curvature relationships in Figure 16 are in close agreement over the entire range of loading. The discrepancy between these results and ULTMAT/LSC is discussed in Section 4.

The deformations predicted by nonlinear FEA are shown in Figure 17 at the ultimate bending moment. At ultimate strength, the maximum deformation is at the loaded end of the model, and the collapse mode is indistinct with both plating and beam-column deformations developing in the two central bays on the bottom and in sides.

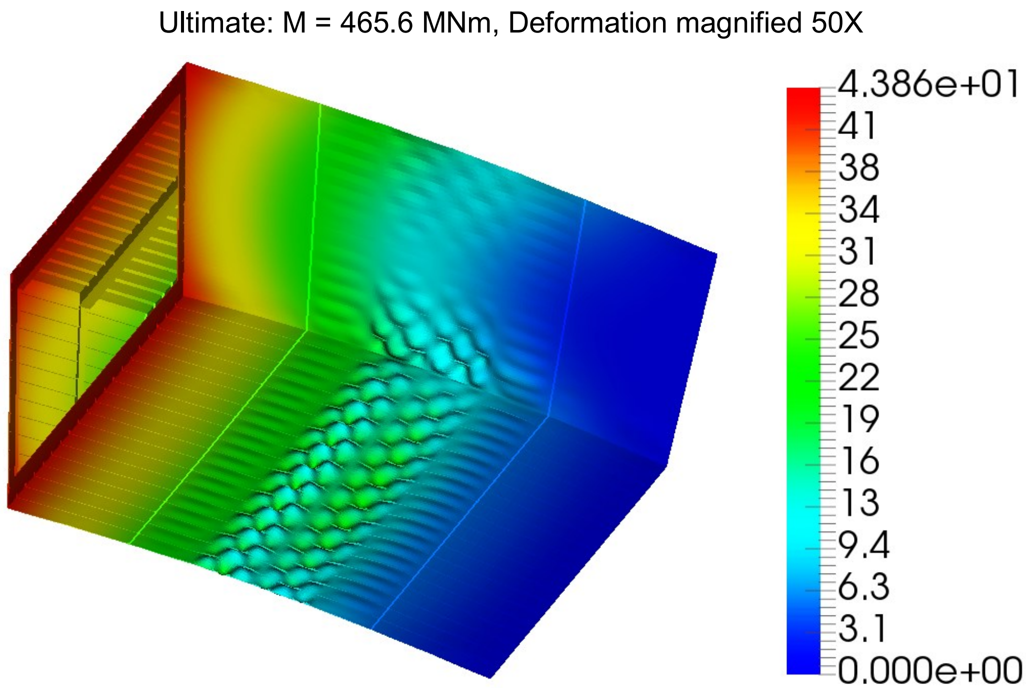

Figure 17: *Total deformation in mm for the intact SSTK-A in hogging at the ultimate moment.*

In the post-collapse region (Figure 18), the maximum deformation has moved to the region of collapse, and the mode can be more clearly identified as an interframe collapse towards the stiffeners that extends across the whole width of the bottom and into the side structure.

A close-up view of the collapse shape is shown in Figure 19, as seen from the inside of the girder. The longitudinals in the bottom and sides are collapsing inward in a beam-column mode. The bottom plate is buckled inward and outward in an alternating shape which precipitates some localized deformation of the longitudinal webs. The side plating buckles primarily inward with the stiffeners, and the alternating pattern is not evident. The structure in the neighboring frame bays deforms outward, creating an alternating deformation pattern across three bays and causing the heavy transverse frames to rotate away from the collapse region. This deformation pattern is consistent with the initial imperfections assumed for this structure. The deformations and collapse shapes in the intact sagging model are very similar to the hogging model, and are shown in Figure C.1 and Figure C.2 in Annex C.

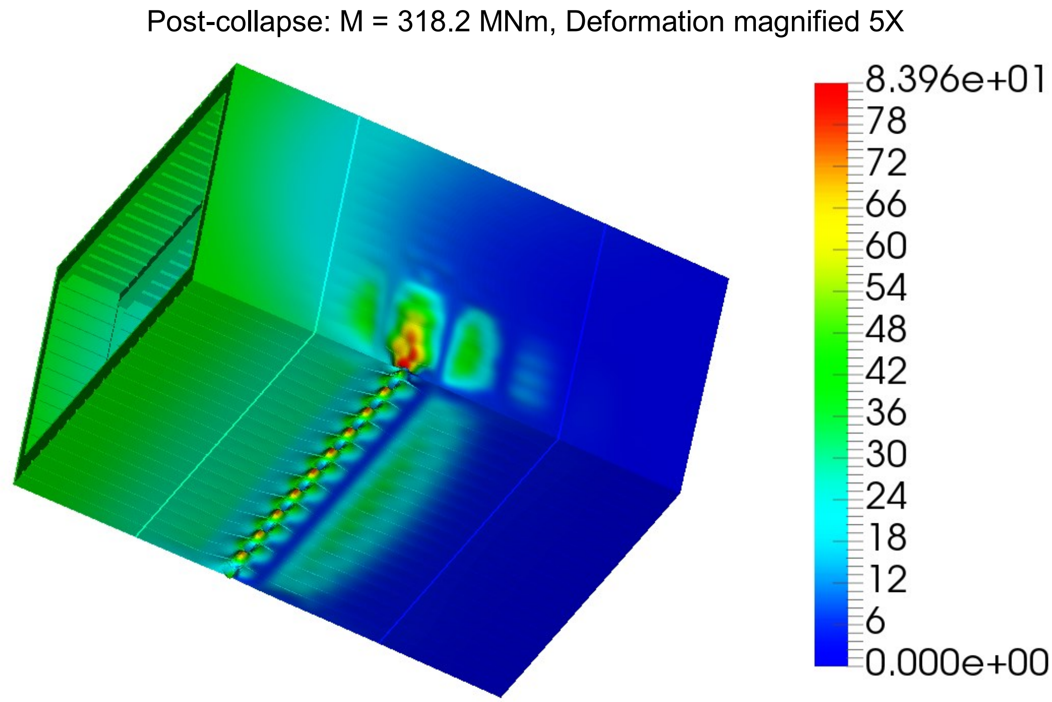

Figure 18: *Total deformation in mm for the intact SSTK-A in hogging during post-collapse.*

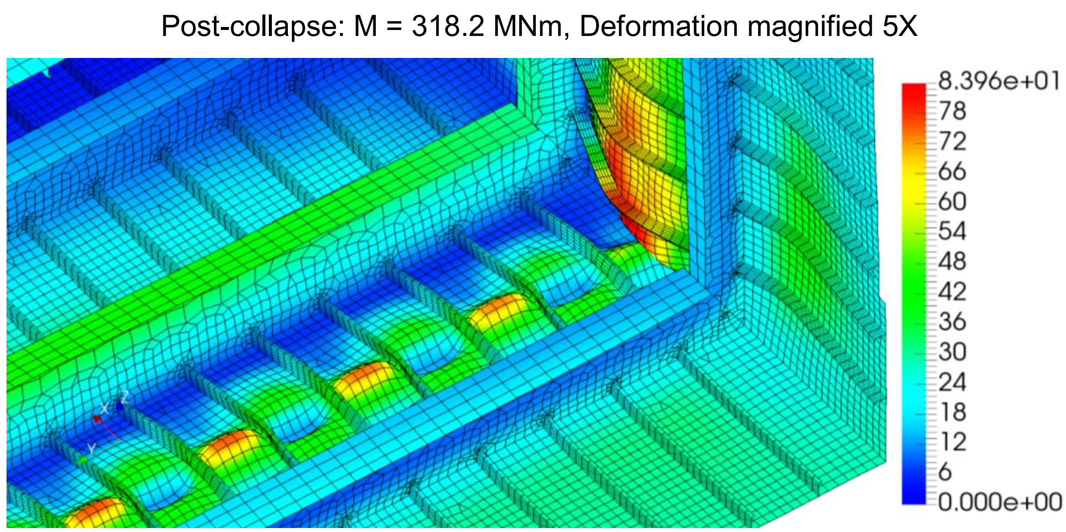

Figure 19: *Close-up view of deformation (total deformation in mm) for SSTK-A in hogging.*

The ultimate strengths for SSTK-A with collision damage are summarized in Table 11. ULTMAT results are presented in Figure 20 as interaction curves with the FEA ultimate strengths in hogging and sagging appearing as single points on the vertical axis. The interaction curves are asymmetric due to the asymmetry in the damage. The dashed lines in this figure are the paths followed by Smith's method using a curvature-controlled incrementing method, showing that the bending moment develops a significant horizontal component due to the asymmetry. Thus the curvature-controlled method does not give an accurate picture of the true ultimate strength under vertical bending moment, which is obtained from the intersections of the interaction curves with the vertical axis. In hogging, the ULTMAT/IACS ultimate strength is within 2.2% of the FEA, while the ULTMAT/LSC prediction is 7.5% lower than the FEA. In sagging the discrepancies are much larger: 34% and 62% for ULTMAT/IACS and ULTMAT/LSC predictions, respectively.

Table 11: *Ultimate strengths in MNm for the SSTK-A with collision damage.*

	Hogging	Sagging
ULTMAT/IACS	408.5	-305.0
ULTMAT/LSC	369.7	-252.9
FEA	399.8	-188.3

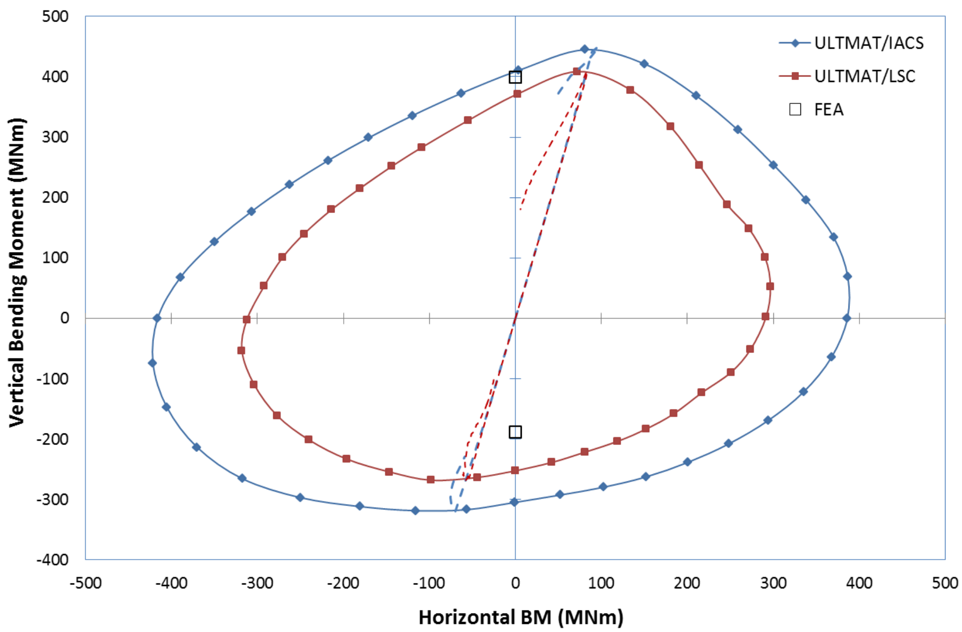

Figure 20: *Interaction curves for SSTK-A with the collision damage.*

The deformed shapes for the nonlinear FEA models are shown in Figure 21 for the hogging case and in Figure 22 for the sagging case. The deformations at the ultimate bending moment in the hogging case are similar to the intact case except deformations are asymmetrically distributed in a manner equivalent to the structure bending about a rotated neutral axis. This is carried through to the post-collapse region, where the buckling of the structure is more pronounced on the side of hull opposite the damaged area. Since the bottom structure is intact it collapses in an interframe collapse mode similar to the intact model.

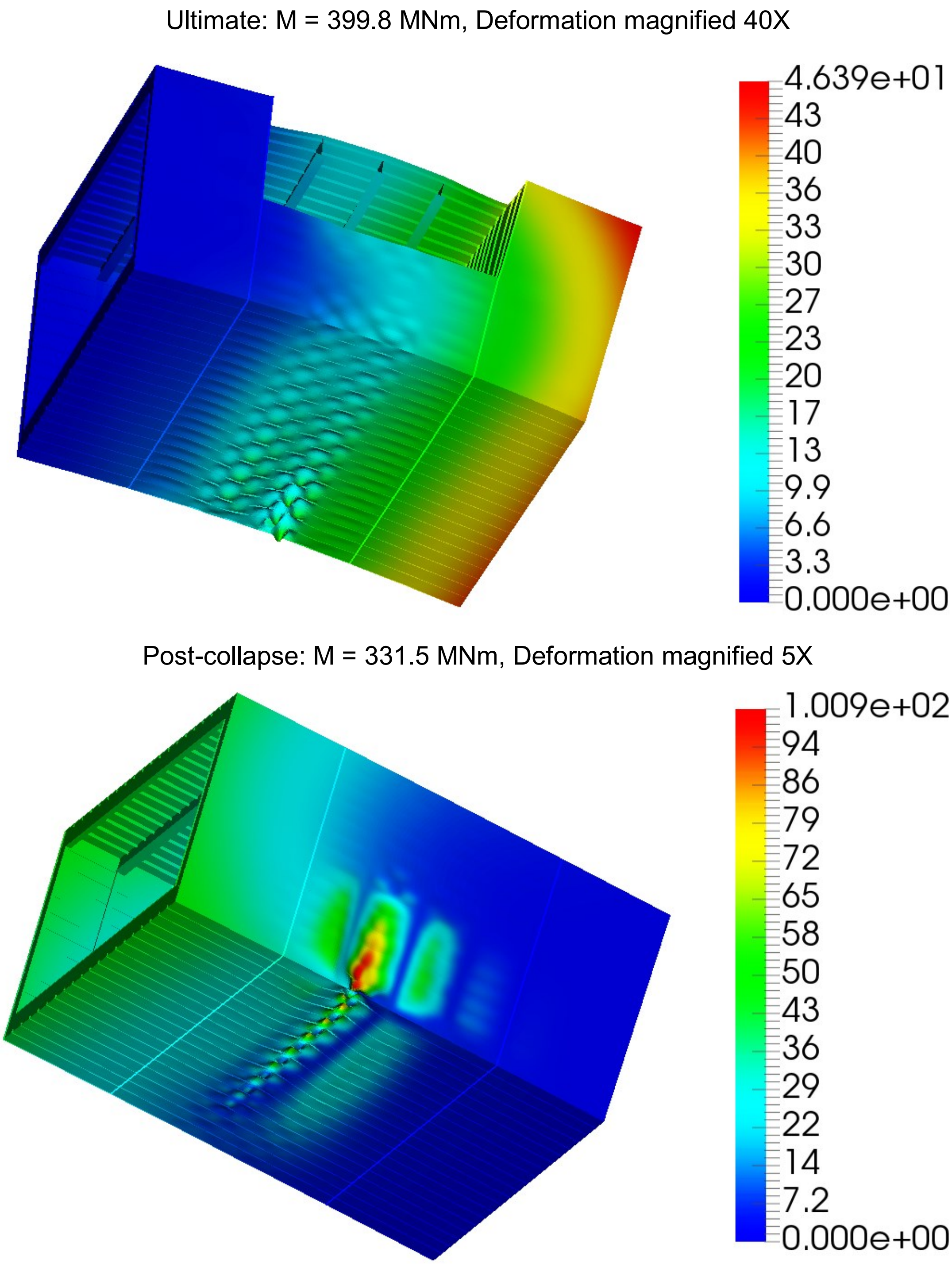

Figure 21: *Total deformation in mm for SSTK-A with collision damage in hogging: at ultimate bending moment (top); in post-collapse (bottom).*

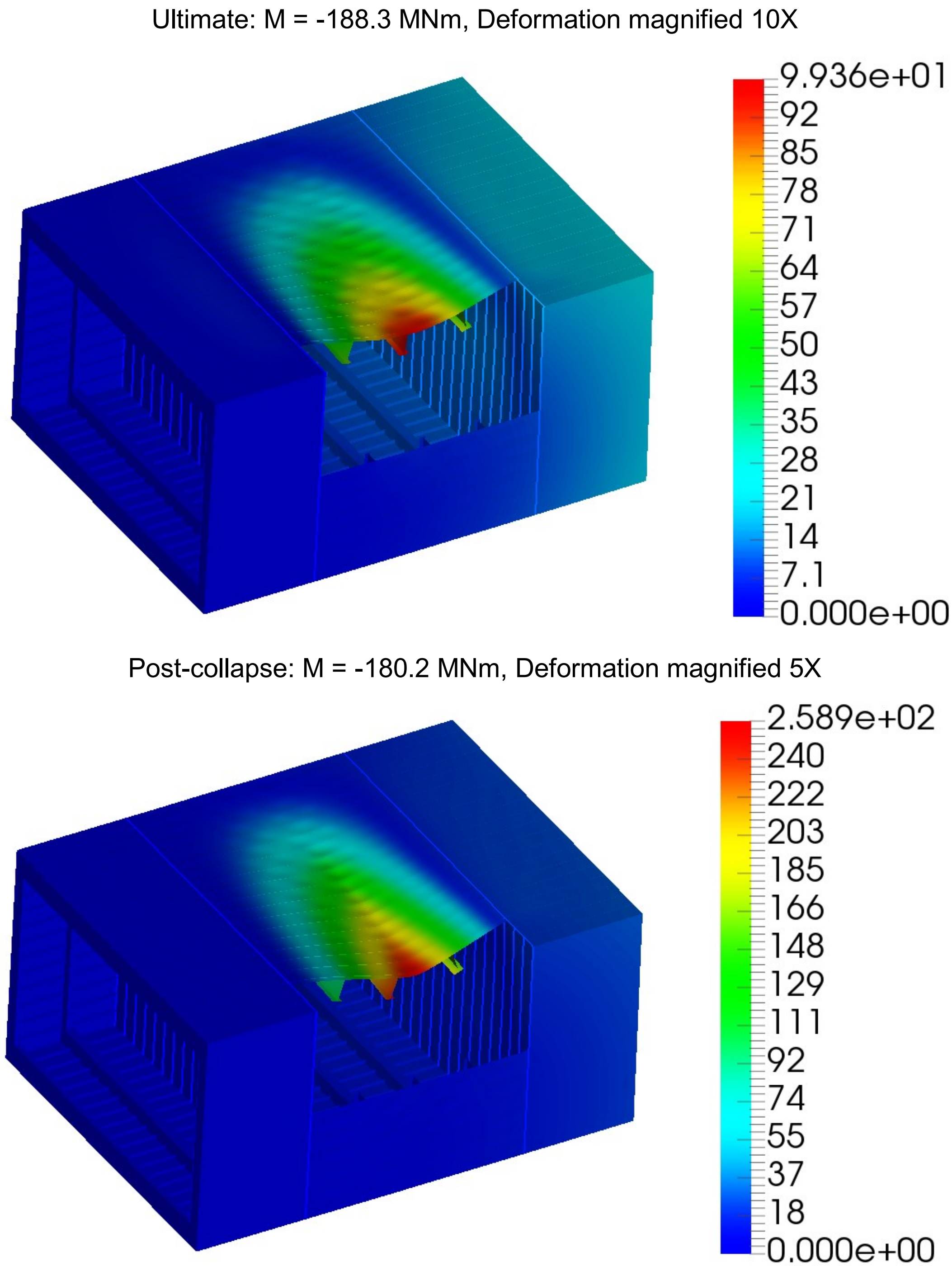

Figure 22: *Total deformation in mm for SSTK-A with collision damage in sagging: at ultimate bending moment (top); in post-collapse (bottom).*

The results for the sagging case show an overall mode of collapse in the damaged deck structure, with the plating, longitudinals and transverse frames collapsing together. This is accompanied by a more than 50% loss in strength compared with the intact case. Since Smith's method always predicts interframe collapse, good agreement between FEA and ULTMAT cannot be expected in this case and as noted ULTMAT predicts much higher sagging strength than does FEA.

The ultimate strengths for SSTK-A with grounding damage are summarized in Table 12. ULTMAT results are presented in Figure 20 as interaction curves with the FEA ultimate strengths in hogging and sagging included as single points on the vertical axis. The ultimate strengths predicted with nonlinear FEA agree with ULTMAT/IACS predictions within 2% in both hogging and sagging. Predictions with ULTMAT/LSC are lower than FEA by 12% in hogging, and by 18% in sagging.

Table 12: *Ultimate strengths in MNm for the SSTK-A with grounding damage.*

	Hogging	Sagging
ULTMAT/IACS	310.3	-363.9
ULTMAT/LSC	270.4	-303.2
FEA	307.4	-370.1

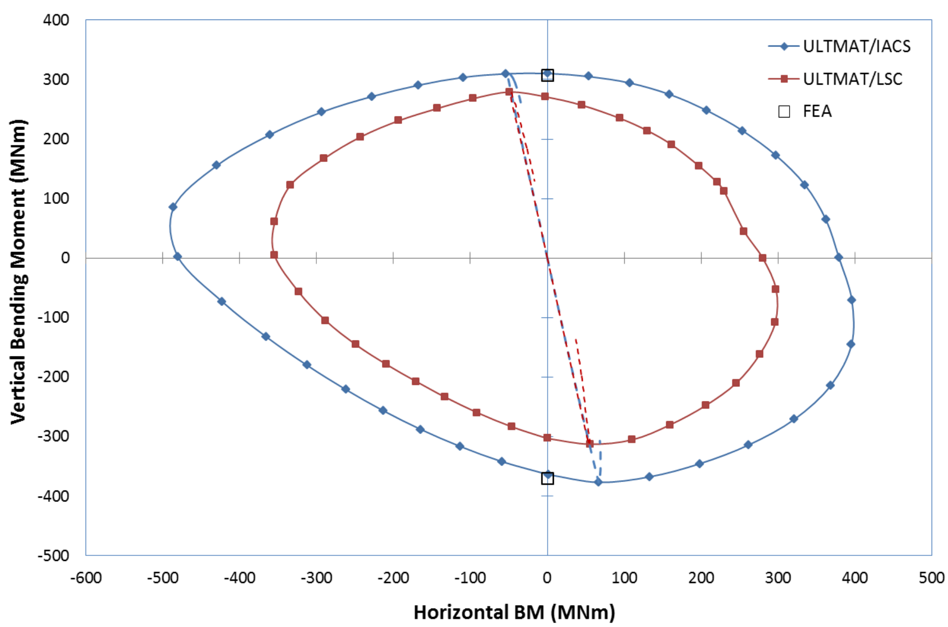

Figure 23: *Interaction curves for SSTK-A with the grounding damage.*

The deformations predicted by nonlinear FEA for the grounding damage case are shown in Figure 24 for hogging. At ultimate bending moment, an overall collapse mode is developing across the damaged bottom of the structure, with interframe collapse in the bottom and in the lower side shell on the opposite side of the damage area. In the post-collapse region, the overall collapse mode did not fully develop, and the damaged hull bottom and lower side shell has primarily failed in an interframe mode.

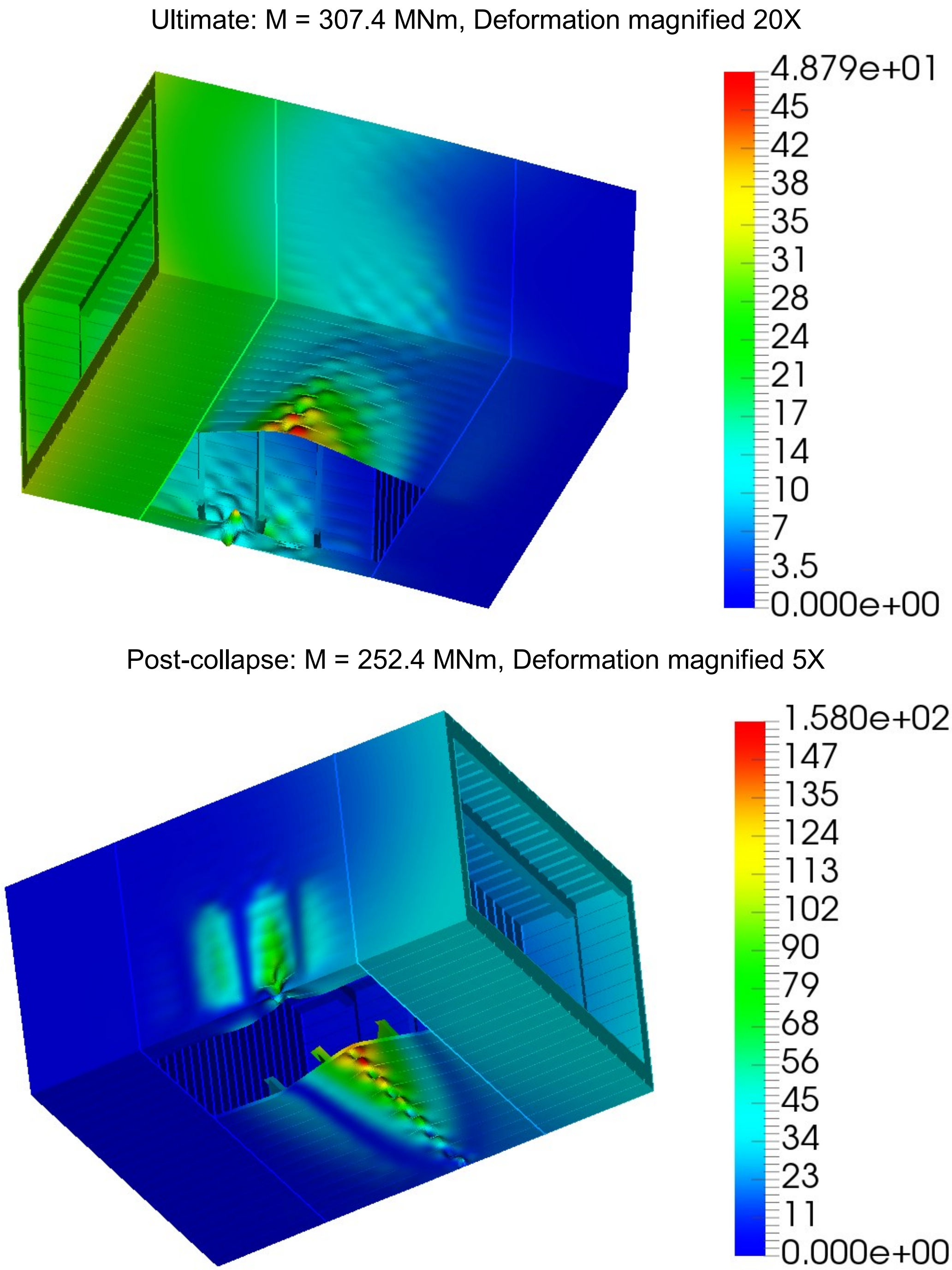

Figure 24: *Total deformation in mm for SSTK-A with grounding damage in hogging: at ultimate bending moment (top); in post-collapse (bottom).*

In the sagging case, shown in Figure 25, the deformations develop in an interframe collapse mode similar to the intact case. That the agreement between the FEA and ULTMAT/IACS predictions is very close in hogging and sagging may be attributed to the interframe mode of collapse.

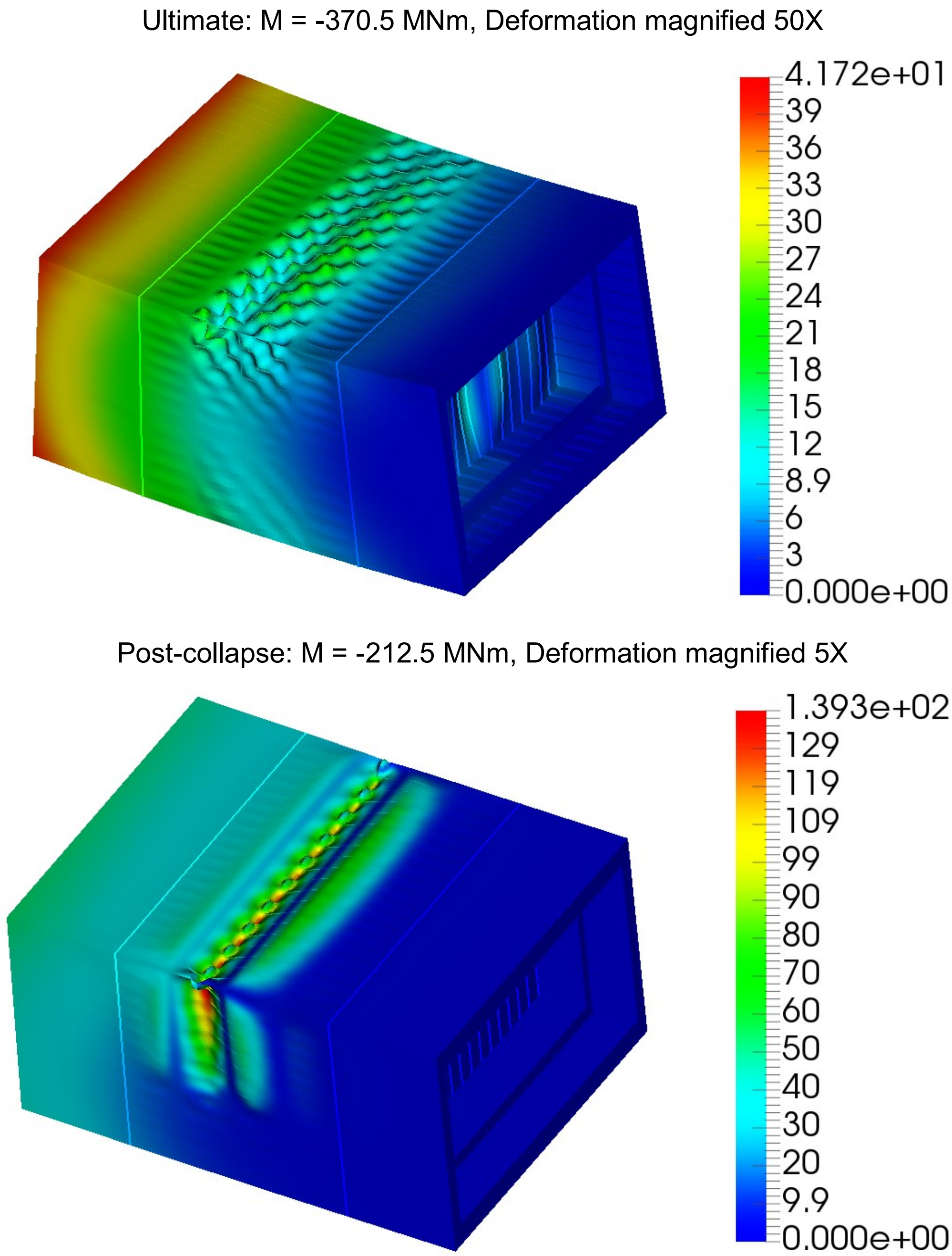

Figure 25: *Total deformation in mm for SSTK-A with grounding damage in sagging: at ultimate bending moment (top); in post-collapse (bottom).*

3.2 SSTK-C results

The ultimate strengths in hogging and sagging for the intact SSTK-C models are summarized in Table 13, and the moment versus curvature relationships are shown in Figure 26. Close agreement is obtained between the FEA and ULTMAT/IACS ultimate strength values, with less than 1% difference in hogging and sagging. The differences between ULTMAT/LSC and FEA are about 13% in hogging and 16% in sagging. Figure 26 shows that the moment-curvature relationships for the FEA and ULTMAT/IACS do not agree very well in the post-collapse regime, although the peak values are close.

Table 13: *Ultimate strengths in MNm for the intact SSTK-C.*

	Hogging	Sagging
ULTMAT/IACS	194.8	-251.9
ULTMAT/LSC	171.1	-212.2
FEA	196.0	-253.1

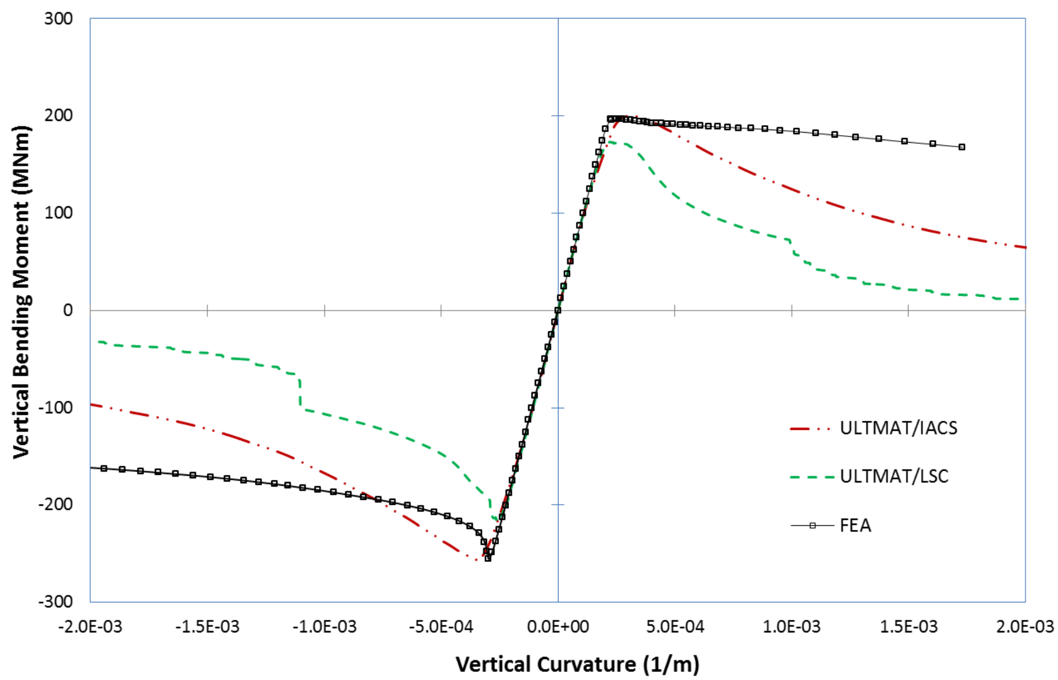

Figure 26: *Moment vs curvature for SSTK-C in the intact condition.*

The deformations predicted by the nonlinear FEA are shown in Figure 27 for the hogging case, where it can be seen that interframe beam-column collapse occurs in the hull bottom structure. Figure D.1 in Annex D shows the deformations in the sagging case where it can be seen that the mode of failure in the sagging case is very similar to the sagging failure of SSTK-A.

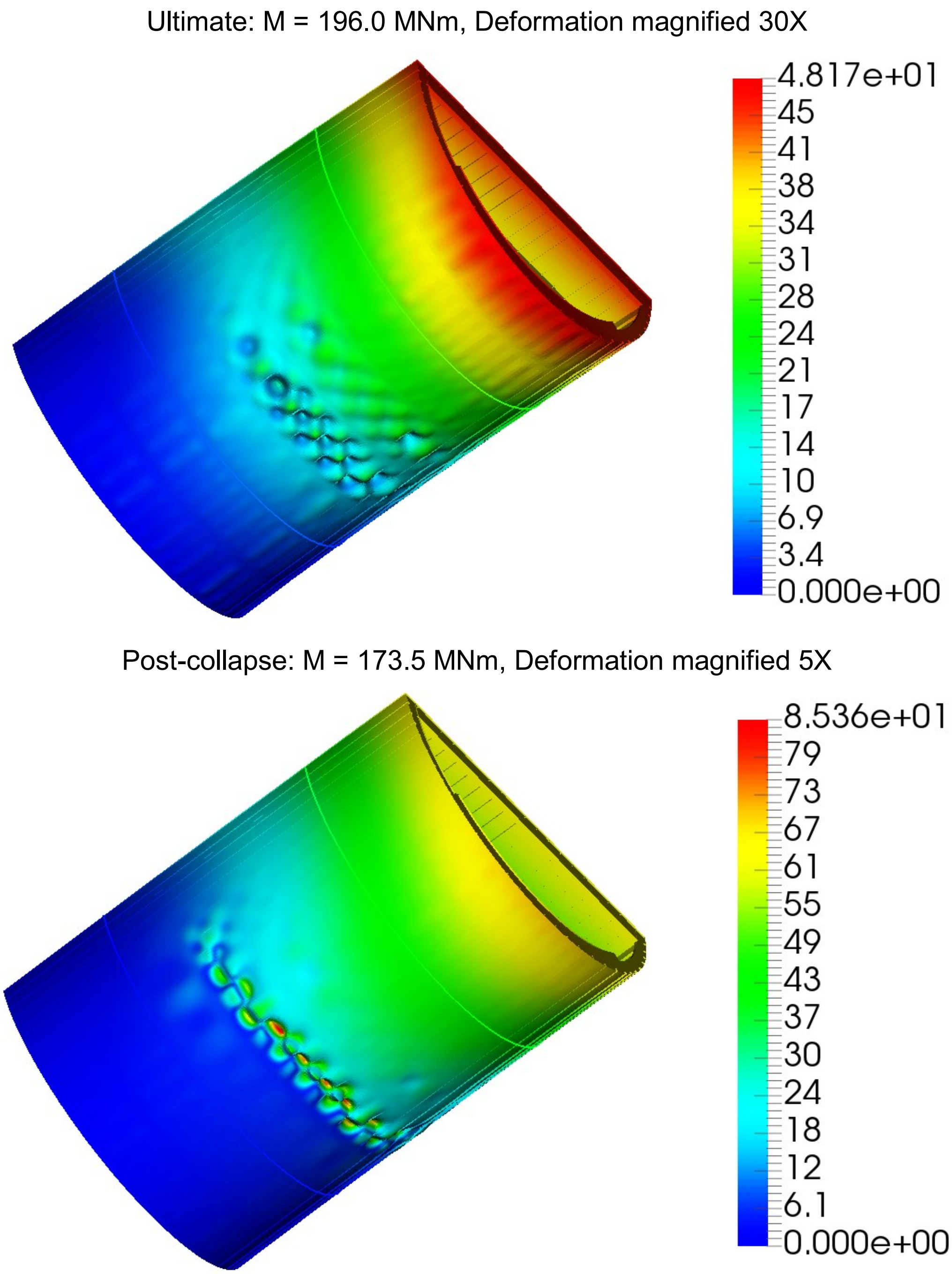

Figure 27: *Total deformation in mm for the intact SSTK-C in hogging: at ultimate bending moment (top); in post-collapse (bottom).*

The ultimate strengths in hogging and sagging for SSTK-C with collision damage are summarized in Table 14, and results in the form of interaction curves are shown in Figure 28. As with SSTK-A, the distribution damage results in asymmetric interaction curves. In hogging, the ultimate strengths predicted by FEA and ULTMAT/IACS agree to within 5%, while ULTMAT/LSC is about 16% lower than FEA. Curiously, the hogging strength is slightly larger than in the intact condition, although the difference is less than the convergence tolerance and therefore probably not significant. In sagging, ULTMAT/LSC and ULTMAT/IACS predictions are 10% and 32% higher than the FEA result, respectively.

Table 14: *Ultimate strengths in MNm for SSTK-C with collision damage.*

	Hogging	Sagging
ULTMAT/IACS	187.2	-182.0
ULTMAT/LSC	165.4	-151.1
FEA	196.3	-137.6

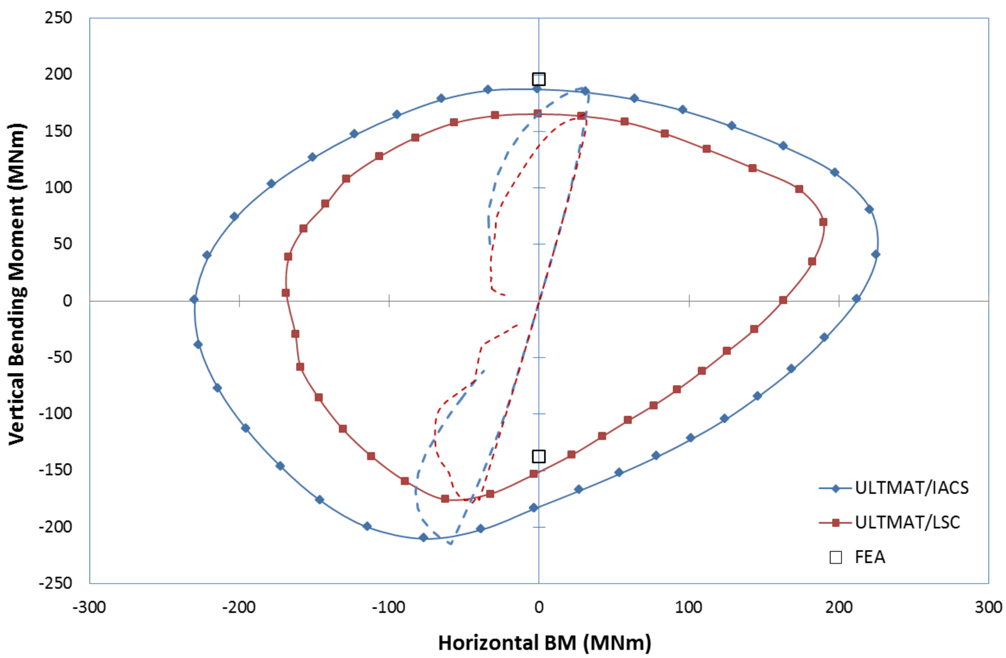

Figure 28: *Ultimate strength interaction curves for SSTK-C with collision damage.*

The deformations predicted by FEA in the hogging case are shown in Figure 29 and Figure 30, indicating that the failure mode is interframe beam-column collapse occurring in the same frame bay as in the intact case. The detailed view in Figure 30 clearly shows beam-column collapse taking place in concert with a higher-order buckling mode in the plate and local buckling of the longitudinal webs.

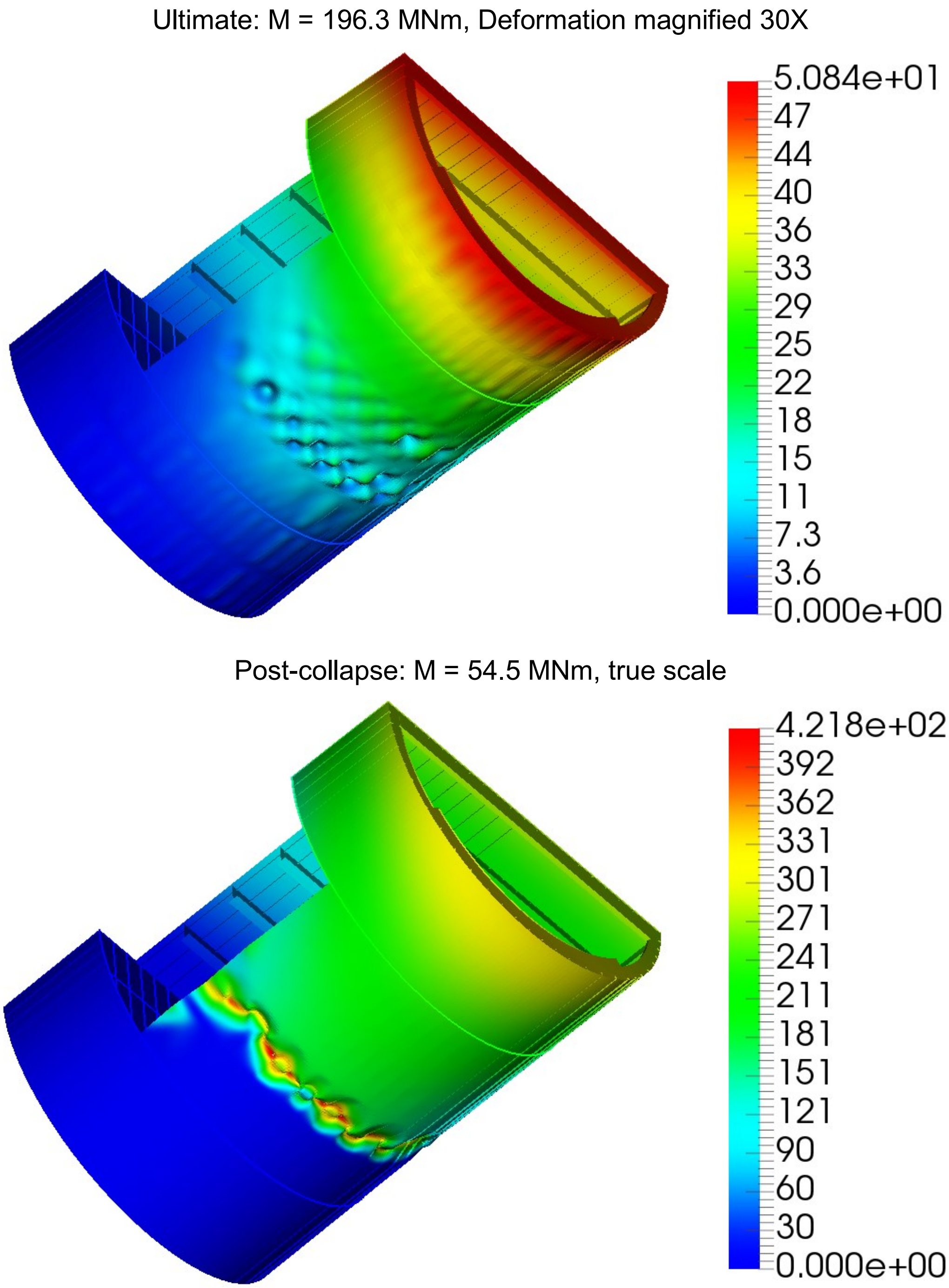

Figure 29: *Total deformation in mm for the SSTK-C with collision damage in hogging: at ultimate bending moment (top); in post-collapse (bottom).*

Post-collapse: M = 54.5 MNm, true scale

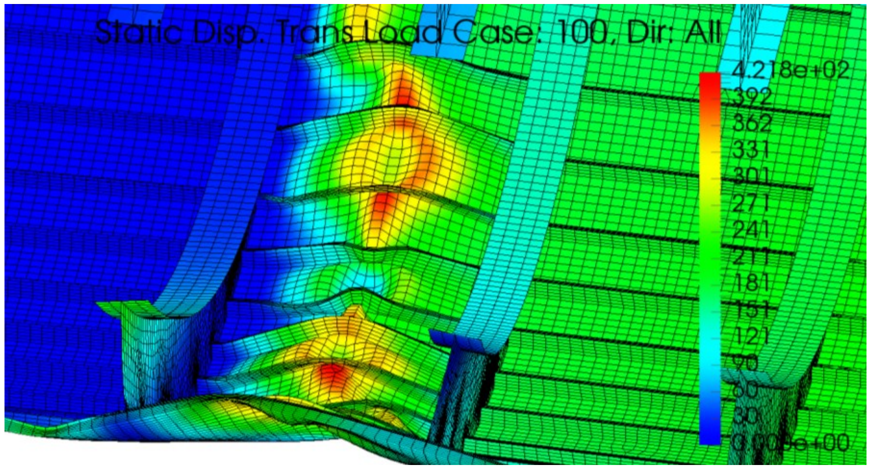

Figure 30: *Detail view of post-collapse deformation (in mm) of SSTK-C with collision damage in hogging condition.*

The deformations predicted by FEA in the sagging case are shown in Figure 31, indicating that the failure mode is overall collapse of the damaged deck, similar to the overall collapse of the collision damage case for SSTK-A. Thus it might be expected that Smith's method can accurately predict the hogging strength, but not the sagging strength.

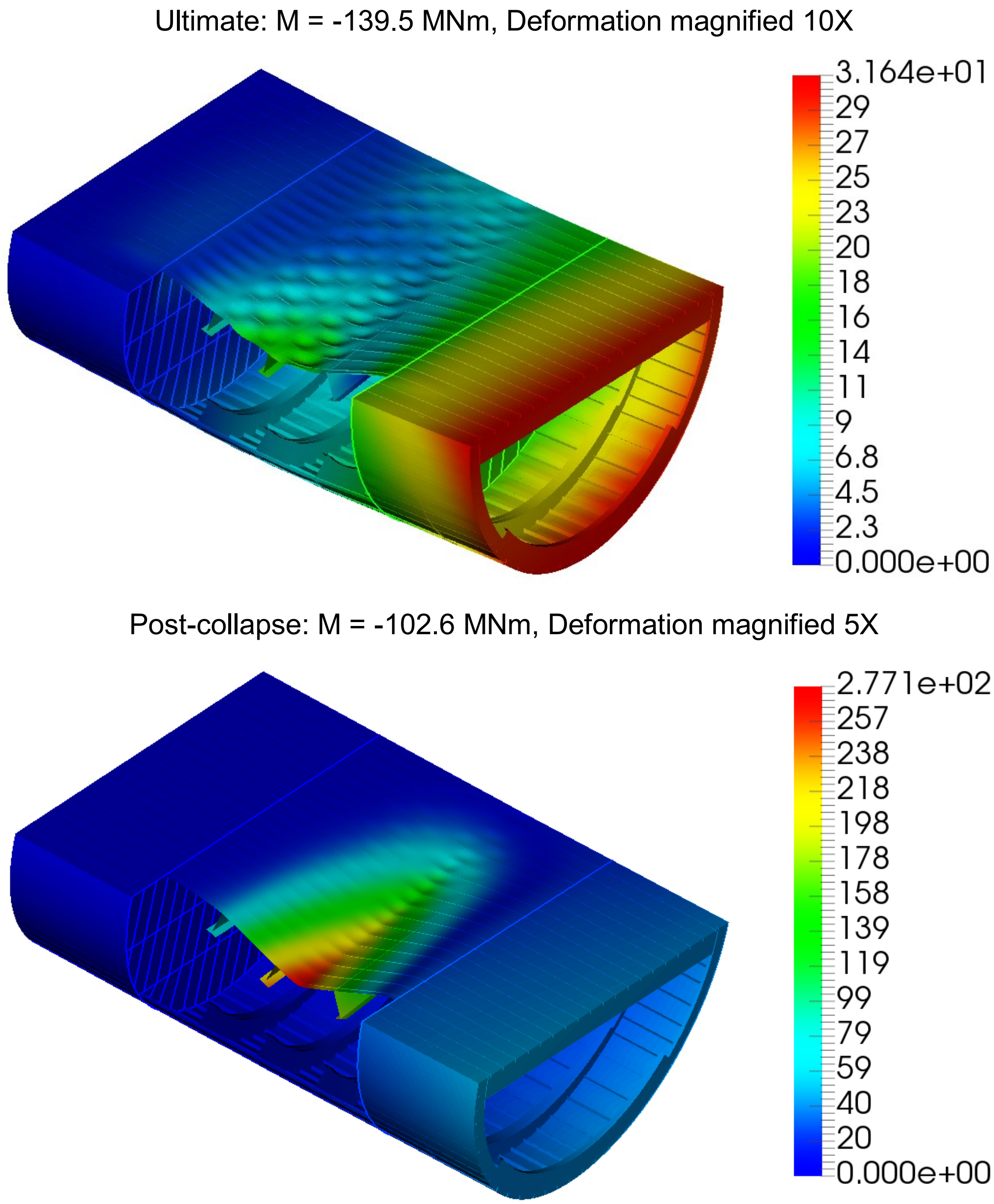

Figure 31: *Total deformation in mm for the SSTK-C with collision damage in sagging: at ultimate bending moment (top); in post-collapse (bottom).*

The ultimate strengths in hogging and sagging for SSTK-C with grounding damage are summarized in Table 15. The ULTMAT/IACS and ULTMAT/LSC agree with the FEA hogging strength prediction to within 31% and 14%, respectively; whereas their agreement with the FEA sagging prediction is within 3% and 14%, respectively. Since the bottom damage is symmetric in this case, a curvature-controlled analysis is adequate, with the resulting moment-curvature relationships given in Figure 32. The FEA calculation in hogging does not reach a peak value, which accounts for why ULTMAT's predicted strength in hogging is so much higher. The FEA moment-curvature in sagging agrees reasonably well with the ULTMAT/IACS curve in the pre-collapse and well into the post-collapse region.

Table 15: *Ultimate strengths in MNm for SSTK-C with grounding damage.*

	Hogging	Sagging
ULTMAT/IACS	115.4	-194.8
ULTMAT/LSC	100.6	-174.1
FEA	88.0	-201.7

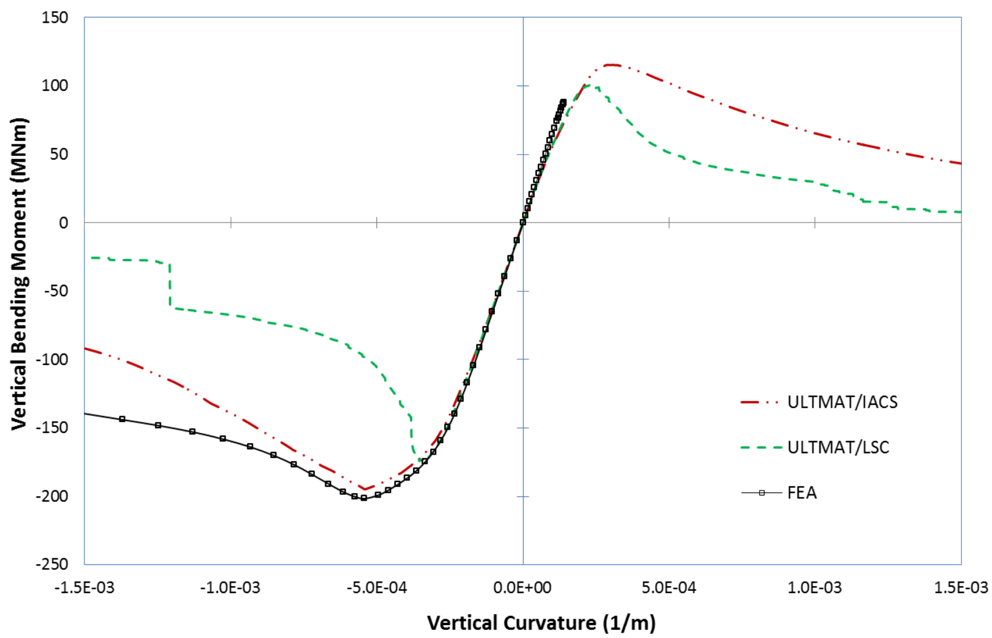

Figure 32: *Moment versus curvature for SSTK-C with grounding damage.*

The deformations predicted by nonlinear FEA are shown in Figure 33 for the hogging case showing large deflections developing at the free edge of plating. The FEA calculation was unable to find convergent solutions at curvatures greater than 1.4×10^{-4} m^{-1} as indicated in Figure 32 due to buckling instabilities arising from these large edge deflections. A pitfall of the nonlinear FE method is that the solution method is often unable to iterate beyond a localized buckling event to get to the ultimate collapse event of interest, and this may be an issue for its future application to analysis of gross damage.

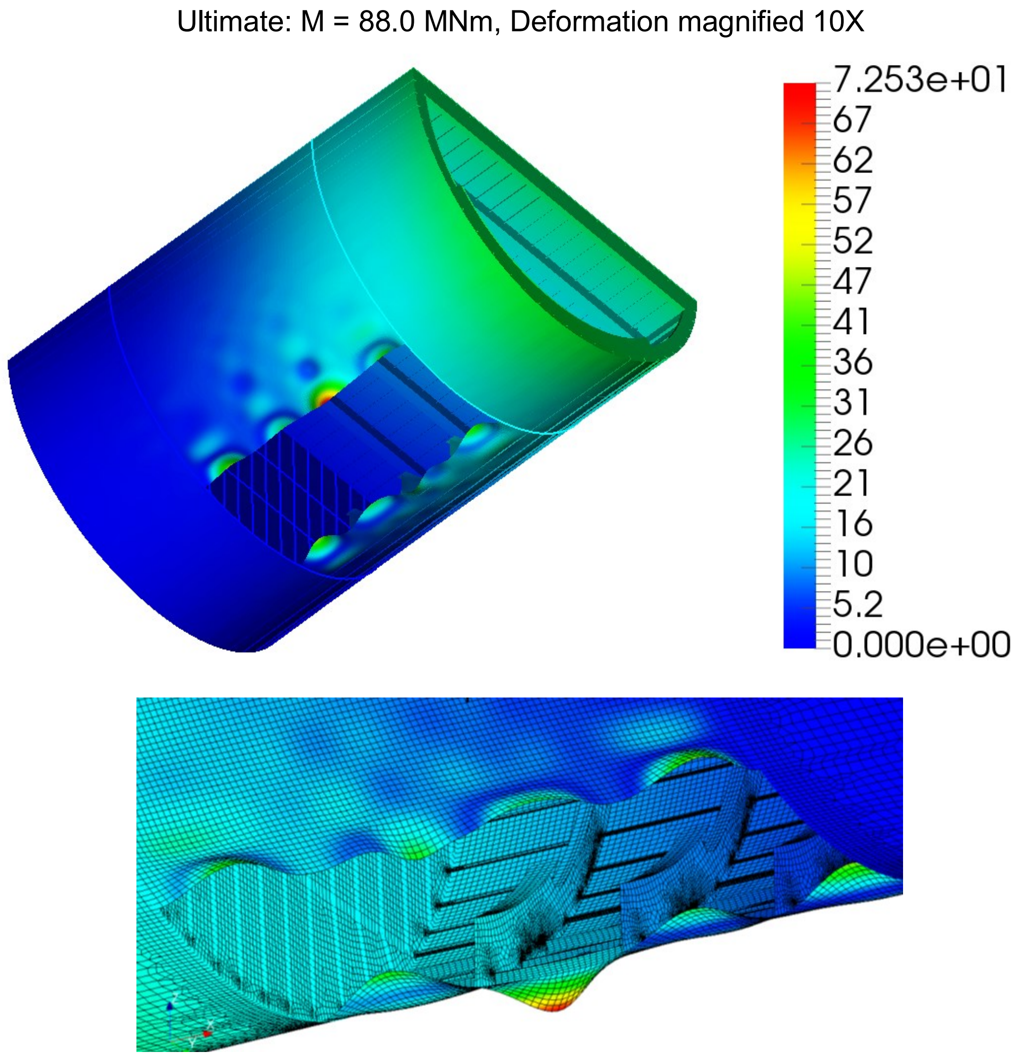

Figure 33: *Total deformation in mm for the SSTK-C with grounding damage in hogging: at ultimate bending moment (top); detail of deformation at edge of damaged area (bottom).*

Because of this difficulty, the breadth of the damage region was increased from 5 m to 6.2 m so as to eliminate most of the free edge of plating that was causing the convergence problems. The cross sectional area for this modified damage case is 0.412 and the ratio to the intact cross sectional area is 0.817, compared with 0.847 with a 5 m wide damage zone. The results for this modified grounding case are summarized in Table 16 and the moment-curvature relationships given in Figure 34. The FEA results now have a clear peak value and post-collapse region. Both the ultimate strength and the moment-curvature relationships agree fairly well with ULTMAT/IACS, while ULTMAT/LSC predicts strengths that are more than 10% lower than the FEA predictions.

Table 16: *Ultimate strengths in MNm for SSTK-C for the modified grounding damage case.*

	Hogging	Sagging
ULTMAT/IACS	102.3	-179.7
ULTMAT/LSC	88.4	-162.4
FEA	100.0	-188.4

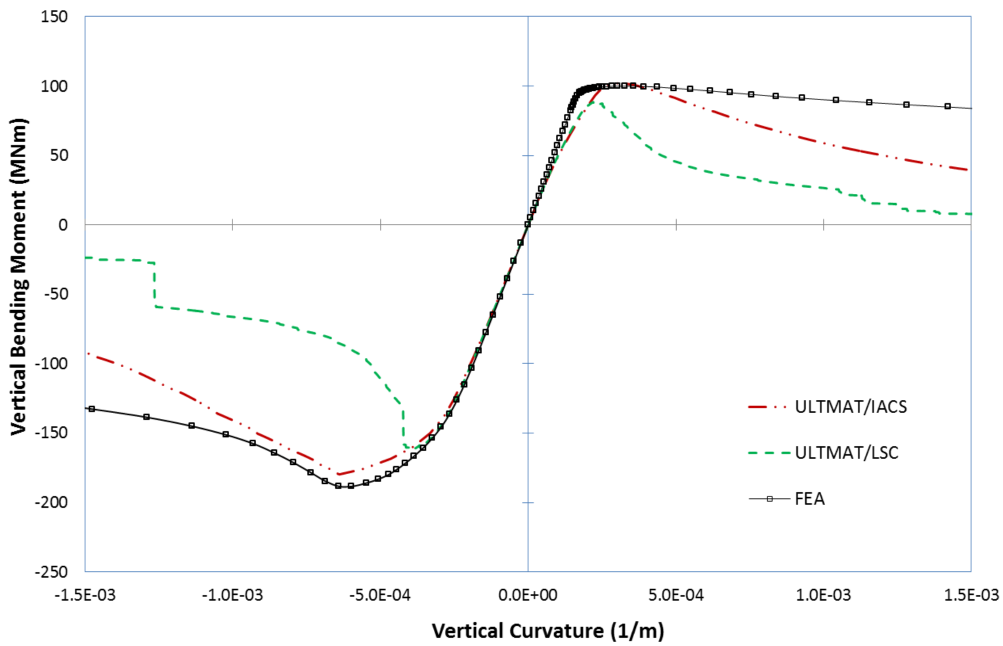

Figure 34: *Moment versus curvature for SSTK-C for the modified grounding damage case.*

The increase in the damage region results in a 3.5% reduction in cross section area. This results in more than 10% drop in the hogging strength (based on the ULTMAT results), and a 7% drop in the sagging strength (ULTMAT and FEA results).

The deformations predicted by nonlinear FEA in the sagging case are shown in Figure 36. This shows the mode of failure to be interframe beam-column collapse, occurring at the same position on the deck as in the intact case (Figure D.1). Thus the close agreement between ULTMAT/IACS and FEA is consistent with that previously seen in the intact case.

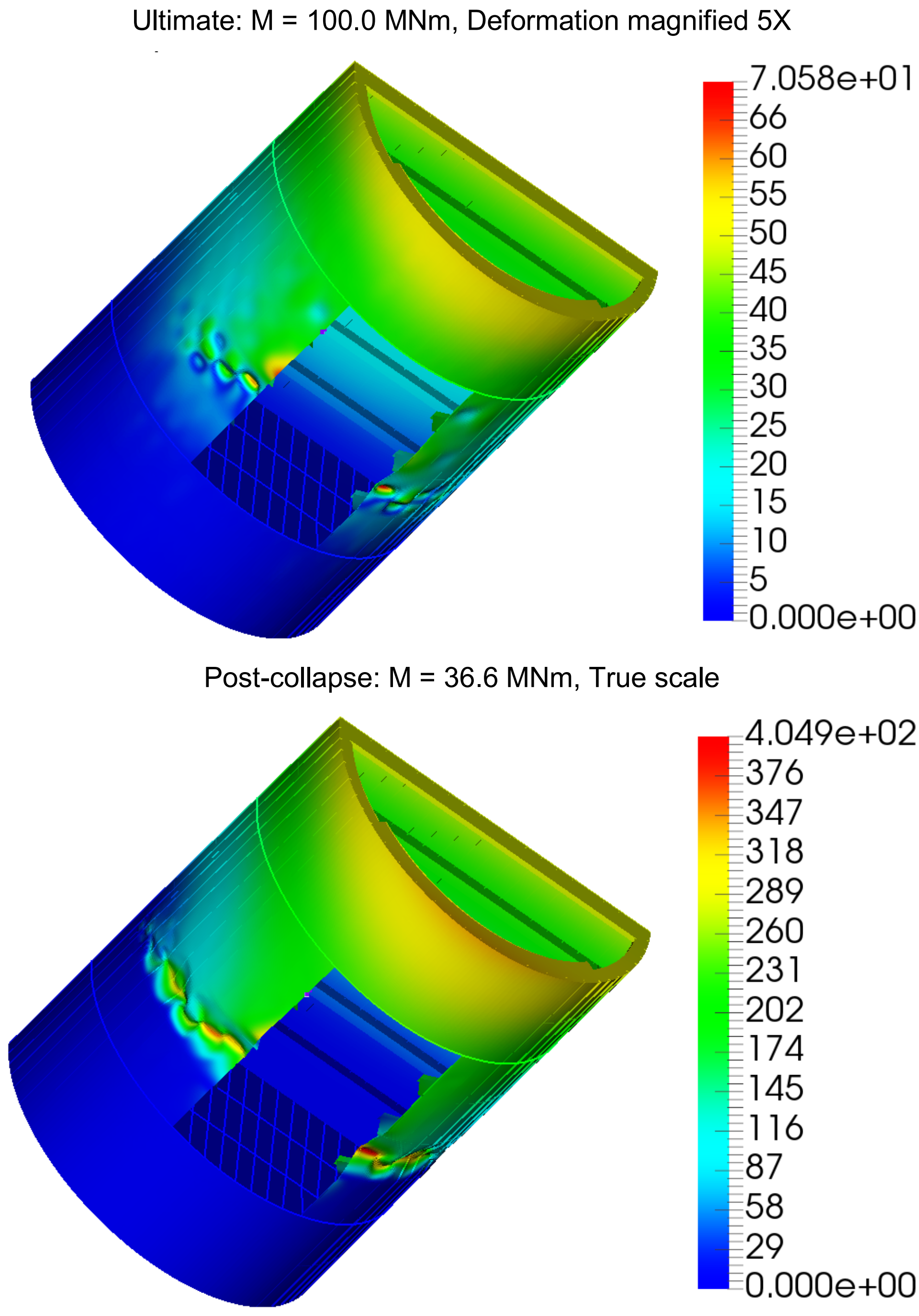

Figure 35: *Total deformation in mm for the SSTK-C in the modified grounding damage case in hogging: at ultimate bending moment (top); in post-collapse (bottom).*

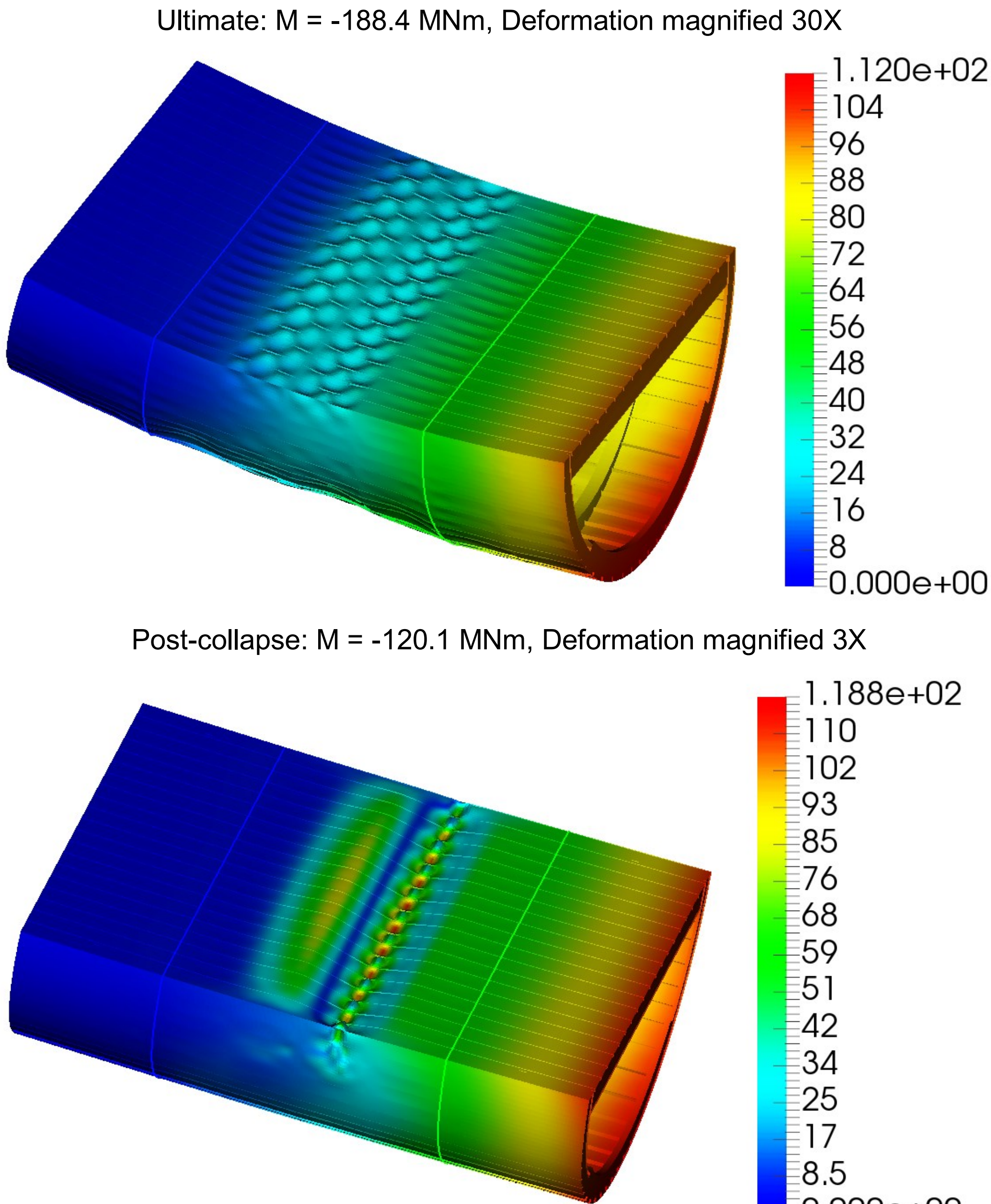

Figure 36: *Total deformation in mm for the SSTK-C with grounding damage in sagging: at ultimate bending moment (top); in post-collapse (bottom).*

3.3 Notional destroyer results

The ultimate strengths predicted for the notional destroyer model in the intact condition are summarized in Table 17. Poor agreement between ULTMAT and nonlinear FEA is obtained in both hogging and sagging. The ULTMAT/IACS prediction is 8.6% higher than FEA in hogging, and 48% higher in sagging. ULTMAT/LSC is 13% higher than FEA in hogging but is only 5.5% higher in sagging. Possible reasons for ULTMAT predicting higher strengths than FEA are discussed below and in Section 4. The moment-curvature plots in Figure 37 show although they do not extend very far into the post-collapse region, the FEA calculations do indicate reasonably clear peak values.

Table 17: *Ultimate strengths in MNm for the intact notional destroyer midsection.*

	Hogging	Sagging
ULTMAT/IACS	1693	-1307
ULTMAT/LSC	1761	-933.9
FEA	1559	-885.4

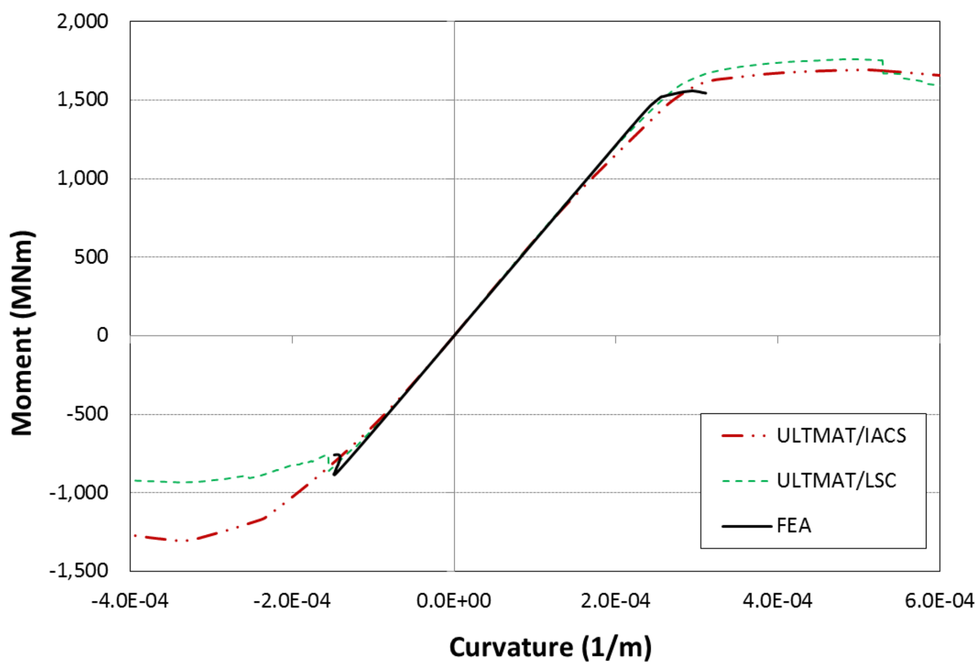

Figure 37: *Moment versus curvature for the intact notional destroyer midsection.*

The deformations in the last converged load step of the nonlinear FEA under a hogging bending moment are shown in Figure 38 and Figure 39. This shows an interframe collapse mode forming in the outer bottom structure which is primarily comprised of buckling of the outer bottom plating and longitudinal webs. The nonlinear simulation could not be progressed far enough to define clearly the final collapse state and location.

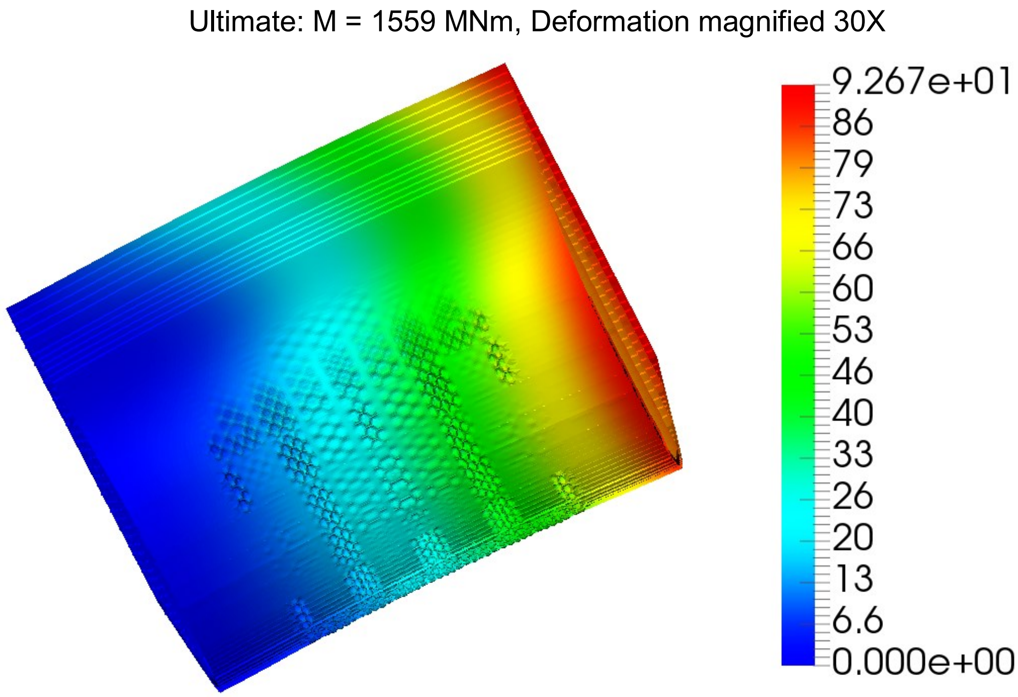

Figure 38: *Total deformation in mm for the intact notional destroyer in hogging: at the ultimate bending moment.*

Post-collapse: M = 1545 MNm, Deformation magnified 20X

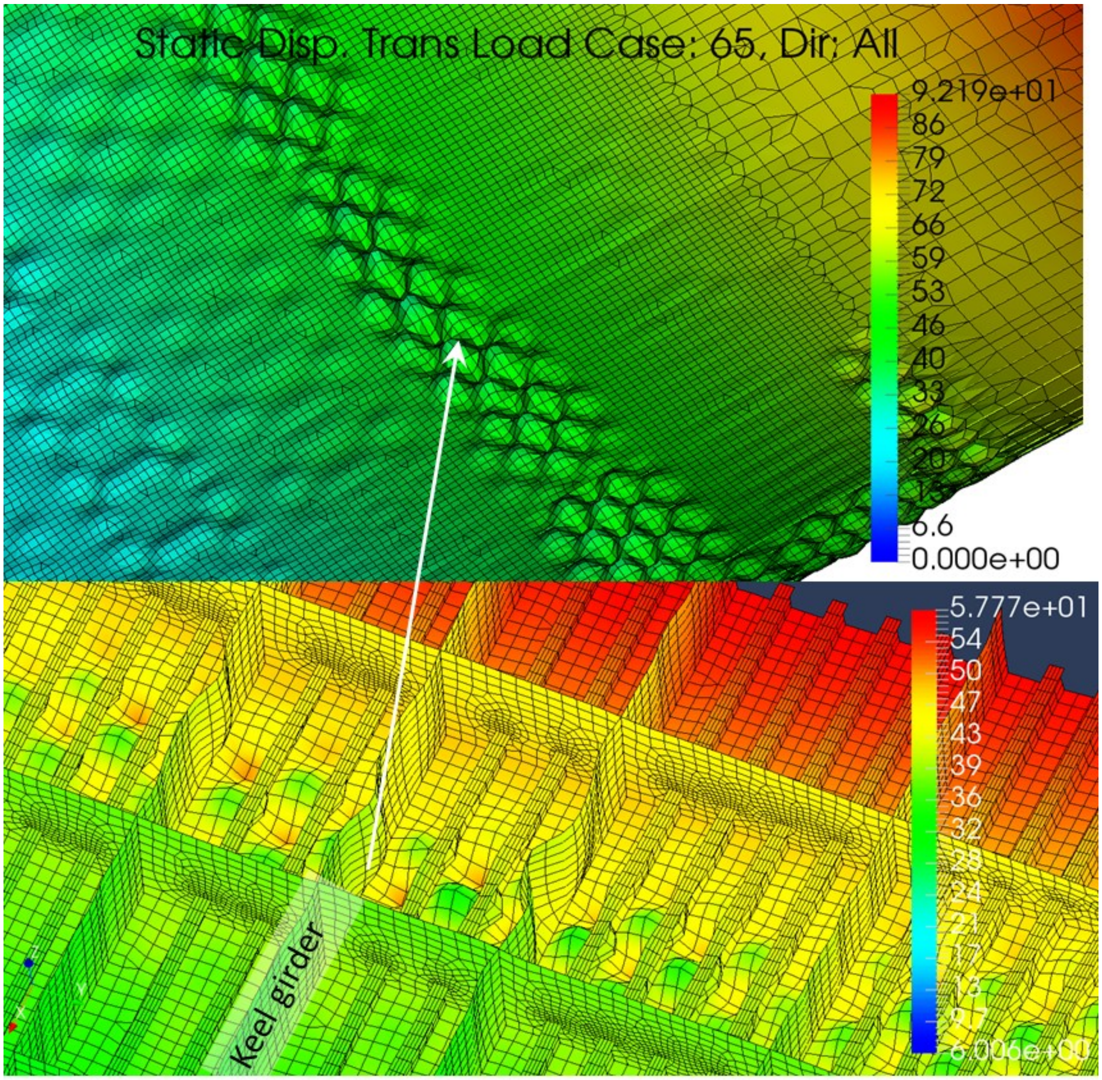

Figure 39: *Close-up view of post-collapse deformation (in mm) in outer-bottom structure of the notional destroyer model in hogging.*

The deformation predicted by nonlinear FEA in the sagging case, shown in Figure 40, indicates an overall collapse of the main deck between the bulkheads. The occurrence of overall collapse in the intact case is not expected, and may be an unintended consequence of lengthening the compartments from 11.43 m to 13.335 m. It explains why ULTMAT predictions in sagging are unconservative. The relatively close agreement between FEA and ULTMAT/LSC in this case is probably fortuitous, given that the latter is predicting an interframe collapse mode.

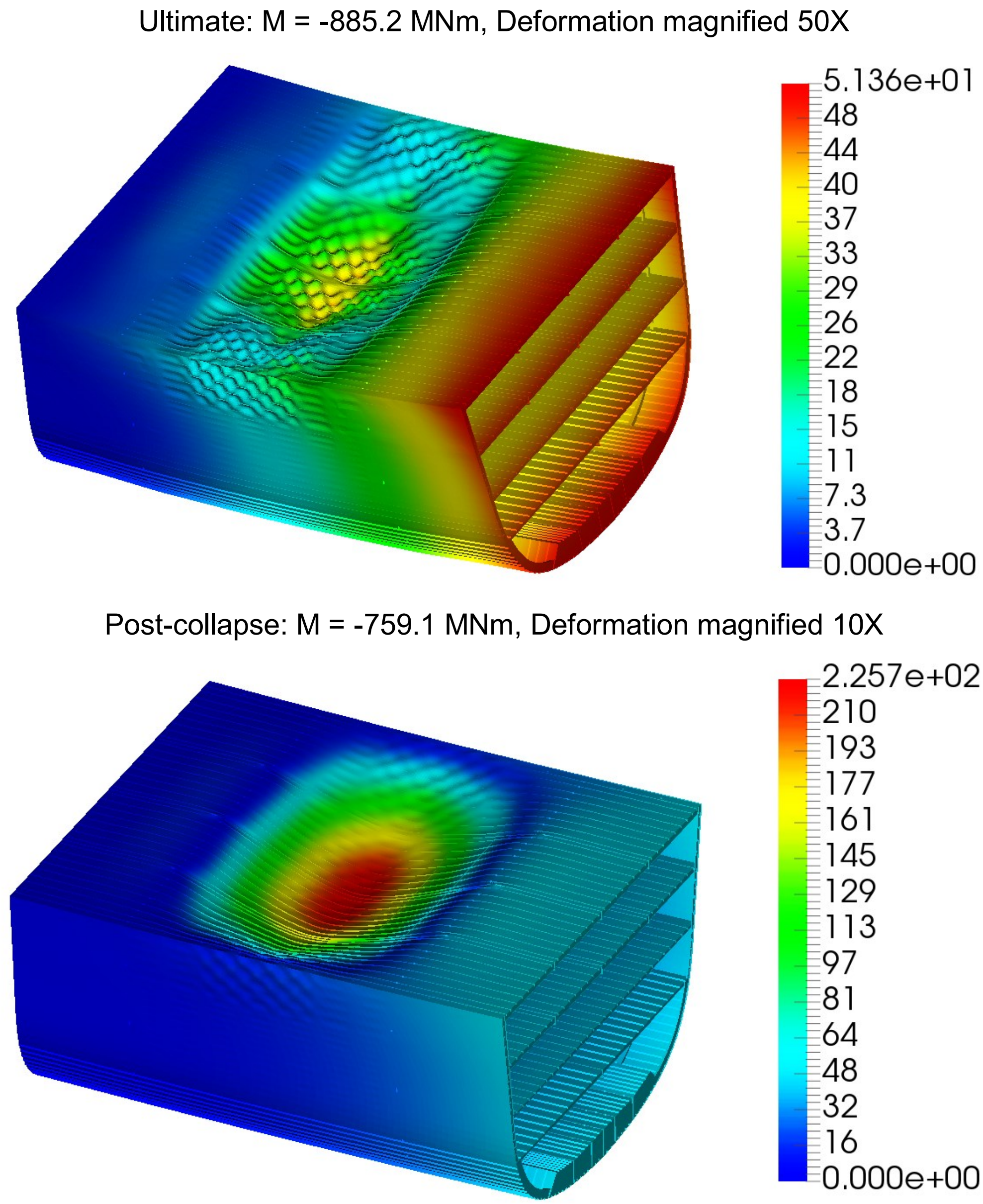

Figure 40: *Total deformation in mm for the intact notional destroyer in sagging at the ultimate bending moment.*

The ultimate strengths predicted for the notional destroyer model with collision damage are summarized in Table 18. As for the intact case, agreement between ULTMAT and nonlinear FEA is significantly better in hogging (within 8%) than in sagging (up to 80% different). The ULTMAT interaction curves are given in Figure 41. In the upper portion of the interaction curves (where the bottom of the vessel is in compression) the ULTMAT/IACS and ULTMAT/LSC curves are in fairly close agreement; whereas in the lower portions of the curve (i.e., when the upper decks and side shell are in compression) the two ULTMAT curves diverge markedly. The upper deck and upper side shell structure has much higher slenderness than the hull bottom structure, and this accounts for the apparent divergence in the accuracy of the ULTMAT methods, as will be discussed in Section 4.

Table 18: *Ultimate strengths in MNm for the notional destroyer midsection with collision damage.*

	Hogging	Sagging
ULTMAT/IACS	1516	-1016
ULTMAT/LSC	1569	-701.2
FEA	1456	-566.4

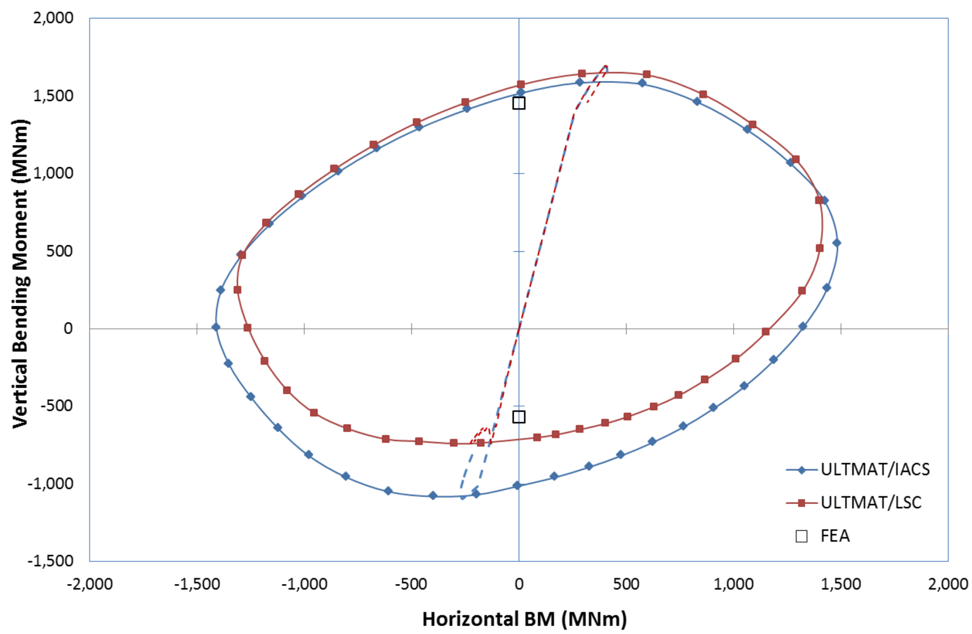

Figure 41: *Ultimate strength interaction curves for the notional destroyer with collision damage.*

The deformations predicted by nonlinear FEA for the destroyer model with collision damage in hogging are shown in Figure 42. As in the intact case, it was only possible to obtain a convergent FEA solution up to the peak hogging bending moment and slightly into the post-collapse region. The mode of collapse is therefore not well defined, but appears to be a developing interframe collapse mode. The deformations for this model under a sagging bending moment clearly indicate an overall collapse mode in the damaged deck.

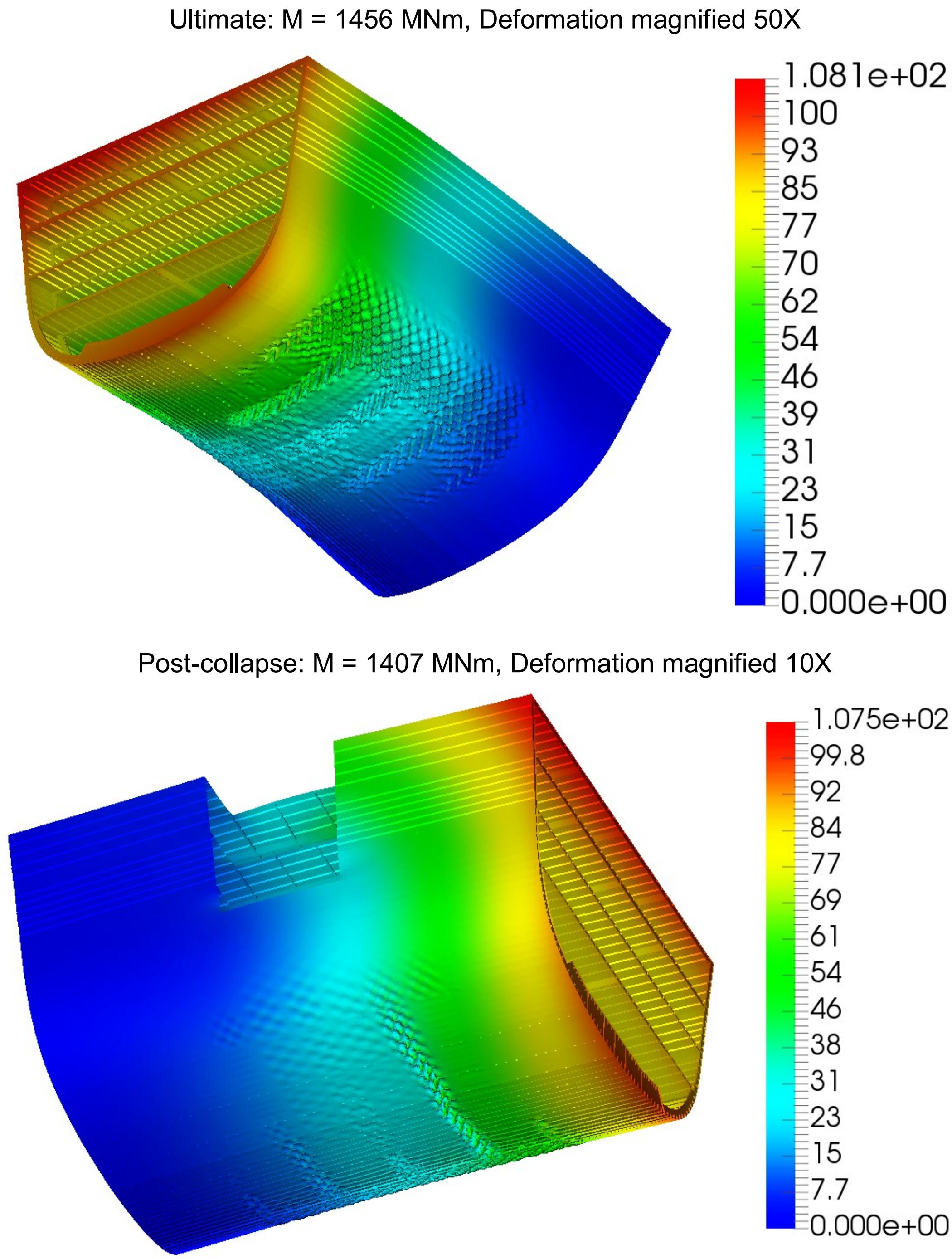

Figure 42: *Total deformation in mm for the notional destroyer with collision damage in hogging: at the ultimate bending moment (top); at post-collapse (bottom).*

Ultimate: M = -566.4 MNm, Deformation magnified 5X

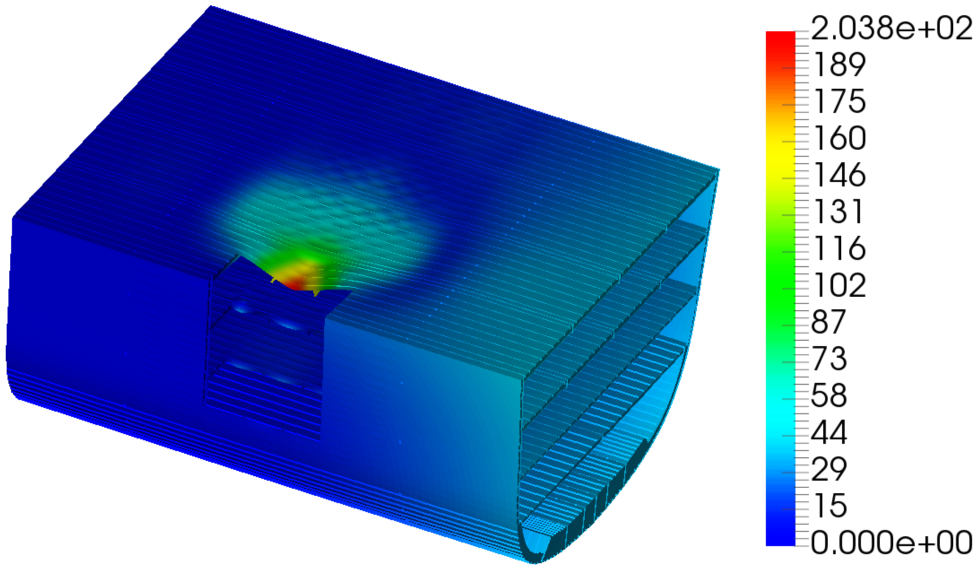

Figure 43: *Total deformation in mm for the notional destroyer with collision damage in sagging at the ultimate bending moment.*

The ultimate strengths predicted for the notional destroyer model with grounding damage are summarized in Table 19. As for the intact case, ULTMAT predicts higher ultimate strength in hogging and sagging than nonlinear FEA, with differences ranging between 6.5% and 48%. The ULTMAT interaction curves are shown in Figure 44. ULTMAT/LSC and ULTMAT/IACS again agree well for hogging moments greater than about 600 MNm, but differ widely for moments less than this. Because the damage is only slight asymmetric, ULTMAT moment-curvature analysis should give results close to the values derived from the interaction curves in Table 19. Figure 45 gives the moment-curvature relationships, which also indicates the extent to which the nonlinear FEA solution progressed into the post-collapse region.

Table 19: *Ultimate strengths in MNm for the notional destroyer midsection with grounding damage.*

	Hogging	Sagging
ULTMAT/IACS	1413	-1220
ULTMAT/LSC	1441	-875.2
FEA	1228	-822.8

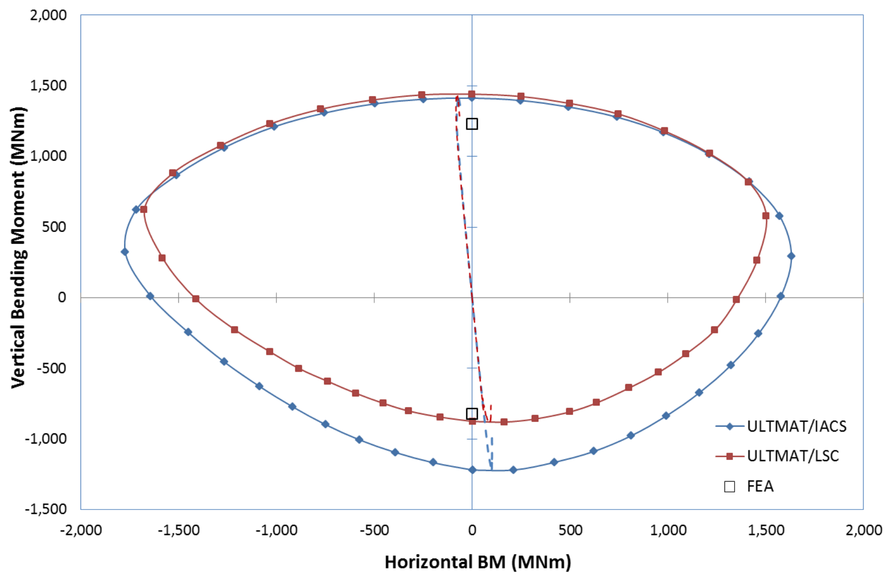

Figure 44: *Ultimate strength interaction curves for the notional destroyer with grounding damage.*

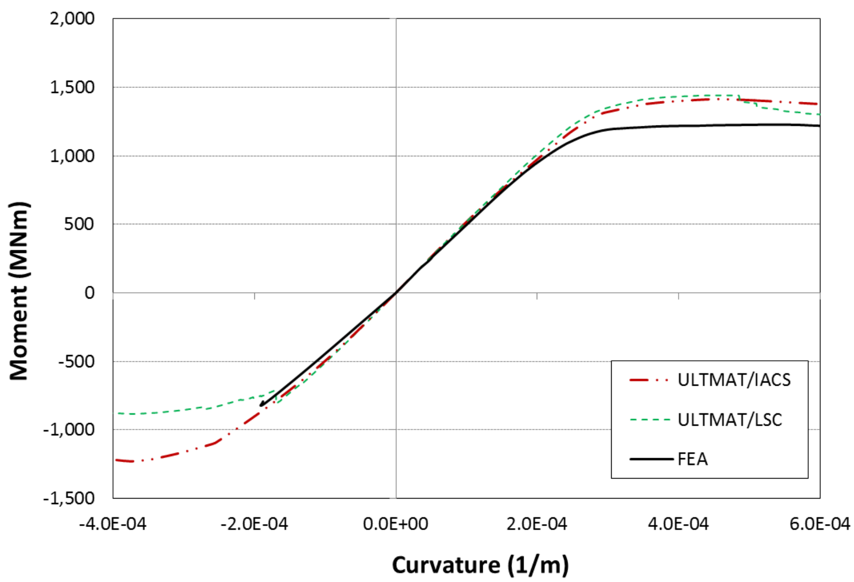

Figure 45: *Moment-curvature relationships for the notional destroyer with grounding damage.*

Deformations predicted by nonlinear FEA in the hogging case are shown in Figure 46. An interframe collapse pattern is developing with large deformations at the free edge of the damaged area. The hull bottom structure seems to be collapsing in the frame bays at either end of the damage area. Figure 47 shows the deformations under a sagging ultimate bending moment, showing that, as in the intact case, the entire main deck structure undergoes overall collapse.

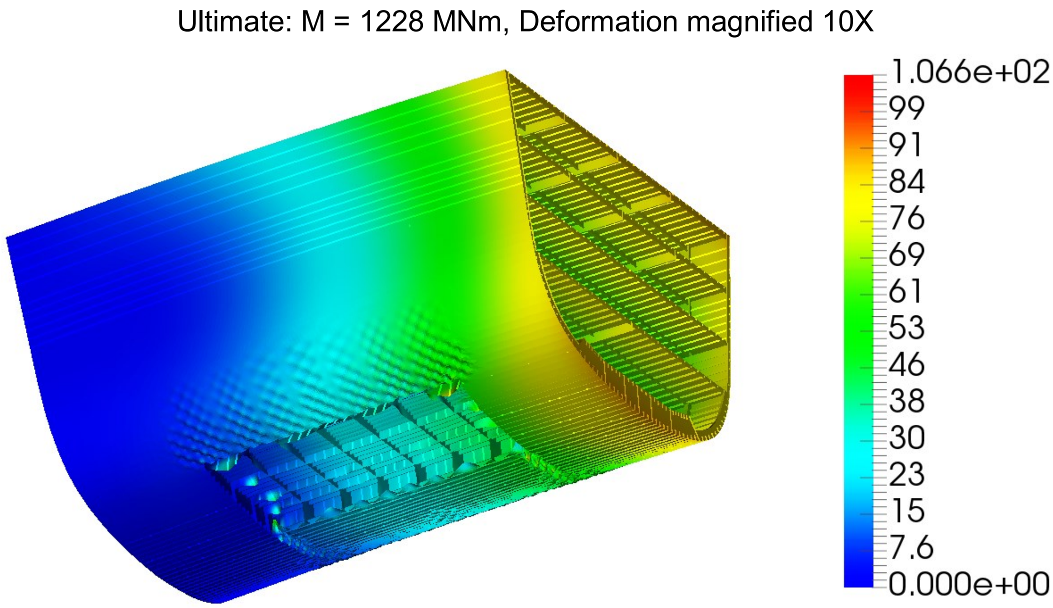

Figure 46: *Total deformation in mm for the notional destroyer with grounding damage in hogging at the ultimate bending moment.*

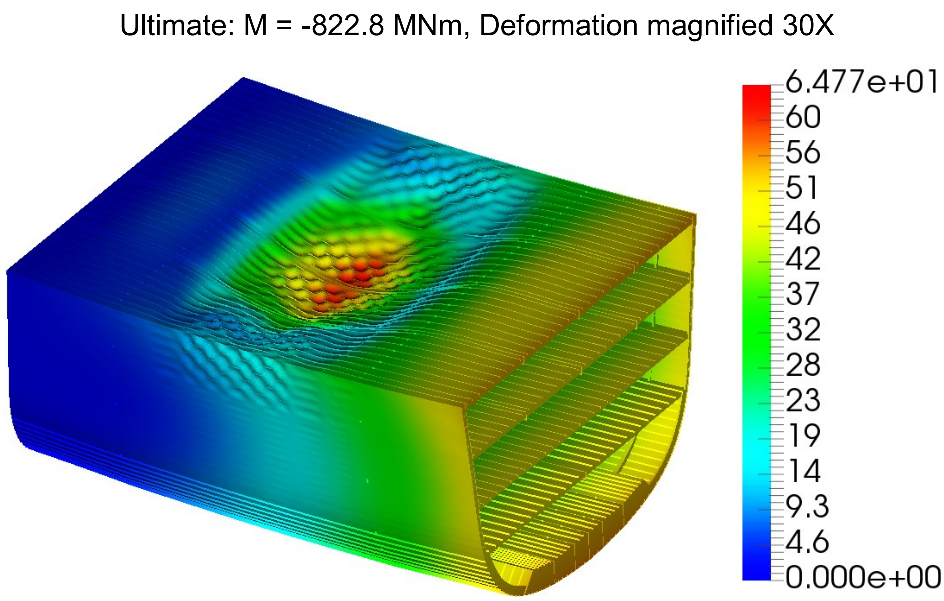

Figure 47: *Total deformation in mm for the notional destroyer with grounding damage in sagging at the ultimate bending moment.*

4 Discussion

The results of Section 3 show that nonlinear FEA can consistently provide converged solutions of relatively simple hull girder structures like SSTK-A and SSTK-C except where local buckling instabilities prevent the solutions from reaching the ultimate collapse load. With more complex structures like the notional destroyer, it is more difficult to achieve convergence of the method close to the point of collapse due to the loss of positive definiteness in the tangent stiffness matrix $\boldsymbol{K_T}$ in the nonlinear equilibrium equation (5). Using an explicit solution method, in which the application of the bending load is treated as a slowly moving dynamic process instead of as a quasi-static process, may help to avoid this difficulty [17].

The extent of the hull girder FE models needs to be sufficiently large so that the collapse mode is adequately represented in the model. To ensure consistency in the application of the finite element methodology, a two-compartment length of hull girder was used for all models, although in some cases of interframe collapse a shorter model length could have been used.

ULTMAT/IACS predictions were found to agree closely with the nonlinear FEA solutions for the intact SSTK models. ULTMAT/LSC predictions were on the other hand significantly lower than nonlinear FEA and ULTMAT/IACS for the intact SSTK models. Both ULTMAT methods predict higher strengths than FEA for the destroyer design. To make sense of these comparisons, Table 20 summarizes the range of slenderness values found in the longitudinal structure for these models. The plate slenderness, β, is defined in (1), and the column slenderness, λ, is defined in (2).

Table 20: *Column and plating slenderness ranges for three models.*

	λ	β
SSTK-A	0.57–0.84	2.11–3.37
SSTK-C	0.57–0.87	2.11–2.83
Destroyer—Deck 1 regular longitudinals + plating	0.72–0.90	1.52–3.35
Destroyer—Outer Bottom	0.26–0.32	2.00–3.07

The column slendernesses are in a relatively high range for both SSTK models. In the destroyer model, the stiffened panels in Deck 1 (regular longitudinals and plating) have high column slenderness, while the outer bottom structure has low column slenderness.

Thus the close agreement between FEA and ULTMAT/IACS for the SSTK models confirms the accuracy of the latter method for structure with relatively high column slenderness. The less satisfactory comparison between FEA and ULTMAT/IACS for the destroyer model is most likely due to two factors: in sagging, the FEA model failed in overall collapse of the main deck, which cannot be predicted with ULTMAT; while in hogging, it is the stockier outer bottom structure that is in compression.

The comparatively poor performance of ULTMAT/LSC for the SSTK models suggests the following:

– that load shortening curve libraries used by this method are too conservative in the higher slenderness range;

– the load shortening curve libraries may not be conservative enough for low-slenderness structure, which could explain the overestimation of the hogging strength for the intact destroyer model.

That both ULTMAT/IACS and ULTMAT/LSC overestimate the hogging strength of the destroyer model suggests another possibility, which is that the subdivision of the cross sectional structure into stiffened panel elements and hard corners may not judicious. The sizing of the hard corners in the bottom of the structure, in particular, will have a large influence on the hogging strength. As was discussed in Section 2.2.1, the width of plating included in each hard corner was determined, following the guidance in the IACS rules [1], as the lesser of half the distance to the next longitudinal support or $20t$, where t is the plate thickness.

However, the plate buckling in the hull bottom structure shown in Figure 38, particularly the buckling of the longitudinal webs spanning the inner and outer bottom, suggests that a smaller portion of the plating is actually behaving like a hard corner (i.e., elasto-plastic deformation without buckling). Determining a better criterion for sizing of hard corners would require considerable investigation, however, and this is left for a future study.

The results of the damage cases largely confirm the above conclusions regarding the accuracy and limitation of the tools. For interframe collapse of slender structure, ULTMAT/IACS generally agrees well with FEA while ULTMAT/LSC is too conservative. Neither ULTMAT method is accurate when overall collapse is the mode of failure.

Based on the FEA results alone, the relative strengths for the various models and damage cases are summarized in Table 21. As might be expected, the collision damage affects the sagging strength much more than the hogging strength, while the grounding damage affects the hogging strength more than the sagging strength.

Table 21: *Relative strengths in the intact and damaged condition (FEA).*

	Collision/Intact	Grounding/Intact
SSTK-A - Hogging	0.858	0.660
SSTK-C - Hogging	1.001	0.449*
Destroyer - Hogging	0.934	0.788
SSTK-A - Sagging	0.471	0.927
SSTK-C - Sagging	0.544	0.797*
Destroyer - Sagging	0.640	0.929

*Modified grounding damage case.

In the SSTK models, strength reductions in excess of 50% are found for cross sectional area reductions in the range 12-18%. For the destroyer model, the strength reductions are 36% in sagging and 21% in hogging for cross sectional area reductions of 10%. Thus the loss in ultimate strength in percentage terms can be expected to be three to four times the percentage reduction in effective cross sectional area, depending on the damage location. Obviously, gross damage occurring in the side shell near the neutral axis of the cross section will have much less effect on the ultimate strength in vertical bending. However, this may significantly reduce vertical shear strength, which was not investigated in this study.

All of the collision damage cases undergo overall collapse in sagging, while all of the grounding damage cases undergo interframe collapse in hogging. The preference for interframe collapse with grounding damage is due to the heavier transverse members using in the hull bottom structure of these models, which is typically the case in real vessels. Thus the development of overall collapse in steel monohull construction seems to be primarily a concern under extreme sagging bending moments when there is gross damage to the upper decks.

5 Conclusion

The results presented in this report indicate that nonlinear FEA is generally effective for relatively simple hull girder structures that are either in the intact or damaged condition. With more complex hull girder models, nonlinear FEA is more difficult to use because of the large model sizes, and because of difficulties in achieving convergent solutions near the collapse point and in the post-collapse region. Extending the nonlinear solution into the post-collapse is generally found to be beneficial for resolving the ultimate strength and the mode of collapse.

Comparison of the results from FEA and ULTMAT shows that close agreement is obtained between FEA and ULTMAT/IACS for hull girder structure with high column slenderness where an interframe collapse mode occurs. This is true regardless of whether the model is in an intact or damaged condition. ULTMAT/LSC gives predictions in this case that are 12-18% lower than FEA, which suggests that the load-shortening curve database is too conservative for high column slenderness structure. For hull girder structure with low column slenderness and which fails in an interframe mode, ULTMAT/IACS and ULTMAT/LSC agree with each other fairly well but both overestimate the strength in comparison to nonlinear FEA. This may be indicating that hard corners are being oversized in ULTMAT's cross section modelling. Neither version of ULTMAT is accurate when overall collapse is the failure mode, as is expected given that ULTMAT is based interframe collapse assumptions.

Based on the damage cases investigated, reductions in the ultimate strength in vertical bending due to gross damage of the main deck and shear strake, or to the hull bottom, can generally be expected to be 3 to 4 times the reduction in effective cross sectional area.

For future validation efforts, it would be useful to use a simplified hull girder structure design similar to the SSTK models, but with a wider range of column slenderness values than is represented in SSTK-A and SSTK-C. Greater variation in the dimensions of the longitudinal stiffeners would accomplish this. The issue of correct sizing of hard corner elements needs to be resolved through a separate investigation.

While nonlinear FEA may generally be effective in assessing residual strength with gross damage, it is too slow for use in the immediate response to a damage incident. One approach for the latter would be to use FEA to precalculate the residual strength for a large number of possible damage scenarios, for quick reference in an actual damage event [18]. Another approach would be to develop or acquire a simplified analysis method for quick analysis of gross damage events that can take into account overall and interframe collapse modes. The progressive collapse method developed by Benson [19] and implemented in the MAESTRO software is an example of one such method.

References

[1] IACS (2017), Common Structural Rules for Bulk Carriers and Oil Tankers, Dated 01 Jan 2017, London UK: International Association of Classification Societies.

[2] Lloyd's Register (2017), Rules and Regulations for the Classification of Naval Ships, January 2017 Edition. London UK: Lloyd's Register Group Limited.

[3] Smith, C. (1977), Influence of local compressive failure on ultimate longitudinal strength of a Ship's hull, In *Proceedings of 3th international symposium on practical design in shipbuilding*, pp. 73–79.

[4] TTCP (2017), Survivability and Resilience of Damaged and Degraded Hulls, Task Proposal for TTCP MAR TP4 KTA-1.

[5] Martec Ltd (2006), Vibration and Strength Analysis Program (VAST), Version 9.0, User's Manual, Martec Limited (Lloyd's Register Applied Technology Group), Halifax, Nova Scotia.

[6] Smith, M. (2006), ULTMAT 2.1 User's Manual, Defence R&D Canada – Atlantic, (DRDC Atlantic TM 2006-049).

[7] MoD (2012), Structures Software Test Kit, 37401/R4729, Issue 01, Ministry of Defence, UK.

[8] Ashe, G., et al. (2009), Committee V.5: Naval Ship Design, In C.D. Yang and S. Y. Hong (Eds.), *Proceedings of the 17th International Ship and Offshore Structures Congress*, Vol 2, pp. 259–307.

[9] Hess, P. (2007), Notional US Navy Destroyer Rev 2, unpublished document, Naval Surface Warfare Center Carderock Division.

[10] Fujikubo, M., Muis Alie, M., Takemura, K., Iijima, K., and Oka, S. (2012), Residual Hull Girder Strength of Asymmetrically Damaged Ships. *Journal of the Japan Society of Naval Architects and Ocean Engineers*, 16, pp. 131–140.

[11] Smith, M. and Pegg, N. (2003), Automated Assessment of Ultimate Hull Girder Strength, *Journal of Offshore Mechanics and Arctic Engineering*, 125 (3), pp. 211–218.

[12] Smith, M. (2010), A load shortening curve library for longitudinally stiffened panels, Defence R&D Canada – Atlantic, (DRDC Atlantic TM 2010-140).

[13] Amlashi, H. and Moan, T. (2008), Ultimate strength analysis of a bulk carrier hull girder under alternate hold loading condition – A case study Part 1: Nonlinear finite element modelling and ultimate hull girder capacity, *Marine Structures*, 21, pp. 327–352.

[14] Muis Alie, M., Sitepu, G., Sade, J., Mustafa, W, Nugraha, A., and Saleh, A. (2016), Finite Element analysis on the hull girder ultimate strength of asymmetrically damaged ships, In *Proceedings of the ASME 2016 35th International Conference on Ocean, Offshore and Arctic Engineering*, OMAE2016-54041.

[15] Petricic, M. (2015), Survivability of hull girder in damaged condition, SSC report SSC-442, Ship Structures Committee.

[16] Martec Ltd (2015), SubSAS User's Guide, Version 1.0, Martec Limited (Lloyd's Register Applied Technology Group), Halifax, Nova Scotia.

[17] Yoshikawa, T., et al. (2015), Committee III.1: Ultimate Strength, In C. Guedes Soares and Y. Garbatov (Eds.), *Proceedings of the 19th International Ship and Offshore Structures Congress*, Vol 1, pp. 279–349, London: CRC Press.

[18] Paik, J. K., Kim, D. K., Park, D. H., Kim, H. B., and Kim, M. S. (2012), A new method for assessing the safety of ships damaged by grounding. *International Journal of Maritime Engineering* 154 (A1), pp. 1–20.

[19] Benson, S. (2011), Progressive Collapse Assessment of Lightweight Ship Structures, PhD Thesis, Newcastle University, Newcastle upon Tyne, UK.

Annex A ULTMAT models

A.1 Intact models

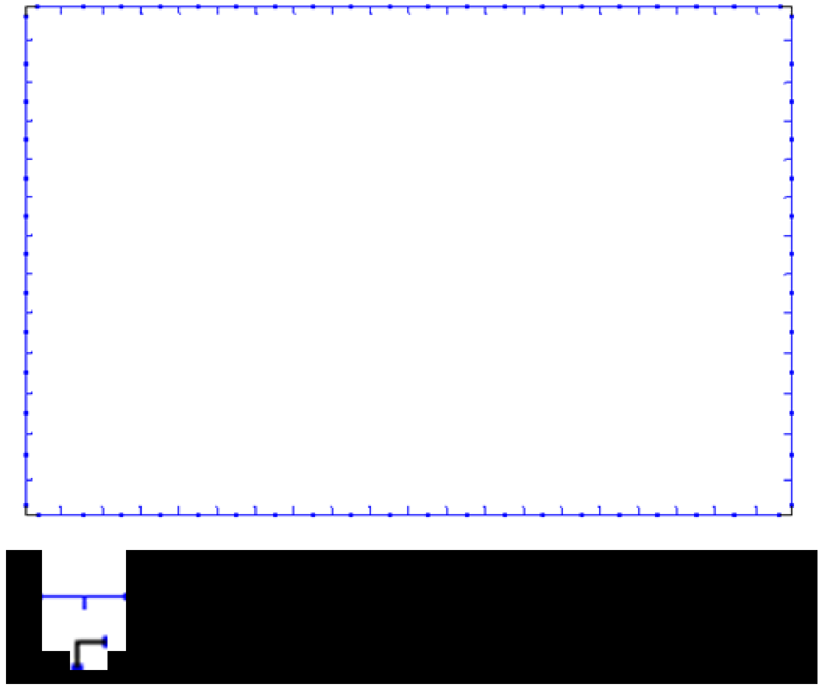

Figure A.1: *ULTMAT model for the intact SSTK-A showing arrangement of structural units.*

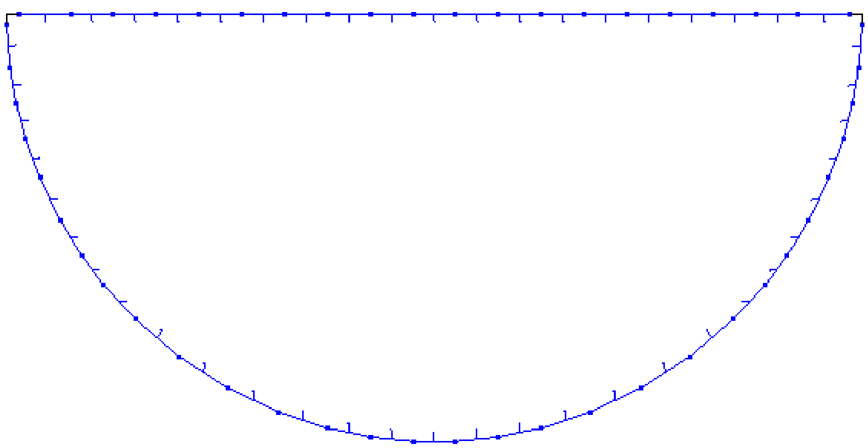

Figure A.2: *ULTMAT model for the intact SSTK-C showing arrangement of structural units.*

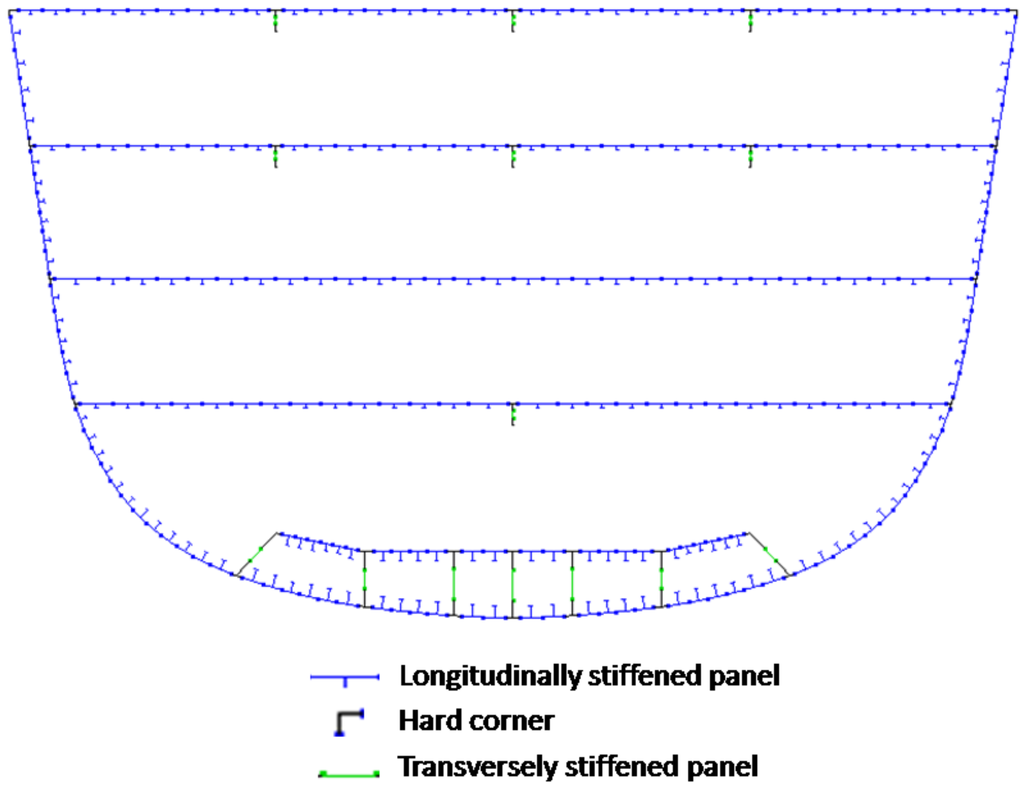

Figure A.3: *ULTMAT model for the intact SSTK-C showing arrangement of structural units.*

A.2 Damage models

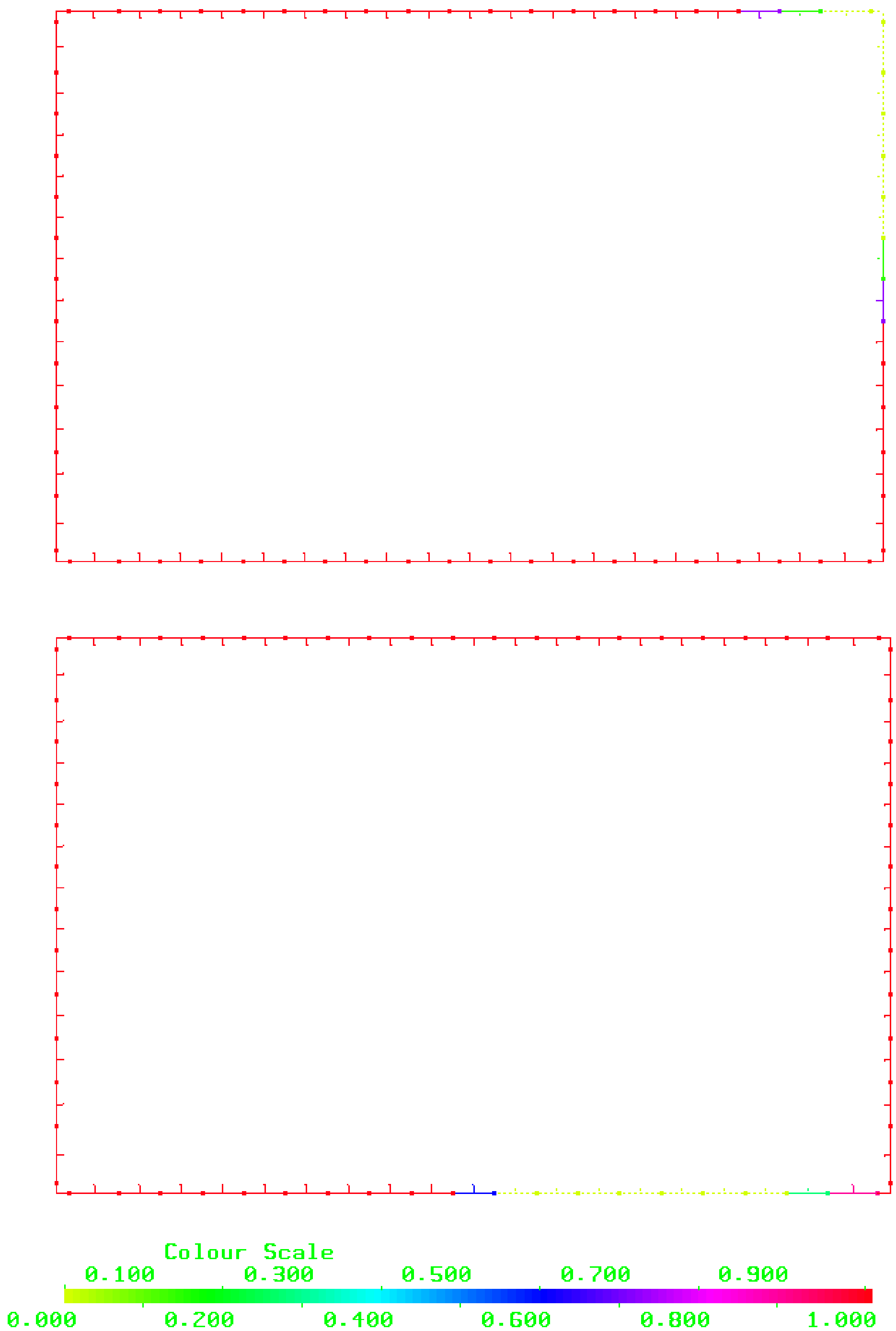

Figure A.4: *ULTMAT models for SSTK-A with collision (top) and grounding (bottom) damage showing unit effectiveness.*

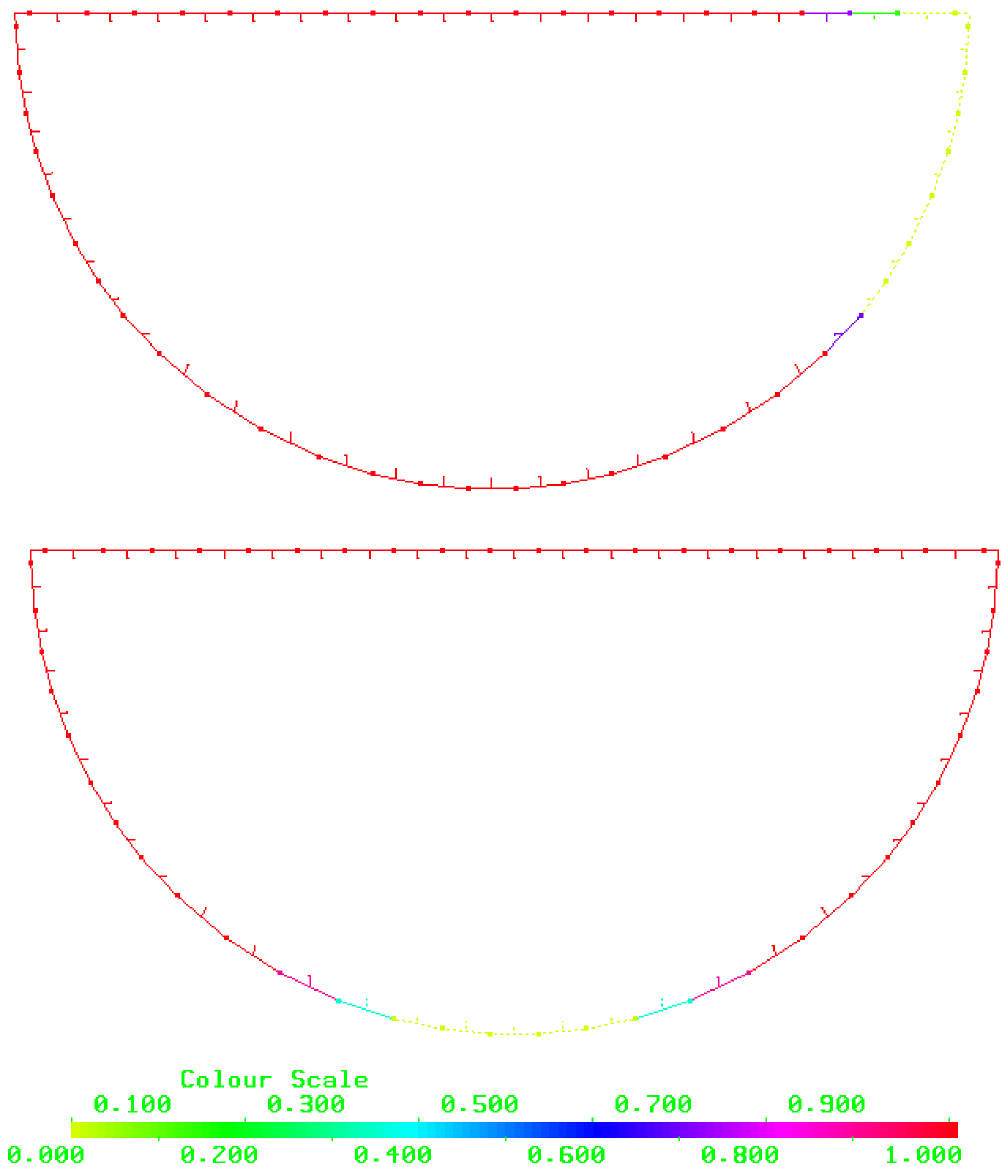

Figure A.5: *ULTMAT models for SSTK-C with collision (top) and grounding (bottom) damage showing unit effectiveness.*

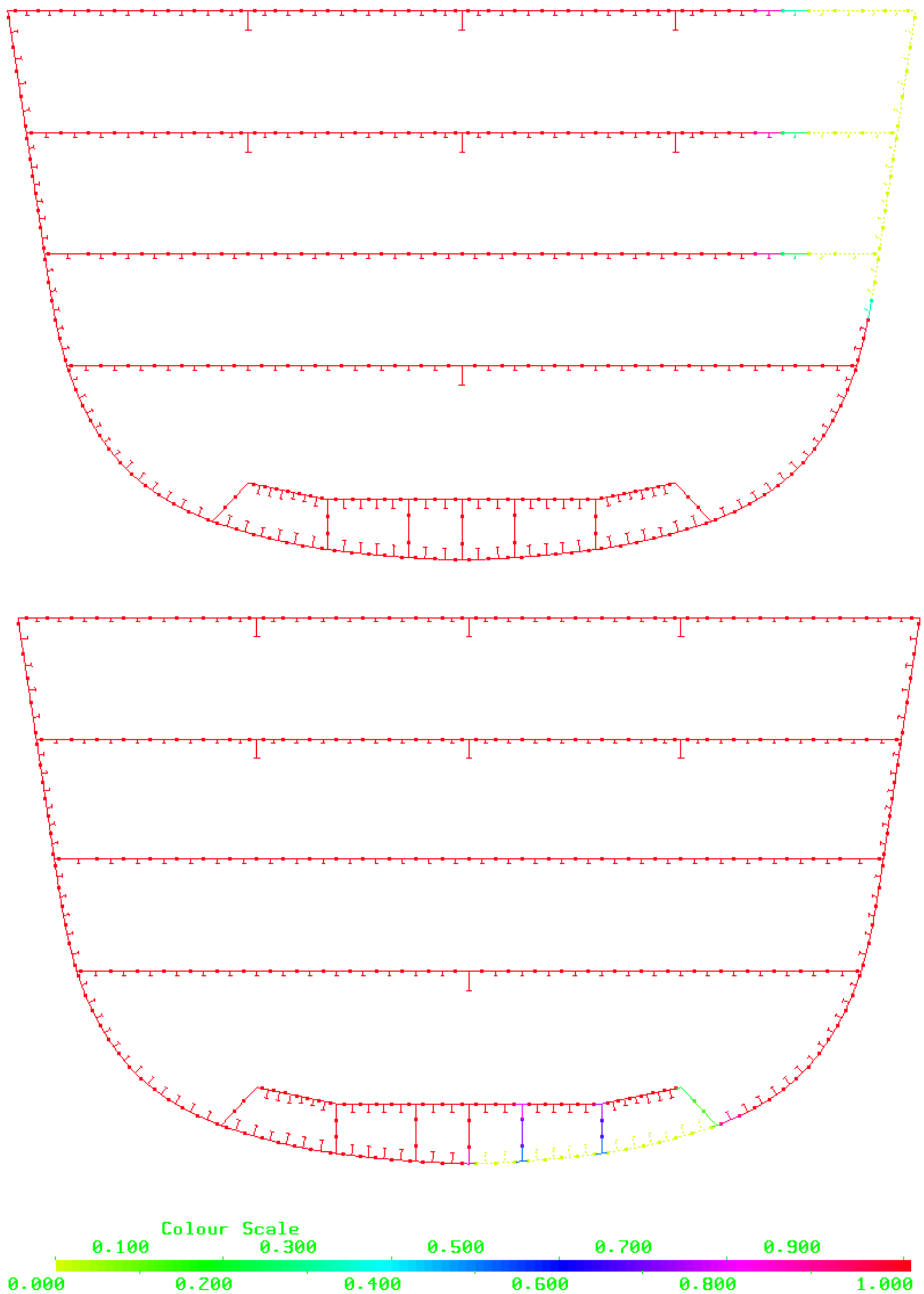

Figure A.6: *ULTMAT models for midships section of the notional destroyer design with collision (top) and grounding (bottom) damage showing unit effectiveness.*

Annex B Finite element models

B.1 FE meshes for SSTK-A

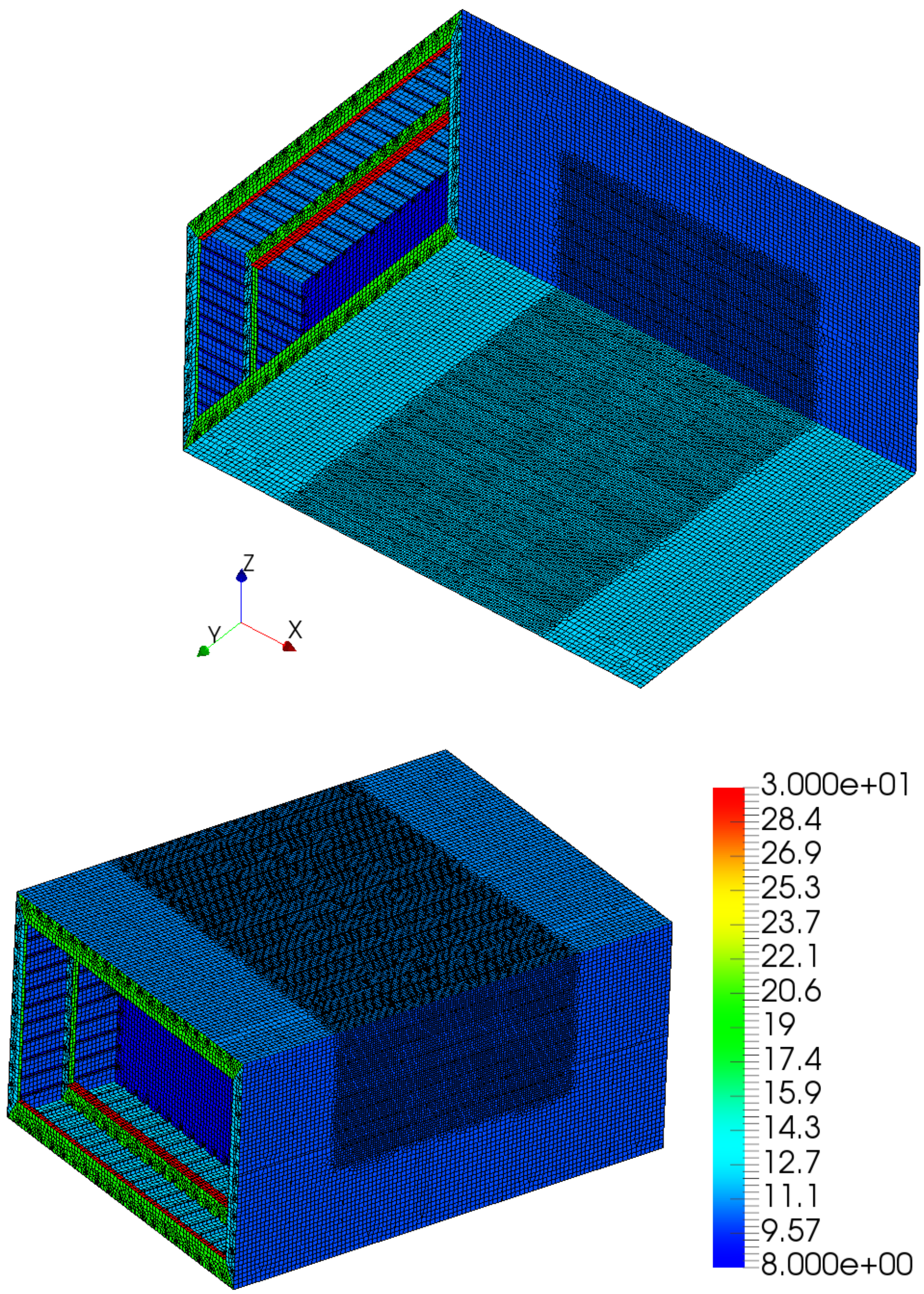

Figure B.1: *FE models for intact SSTK-A showing plate thickness in mm: hogging case (top); sagging case (bottom).*

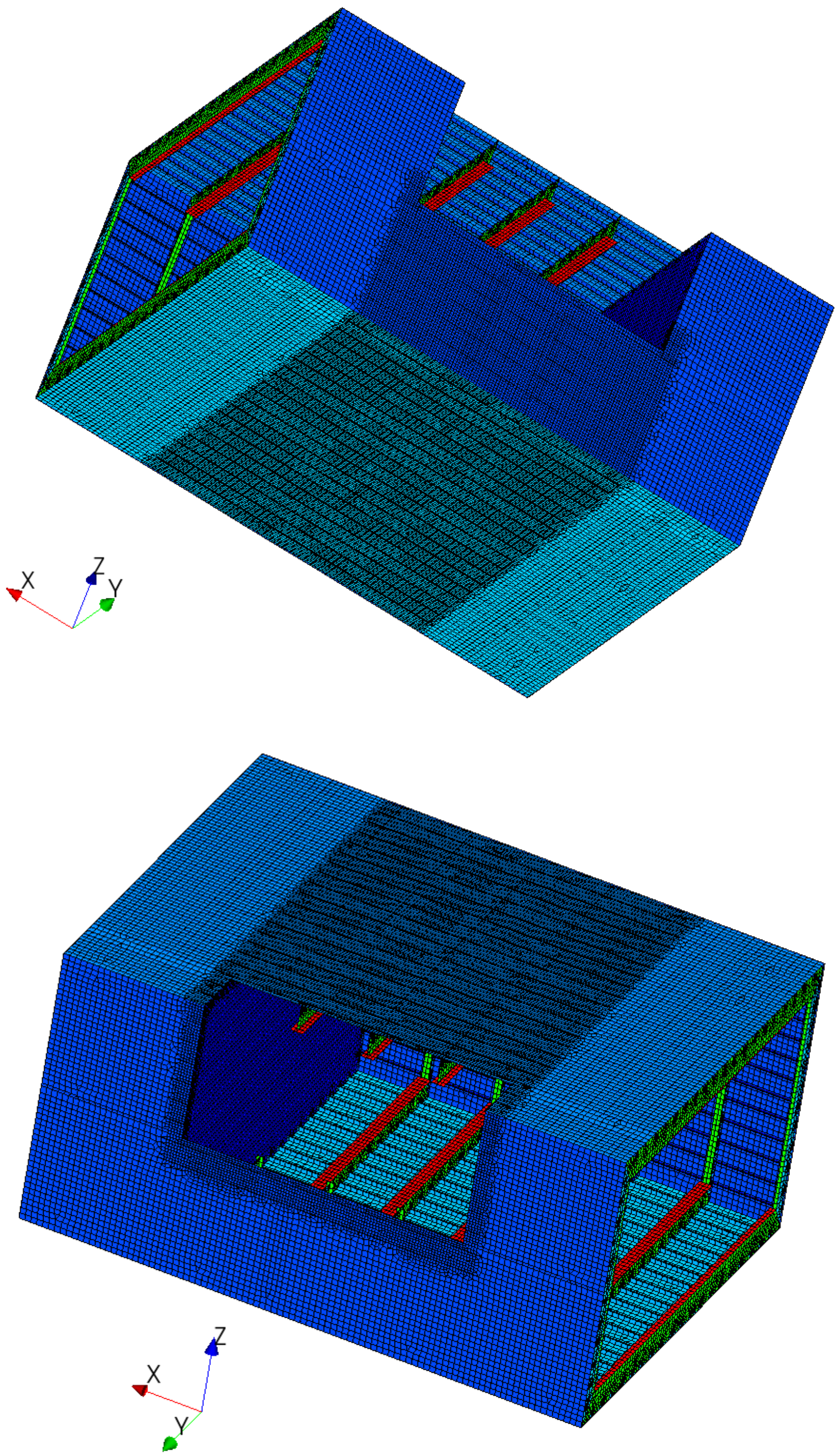

Figure B.2: *FE models for SSTK-A with collision damage: hogging case (top); sagging case (bottom).*

B.2 FE models for SSTK-C

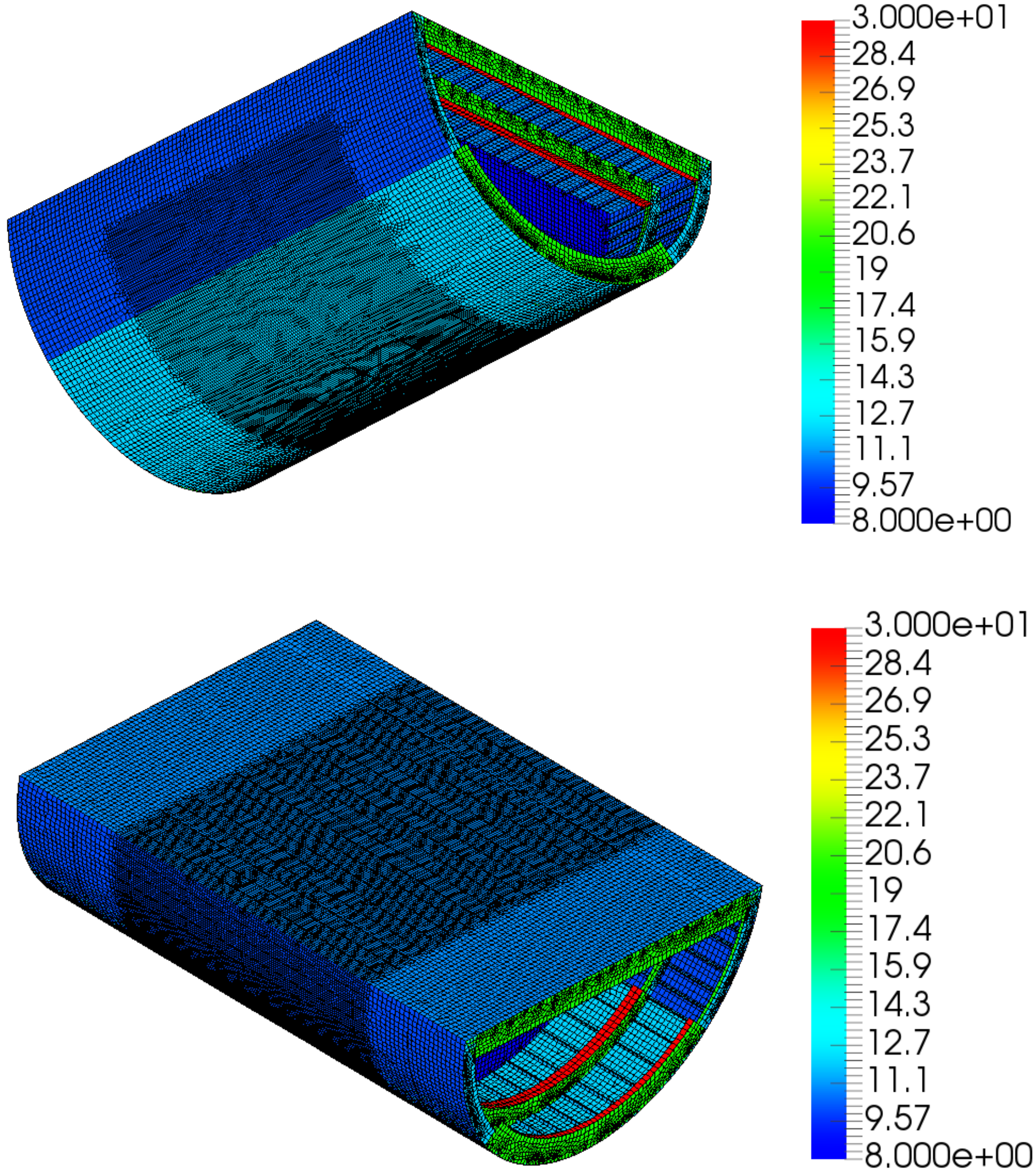

Figure B.3: *FE models for intact SSTK-C showing plate thickness in mm: hogging case (top); sagging case (bottom).*

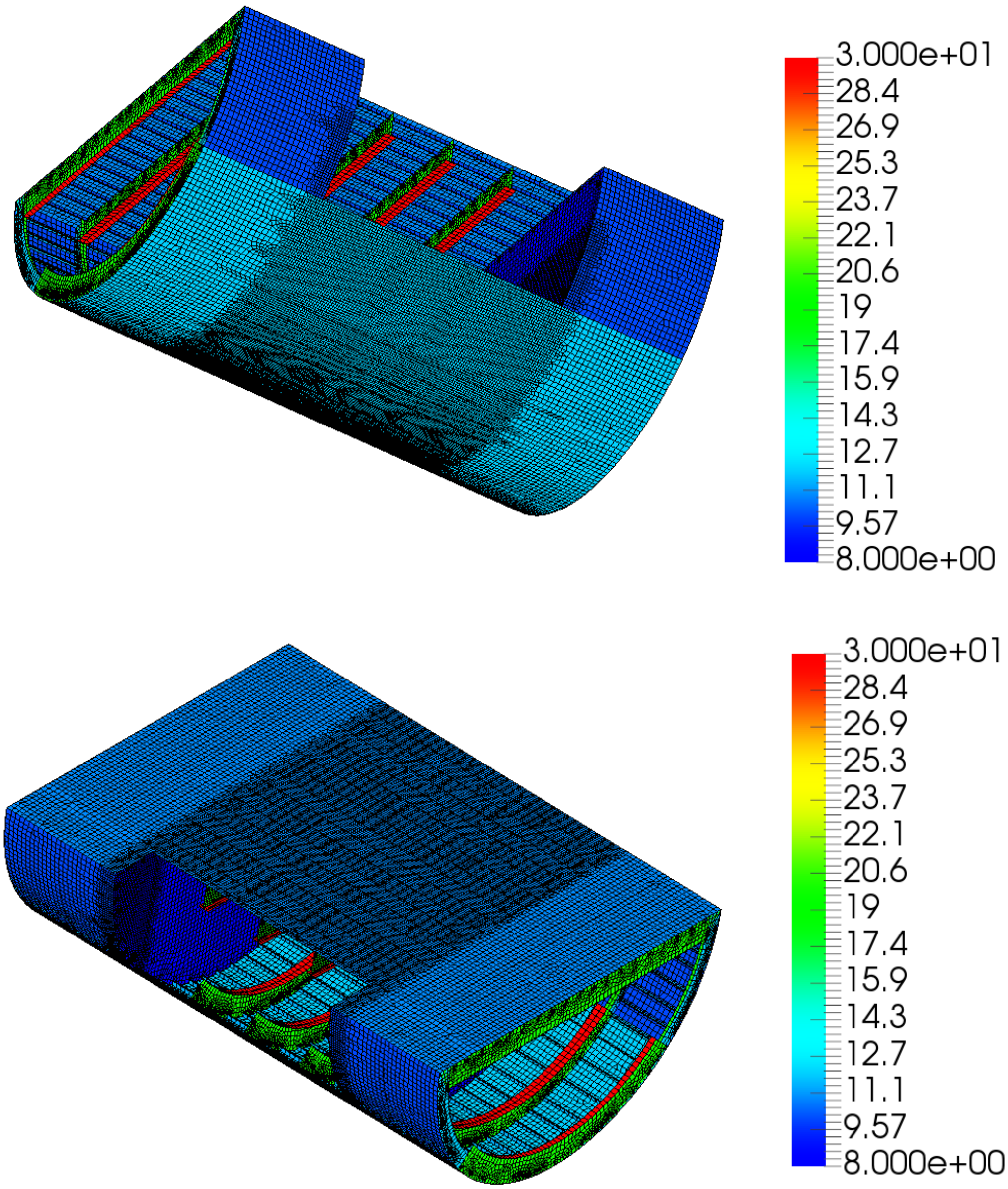

Figure B.4: *FE models for SSTK-C with collision damage showing plate thickness in mm: hogging case (top); sagging case (bottom).*

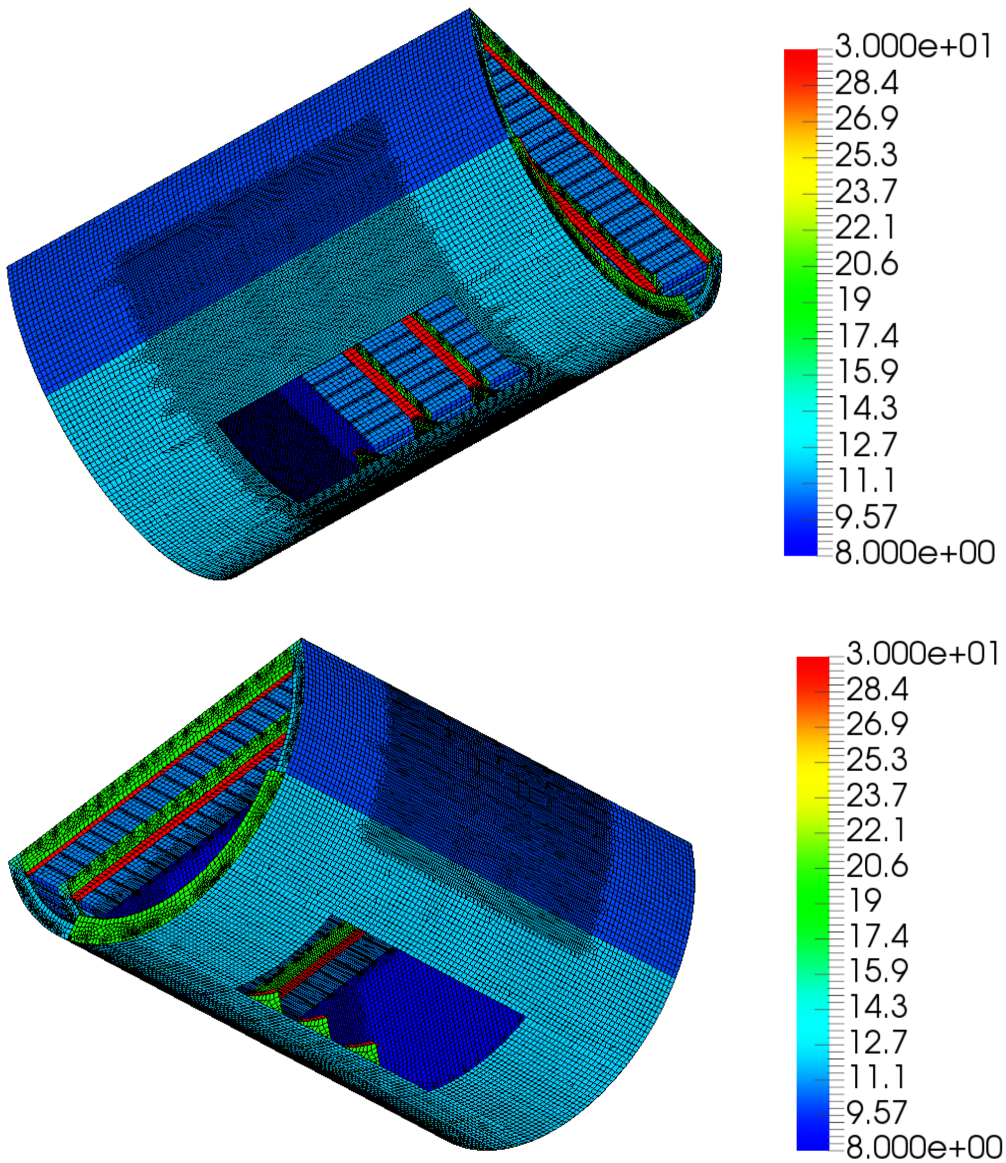

Figure B.5: *FE models for SSTK-C with grounding damage showing plate thickness in mm: hogging case (top); sagging case (bottom).*

B.3 FE models for the notional destroyer midsection

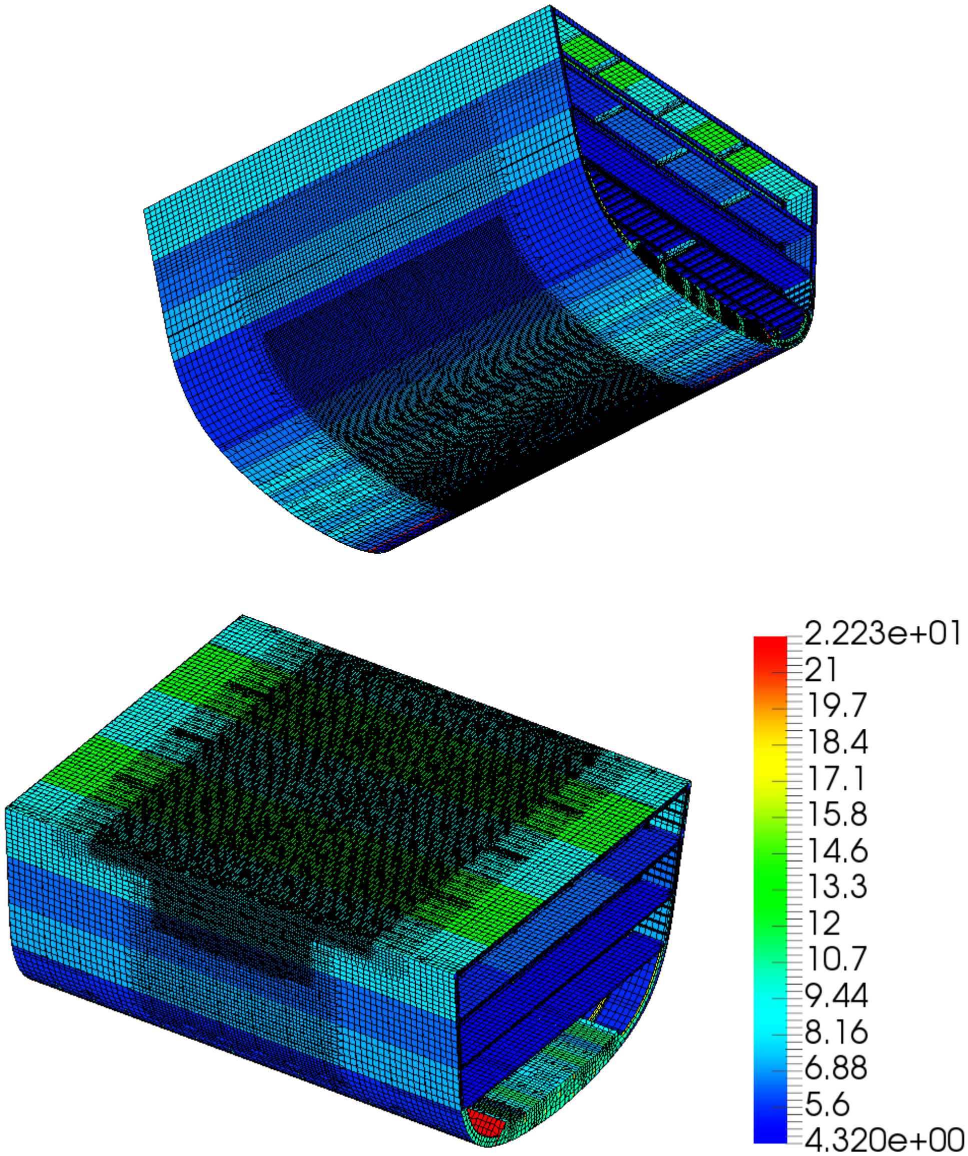

Figure B.6: *FE models for intact notional destroyer midsection showing plate thickness in mm: hogging case (top); sagging case (bottom).*

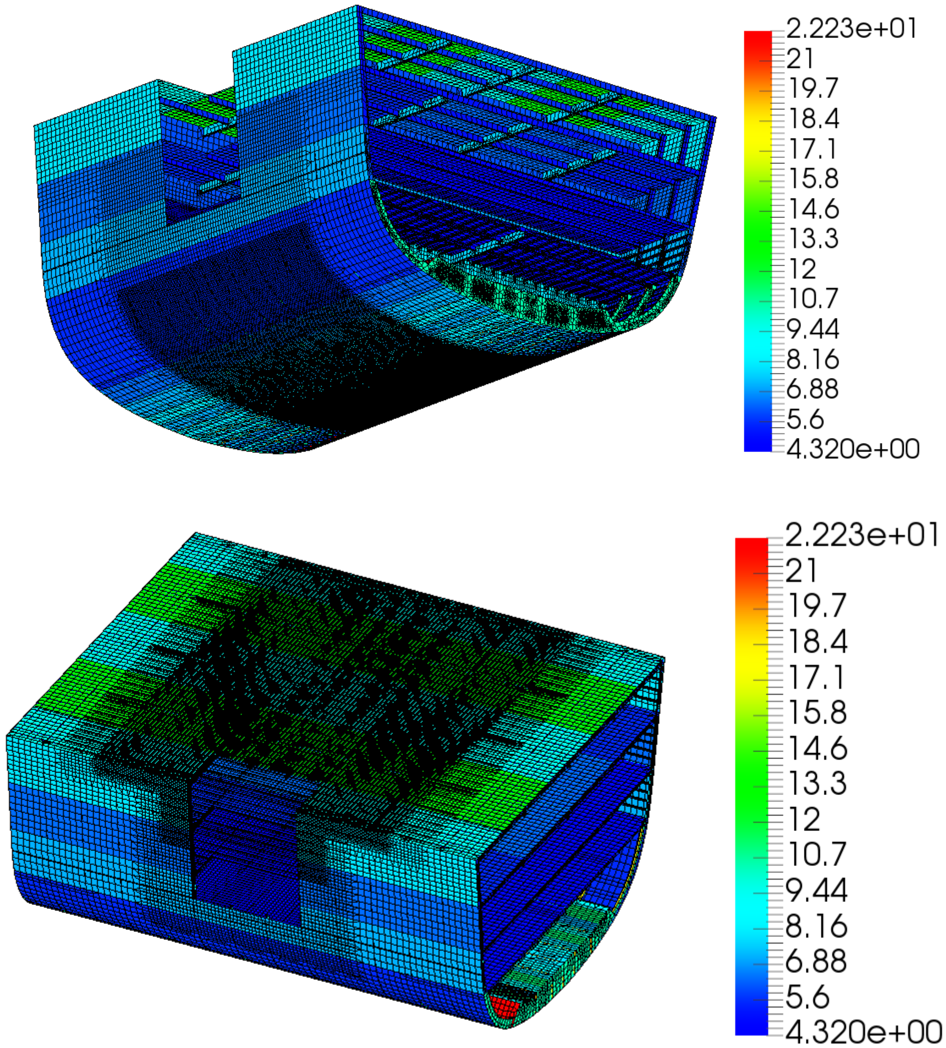

Figure B.7: *FE models for the notional destroyer with collision damage showing plate thickness in mm: hogging case (top); sagging case (bottom).*

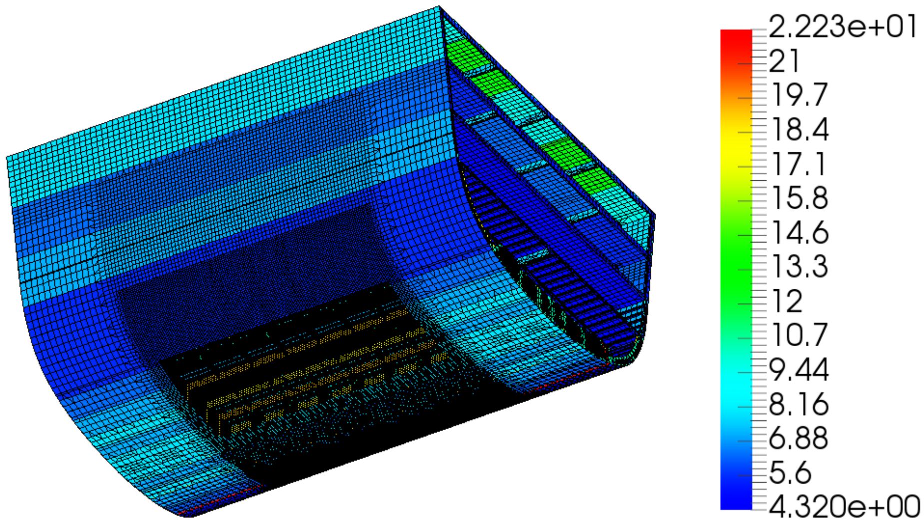

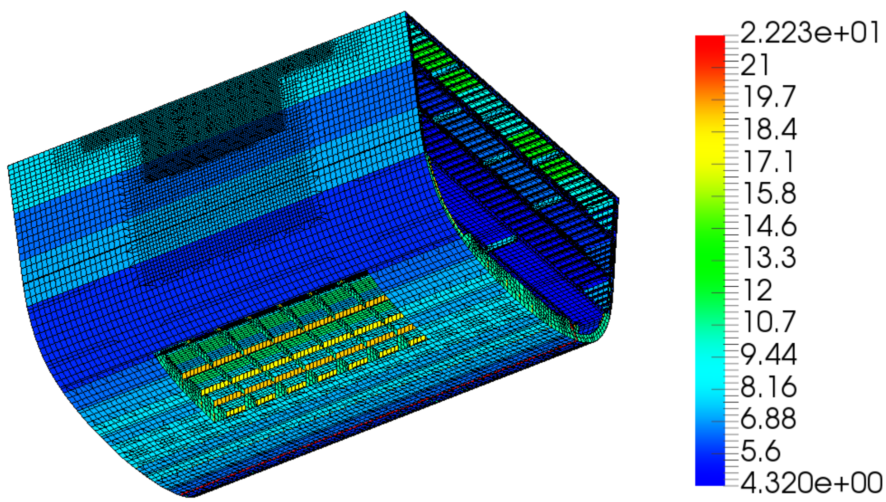

Figure B.8: *FE models for the notional destroyer with grounding damage showing plate thickness in mm: hogging case (top); sagging case (bottom).*

Annex C   Nonlinear FEA results for SSTK-A

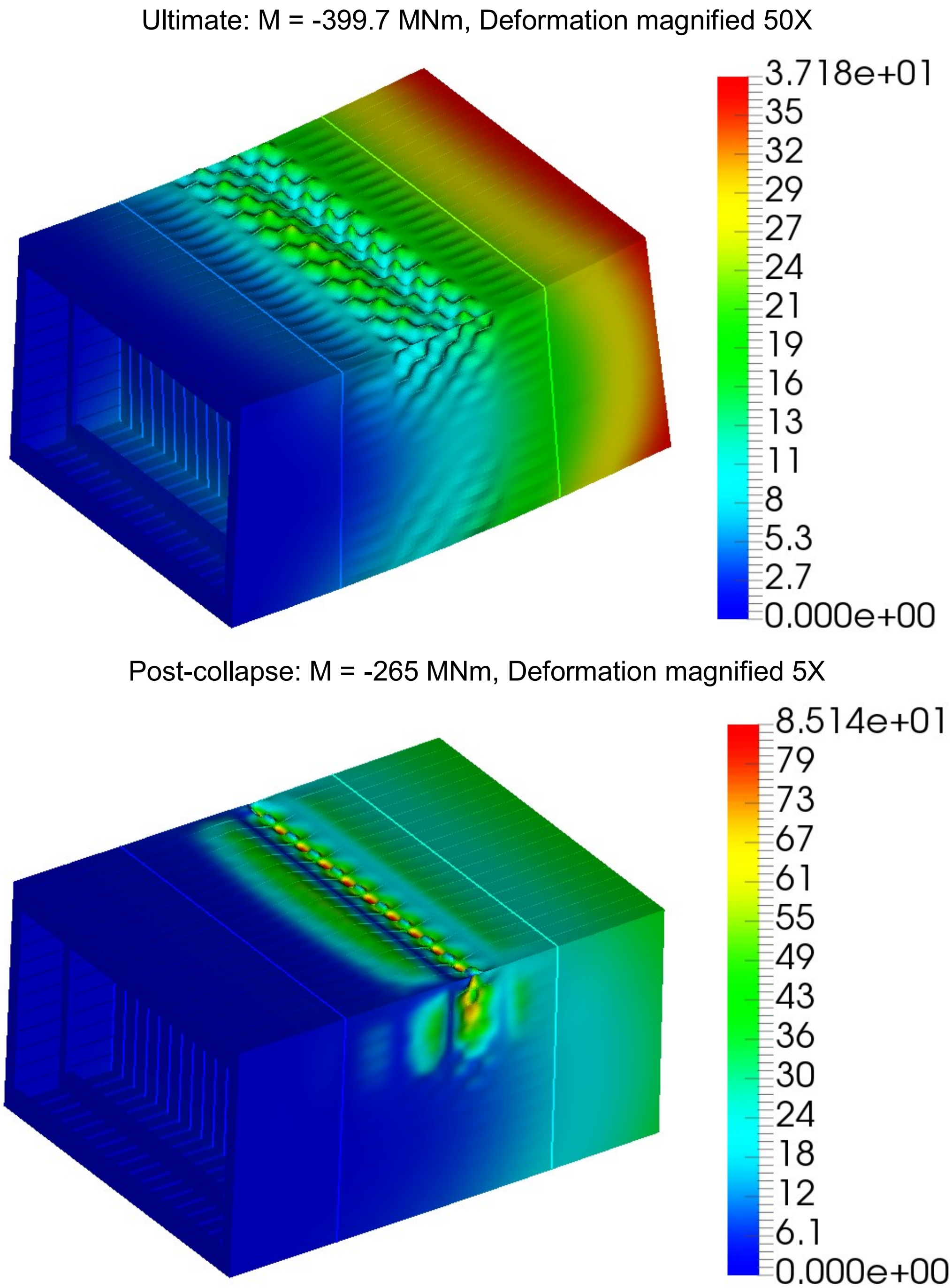

Figure C.1: *Total deformation in mm for SSTK-A in sagging: at ultimate bending moment (top); in post-collapse (bottom).*

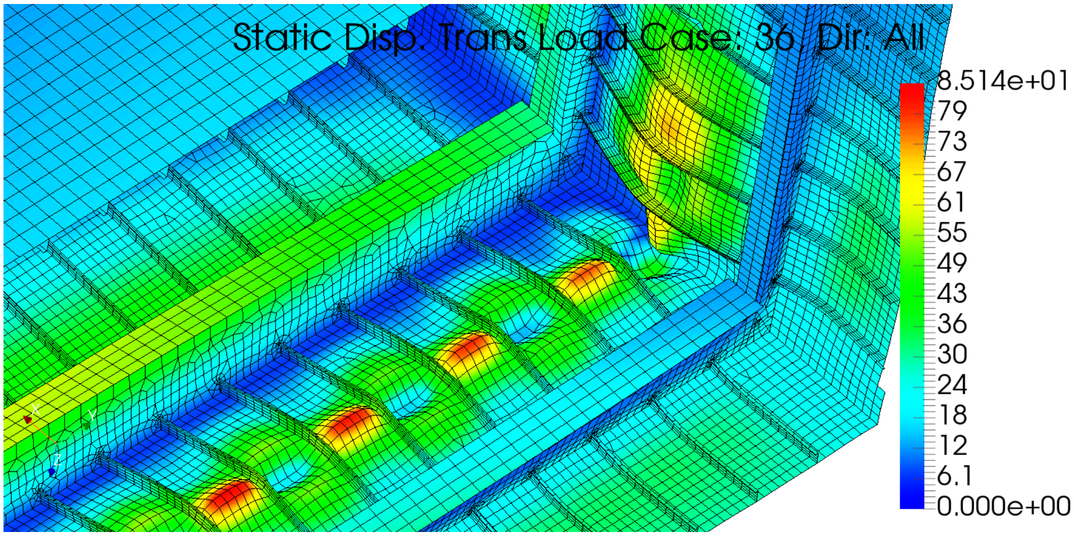

Figure C.2: *Close-up view of deformation (total deformation in mm) for SSTK-A in sagging.*

Annex D Nonlinear FEA results for SSTK-C

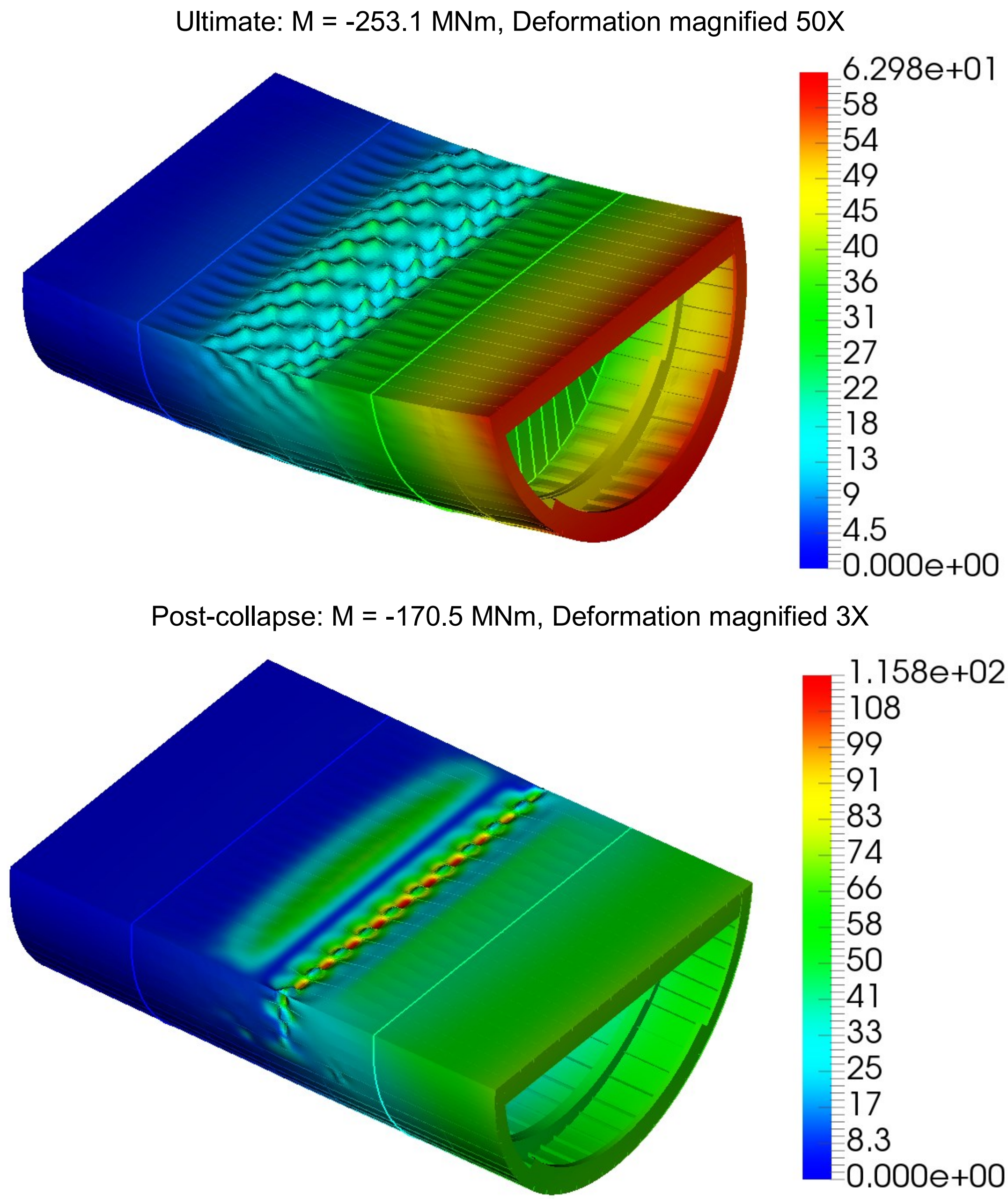

Figure D.1: *Total deformation in mm for the intact SSTK-C in sagging: at ultimate bending moment (top); in post-collapse (bottom).*

List of symbols/abbreviations/acronyms/initialisms

BM	Bending Moment
BP	Bulbplate
DND	Department of National Defence
DRDC	Defence Research and Development Canada
FE	Finite Element
FEA	Finite Element Analysis
HAZ	Heat-Affected Zone
HSS	High-Strength Steel
HY	High-Yield
IACS	International Association of Classification Societies
in	inches
ISSC	International Ship and Offshore Structures Congress
LSC	Load-Shortening Curve
m	metres
mm	millimetres
MNm	Mega-newton-metres
MoD	Ministry of Defence
MPa	Megapascals
NSWC	Naval Surface Warfare Center
SSTK	Structures Software Test Kit
RCN	Royal Canadian Navy
TTCP	The Technical Cooperation Program
ULTMAT	Ultimate Strength (analysis program)
VAST	Vibration and Strength Analysis

DOCUMENT CONTROL DATA

*Security markings for the title, authors, abstract and keywords must be entered when the document is sensitive

1. ORIGINATOR (Name and address of the organization preparing the document. A DRDC Centre sponsoring a contractor's report, or tasking agency, is entered in Section 8.) DRDC – Atlantic Research Centre Defence Research and Development Canada 9 Grove Street P.O. Box 1012 Dartmouth, Nova Scotia B2Y 3Z7 Canada	2a. SECURITY MARKING (Overall security marking of the document including special supplemental markings if applicable.) CAN UNCLASSIFIED 2b. CONTROLLED GOODS NON-CONTROLLED GOODS DMC A

3. TITLE (The document title and sub-title as indicated on the title page.)

Ultimate and residual strength of benchmark hull models

4. AUTHORS (Last name, followed by initials – ranks, titles, etc., not to be used)

Smith, M. J.

5. DATE OF PUBLICATION (Month and year of publication of document.)	6a. NO. OF PAGES (Total pages, including Annexes, excluding DCD, covering and verso pages.)	6b. NO. OF REFS (Total references cited.)
March 2019	77	19

7. DOCUMENT CATEGORY (e.g., Scientific Report, Contract Report, Scientific Letter.)

Scientific Report

8. SPONSORING CENTRE (The name and address of the department project office or laboratory sponsoring the research and development.)

DRDC – Atlantic Research Centre
Defence Research and Development Canada
9 Grove Street
P.O. Box 1012
Dartmouth, Nova Scotia B2Y 3Z7
Canada

9a. PROJECT OR GRANT NO. (If appropriate, the applicable research and development project or grant number under which the document was written. Please specify whether project or grant.)	9b. CONTRACT NO. (If appropriate, the applicable number under which the document was written.)
01ea	

10a. DRDC PUBLICATION NUMBER (The official document number by which the document is identified by the originating activity. This number must be unique to this document.)	10b. OTHER DOCUMENT NO(s). (Any other numbers which may be assigned this document either by the originator or by the sponsor.)
DRDC-RDDC-2019-R021	

11a. FUTURE DISTRIBUTION WITHIN CANADA (Approval for further dissemination of the document. Security classification must also be considered.)

Public release

11b. FUTURE DISTRIBUTION OUTSIDE CANADA (Approval for further dissemination of the document. Security classification must also be considered.)

12. KEYWORDS, DESCRIPTORS or IDENTIFIERS (Use semi-colon as a delimiter.)

Ship Structure; ultimate strength; residual strength; gross damage; Finite Element Analysis

13. ABSTRACT (When available in the document, the French version of the abstract must be included here.)

The ultimate and residual strength in vertical bending of three benchmark hull girder models are evaluated using nonlinear Finite Element Analysis (FEA) and using Smith's simplified method. The benchmark models are evaluated in three conditions: intact, with simulated grounding damage, and with simulated collision damage. Two different Smith's method calculations are performed for each model, in which load shortening curves are generated either using the International Association of Classification Societies (IACS) analytical formulas, or by interpolating from the Ultimate Strength ULTMAT database of pre-calculated curves. Smith's method predictions using the IACS formulas are found to agree well with FEA predictions for interframe collapse of longitudinal structure with high-column slenderness, whereas Smith's method does not agree well with FEA when an overall collapse mode is predicted. For structures with low-column slenderness, Smith's method is found to predict ultimate strengths that are higher than the FEA predictions. Gross damage to the main deck and shear strake, or to the hull bottom, is found to reduce ultimate strength by more than 50% in some cases. In percentage terms, strength reductions are up to three to four times the percentage reduction in the effective cross sectional area. Overall collapse is the preferred mode of failure with collision damage, whereas interframe collapse is preferred with grounding damage.

La résistance à la rupture détermine la capacité portante globale de la coque des grands navires de combat de surface. La résistance à la rupture peut varier tout au long de la vie d'un navire en fonction des changements à sa conception et des effets de la dégradation en service tels que la corrosion et les déformations. Les incidents qui causent de graves avaries peuvent réduire considérablement la résistance restante ou résiduelle au point où la sécurité du navire s'en trouve compromise. Les présents travaux font partie d'une collaboration internationale visant à valider les outils de prévision de la résistance à la rupture et de la résistance résiduelle par des jeux d'essai réalistes Ces efforts ont permis d'accroître la connaissance des limites opérationnelles des coques de la Marine royale canadienne (MRC), ce qui vient appuyer les objectifs du ministère de la Défense nationale (MDN) en matière d'assurance de l'équipement naval.